Indentation of Multi-Layered Materials Using Spherical Indentation

James A. Mills

Submitted in partial fulfillment of the Requirements for the degree of Doctor of Philosophy in the Graduate School of Arts and Sciences

COLUMBIA UNIVERSITY

2020

© 2020

James A. Mills

All Rights Reserved

Abstract

Indentation of Multi-Layered Materials Using Spherical Indentation

James A. Mills

In the field of indentation there is a subset of study that examines indentation of thin films on substrate materials. Early work in this area primarily focused on the properties of the film, neglecting the substrate. However, there are a great many instances where understanding the substrate may be as important if not more important than understanding the film properties. The primary focus of this research and associated thesis is to extend the level of knowledge of the moderately deep spherical indentation of film-substrate systems, investigating both film and substrate. By choosing to use a spherical indenter the effects of damaging the test material at these moderate depths is reduced. It also allows for the incorporation of the innovative technique of invoking the non-self-similarity characteristics of this type of indenter. This thesis is focused on this phenomenon and furthers the present knowledge that exists today of thin film-substrate elastic indentation.

The beginning of this thesis reviews the historical path that indentation has followed from the early work of Hertz to present day research in thin film on substrate materials. The next section focuses on thin films on substrates under spherical indentation in a fully elastic condition, investigating both film and

substrate. A forward analysis incorporating Dimensional Analysis will be performed that will determine two relationships that can be used to solve for material properties of both film and substrate. Moderate indentation depths are chosen that will allow for the addition of the substrate effect while directly avoiding problems related to shallow indentation. A full numerical reverse analysis is performed using simulations that will check the applicability and accuracy of the relationships developed from the forward analysis. In the reverse analysis, different input values are used providing for a unique and unbiased review of the work performed. The next section will extend this research into the area of fully elastic film affixed on substrate systems with the film under an applied equi-biaxial steady-state stress. A forward analysis is performed incorporating dimensional analysis to help reduce the number of variables. A set of relationships are established that are then tested by an independent numerical reverse analysis using a full set of discreet and arbitrary input values. Finally a general examination of multi-layered systems is performed. This is done by first examining a specific problem that exists in industry today, water filtration, then extending this to a general relationship as a proof-of-principal investigation of a multi-layered system. Throughout this work an independent and rigorous error analyses is performed in order to identify potential instabilities in the proposed solutions. Finally an examination and proposal is made of how this work can be used to further extend specific areas of both research and commercial applications of indention of materials to moderate depth, incorporating the substrate effect.

Table of Contents

List of Figures

List of Tables

Notations and Symbols

A_p	projected contact surface area
A	coefficient for variables A_i, B_i, C_i,…
A	constant
a	radius of contact of circle
a_i, b_i, c_i,…	coefficients for variables A_i, B_i, C_i,…
A_i, B_i, C_i,…	functional coefficients for fitting functions, forward analysis
B	constant
C	normalized indentation loading curvature
d	deformed contact surface or chordal diameter of contact surface
D	indenter diameter (spherical)
E	Modulus of Elasticity, Elastic Modulus
E*	effective or Reduced Elastic Modulus
E_f	film elastic modulus
E_i	indenter elastic modulus
EMR	elastic modulus ratio, E_f/E_s
E_{ps}	polysulfone elastic modulus
E_r	effective or reduced elastic modulus
E_s	substrate elastic modulus
f_i	function, forward analysis
G	energy release rate
G_s	shear modulus

h	film thickness
H	hardness
h_f	algae film thickness
$h_{ps}= t_p$	polysulfone thickness
i	coefficient
I	functional variable used for derivation, Rockwell
j	coefficient
k	constant, or relative density
K	strength coefficient
l_d	length of the longest diagonal, Knoop indenter
M, m	coefficients from Oliver and Pharr least squares fit
n	coefficient, work hardening exponent
p	pressure
p (r)	pressure over contact surface
P	force
P	indentation load
p_0	maximum pressure
P_m	mean pressure
q_i	variable 1-3
Q_t	perturbation coefficient, error analysis, t = x,y
r	radial position measured from ordinate to the point of surface contact, also variable 1-4
R	curvature of two surfaces
R	radius of spherical indenter

R^*	circular interface crack
R_i	curvature of surfaces
S	stiffness of the unloading curve
t	Rockwell penetration depth
t_f	algae film thickness
V_i	perturbation coefficient, error analysis
V_s	volume of solids
V_t	perturbation coefficient, error analysis, t=x,y
V_t	total volume
V_v	volume of voids
w	coefficients for variables A_i, B_i, C_i,…
w_i	coefficient, error analysis
X	perturbation coefficient, error analysis
x_c	coefficients for variables A_i, B_i, C_i,…
X_i	perturbation coefficient, error analysis
Y	constants
Y_0	coefficients for variables A_i, B_i, C_i,…
Z	constants
α_i, β_i,…	error sensitivity coefficients, error analysis
β	coefficient, Oliver and Pharr coefficient
δ	elastic displacement or indenter displacement
δ_f	elastic displacement
δ_i	prescribed indentation penetration depth

δ_p	plastic indentation depth
δ_s	depth from free surface to point of contact
δ_t	indenter penetration depth
ε	generalized strain
ε_i	coefficient, error analysis
ε_i	perturbation coefficient, error analysis
η_i	perturbation coefficient, error analysis
θ	conical indenter half angle
K	normalized prestress, σ_{ps}/E_f
ν	Poisson's ratio
ν_i	indenter Poisson's ratio
ν_f	film Poisson's ratio
ν_s	substrate Poisson's ratio
ξ_i	coefficient, error analysis
ξ_i	perturbation coefficient, error analysis
Π, Π_i	function form for forward analysis
σ	stress
σ_0	residual stress in film
σ_{ps}	equi-biaxial stress in film
σ_r (R)	stress at crack radius
$\sigma_r^l(R)$	stress due to indentation at crack radius
σ_s	substrate elastic modulus, aromatic polyamide substrate
σ_y	yield strength

τ_i	perturbation coefficient, error analysis
φ	porosity
X_i	parameter for error analysis
Ψ_t	perturbation coefficient, error analysis, t=x,y
ω_i	perturbation coefficient, error analysis
Ω_i	perturbation coefficient, error analysis

Acknowledgements

Over the past many years I have had the wonderful, challenging and fulfilling opportunity to work at Columbia University studying Civil Engineering and Engineering Mechanics. Under the very special guidance and support of Professor Xi Chen this has turned into an exciting, intellectual journey that I had not anticipated but will forever cherish. His continued technical input, helpful suggestions, patience, and unending encouragement have provided the motivation that has made this research and corresponding dissertation possible. His knowledge in indentation and engineering mechanics is second to none. He has challenged me to think critically about engineering mechanics and how it may be applied to the world we live in. I cannot thank him enough for this and will forever respect and admire him; my mentor, colleague, and friend.

I would also like to very much thank Professor's Patricia J. Culligan, Gautam Dasgupta, Ling Liu, and Dr. Manhong Zhao for serving on my Defense Committee and for their thoughtful and critical review of this dissertation.

Finally, I would like to thank my family for their unending encouragement for this endeavor. I am especially appreciative to my wife, for without her unconditional love and support this would not have been possible.

Dedicated to my Wife

1 Introduction and Problem Statement

1.1 Overview

From its earliest days of use indentation was a test used to help understand the quality and mechanical properties of materials. In its early days, hardness was the material term that was determined using indentation testing. Engineers and scientists also tried to understand how indentation load-depth information might be able to predict more common engineering material properties such as elastic modulus, Poisson's ratio, and yield point. It was through a combination of theoretical and empirical investigations that we can now use indentation to measure such engineering properties.

It is the intent of this paper to review the historical progress of indentation technology from its earliest days to the current research being performed to date. The writer will also detail a series of investigations on the use of indentation and its particular use in thin films and how this investigation has provided to us an additional understanding of the correlation between indentation, hardness, and the material properties of common materials used in today's manufacturing. In particular this paper will guide the reader through a study of indentation of thin films attached to a bulk substrate and how we can uniquely derive material properties of both the film and substrate.

1.2 Early Work in Contact Mechanics

The study of elastic bodies in contact was first studied by Heinrich Hertz in the late 1800s. He wrote two seminal papers on the topic [1, 2]. Hertz's first paper considered the general contact between two surfaces. His approach was to consider the bodies as elastic and isotropic. Their contact area was considered small compared to their overall surface area, and their radius of curvature for each body much larger than the radius of curvature for the contacting surfaces. His investigation led to a better understanding of the surface pressure distribution in the area of contact as well as the deformations associated with this contact pressure. Assumptions he made were (1) there is negligible friction acting between contacting surfaces, leading then to only a normal pressure acting on the two surfaces, (2) the bodies in contact are considered to be infinitely large as compared to the contact surfaces. As such the pressure distribution and contact deflections would disappear as one moved away from the contact area. (3) The two surfaces and hence their overall distance apart can be represented by a quadratic function. He then oriented his axis such that the distance to a reference plane could be simply represented by the term $z_i^2 = Ax_i^2 + By_i^2$ (where the term i designates the two contacting bodies, 1 and 2. This distance can also be described by the curvatures representing each solid; $z_i^2 = \frac{1}{2R_i'} x_i^2 + \frac{1}{2R_i''} y_i^2$ (Figure 1-1). Hertz concluded that for general solids of revolution just prior to contact, contours representing constant gap between the two surfaces would be elliptical in shape. In further developing this theory Hertz also concluded that an ellipsoidal pressure

distribution due to contact would satisfy the general differential equations of equilibrium. Hertz's analysis provided an insight into stresses along the surface of the loaded bodies and closely adjacent regions as well as a prediction of how large the contact surface would be. He also provided the stress and displacement distribution along the line of symmetry of the loaded objects.

From Hertz, for solids of revolution ($R_i' = R_i'' = R_i$) in contact, the contours of constant gap would be circular and the contours of constant pressure once contact occurred would be circular as well. The radius of this contact circle is represented by the following:

$$\mathrm{a} = \left(\frac{3}{4}\frac{\mathrm{PR}}{\mathrm{E}^*}\right)^{1/3} \quad \textbf{(1.1)}$$

with P equal to the total contact force, R represents the curvature of the two surfaces in the form $\frac{1}{R} = \frac{1}{R_1} + \frac{1}{R_2}$, and E* the elastic modulus, $\frac{1}{E^*} = \frac{(1-\nu_1^2)}{E_1} + \frac{(1-\nu_2^2)}{E_2}$ again related to the two corresponding surfaces.

The total elastic displacement is represented by:

$$\delta = \frac{a^2}{R} = \left(\frac{9}{16}\frac{P^2}{RE^{*2}}\right)^{1/3} \quad \textbf{(1.2)}$$

The pressure generated over the contact surface then can be represented by:

$$p(r) = p_0\left\{1 - \left(\frac{r}{a}\right)^2\right\}^{1/2} \quad \textbf{(1.3)}$$

where r is the radial position measured from the ordinate to the point of surface contact. The maximum pressure is then described by:

$$p_0 = \frac{3P}{2\pi a^2} = \left(\frac{6}{\pi^3}\frac{PE^{*2}}{R^2}\right)^{1/3} \quad \textbf{(1.4)}$$

As can be seen from the above equations the radius of the contact circle and the contact pressure increase as the cube root of the load. Note that for spheres contacting a flat plate the term $R_2 \rightarrow \infty$ and $1/R_2 \rightarrow 0$, with the above relationships still being applicable.

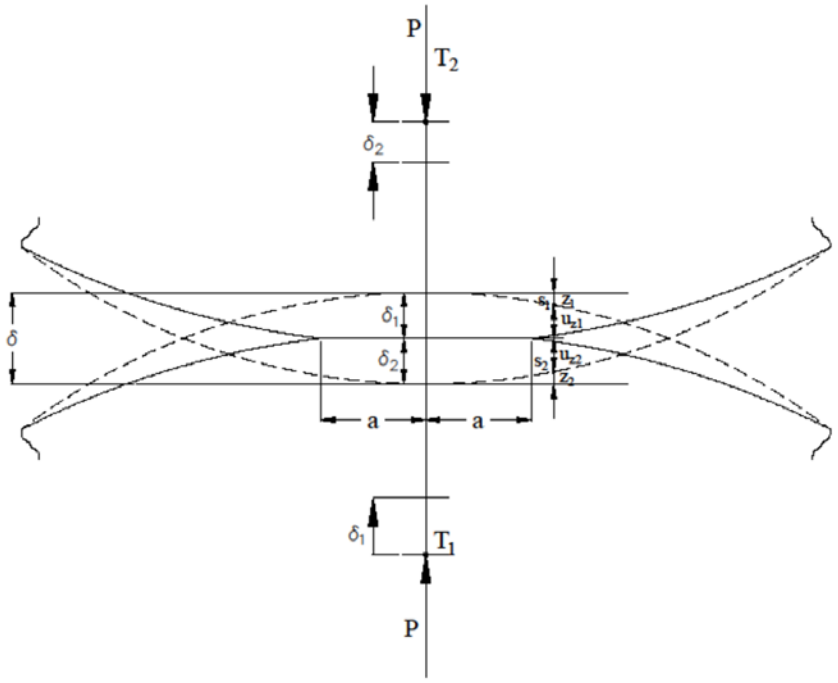

Figure 1-1 Hertz Contact (from Johnson [3])

Boussinesq [4] in 1885 extended this study by solving for the internal stresses of a body under a point load. His analysis used the method of superposition. He looked at a single point load, calculating the ensuing stresses throughout the body

and then applied multiple point loads in order to simulate contact pressure. However, Boussinesq's approach is complicated and therefore limited in its practical application to only the simplest of problems. Further work by Huber [5] in 1904, Fuchs [6] in 1913, and by Huber and Fuchs in 1914 [7] examined the internal stresses developed under various indentation scenarios. Timoshenko and Goodier [8] also examined the internal stresses and displacements based on Boussinesq's solution. They studied in detail the internal stresses from a point load on a contact surface of an axisymmetric body acting as a solid of revolution.
An early application to Hertz and Boussinesq was done by Flamant [9]. Flamant's work dealt with the investigation of stresses and displacement for a type of problem knows as line contact, such as what might be modelled when examining a mechanical bearing. This type of contact is viewed as a line contact along a knife-edge, and represented as a two dimensional problem with a uniform load acting along its length.

Mindlin in the Compliance of Elastic Bodies in Contact [10], examined the displacement and stresses under Hertz's general elliptical contact surface due to a tangential surface traction under the potential of partial slip. His novel approach used elliptic integrals to solve for the tangential surface displacements.

Further work done by A. E. H. Love solved for a conical indenter pressed into an elastic half space in his paper titled, Boussinesq's Problem for a Rigid Cone [11]

in 1939. Harding and Sneddon [12] did additional work in 1945 on this topic as did Gladwell [13].

In particular, Harding and Sneddon [14] proposed a solution to the axisymmetric problem of the elastic stresses produced from the indentation of an object on its surface by a rigid punch; a specific application to the general contact problem. They used the method of integral transforms (Hankel transforms), to reduce the number of variables (r, z) from two to one as shown in the standard bi-harmonic equation, $\Delta^4\phi=0$, where

$$\nabla^2 = \frac{\partial^2}{\partial r^2} + \frac{1}{r}\frac{\partial}{\partial r} + \frac{\partial^2}{\partial z^2} \qquad \textbf{(1.5)}$$

and thus transforming the stress-displacement equations. Applying boundary conditions to this new set of transformed equilibrium equations, they then determined the general solution by incorporation of a solution technique first proposed by Titchmarsh [15]. Sneddon went on to publish additional papers, one of which dealt with the solution of a flat ended, circular cylindrical punch acting on an elastic medium [16]. An additional paper by Sneddon followed in 1948, "Boussinesq's Problem for a Rigid Cone" [17], which analyzed the internal stresses and displacements for an elastic, homogenous, material, such as soil or ductile metals under loading from a conical indenter. In 1965 Sneddon [18] proposed an alternate solution to that developed in the 1944 Harding and Sneddon paper. He still incorporated the use of Hankel transforms but instead of following

the solution technique for these dual integral equations that Titchmarsh proposed, he submitted an alternate and as the author suggests a simpler solution technique.

In 1957 C. M. Segedin proposed an alternate solution to that of Harding and Sneddon [14] and that of Chong [19], in his paper titled The Relation Between Load and Penetration for a Spherical Punch [20]. Instead of using Hankel transforms and dual integral equations he suggested incorporating a set of potentials. He introduced a general solution and then applied this solution to the specific spherical indentation problem of an elastic material.

1.3 Contact, Material Hardness and Indentation

Tabor [21] described hardness as the ability of a material to resist deformation and is a method for determining certain physical properties of a material. Tabor goes on to propose that there are three types of hardness measurements; scratch hardness, indentation hardness, and rebound (dynamic) hardness.

The earliest work of measuring hardness seems to have most likely come from mineralogists. As Tabor describes, the first semi-quantitative measurement was proposed in a paper by Mohs [22] in 1922. This type of hardness testing was also studied by Bierbaum [23], Hankins [24], and O'Neill [25]. However, other than the mineral industry, the scratch sclerometer was not very popular and proved to be a relatively inaccurate form of hardness measurement.

Static indentation hardness has proved to be more resilient and useful as a general purpose testing method for hardness and provides the possibility of estimating other useful mechanical properties of materials. Generally speaking Hardness can be described as the average pressure from an indentation test. This is typically calculated as the applied load divided by the projected contact area made between an indenter and material specimen. Brinell was an early advocate for hardness testing using static methods. The technique, as Brinell [26] proposed and on which A. Wahlberg [27] described in his two papers (1901 V1 and V2), uses a hardened spherical ball firmly pressed into the material under investigation. The diameter of the permanently deformed surface area from the test is then measured. From the measured indented surface diameter, along with knowing the spherical indenter diameter the concavity surface area can be determined. This area is then divided into the applied force from the test. He named this value, the Brinell hardness number. However there were flaws in this technique as Wahlberg spelled out. In particular, the calculated hardness value of a material increases if a smaller diameter indenter is used (at constant indentation pressure). Also if instead, the indentation load is increased with the indenter diameter constant, the hardness also increases. Wahlberg also states that cold-working of the material from the indenter being pressed into the specimen also caused variations in the measured hardness. Brinell accounted for this by using the concavity surface instead of the projected surface. Brinell used his results at the Fagersta Iron and

Steel Works in Westmanland, Sweden not only to provide a relationship of hardness to different materials but also to compare his hardness number to the included percentage of carbon in the steel produced at the facility.

Meyer [28] in 1908 proposed an alternate form for the hardness calculation, using an area as the divisor based on the projected surface area of the indention rather than the actual concavity area of the deformed material. The Meyer Hardness is then:

$$H = \frac{P}{\frac{\pi d^2}{4}} \quad \textbf{(1.6)}$$

in which P is the measured indentation force at full load and d is the diameter of the deformed contact surface (Figure 1-2a). Meyer continued his research by examining the effect of differing spherical indenters and their relationship to indentation load during a hardness test. These new findings, known as Meyer's law takes the form of $P = kd^n$. The coefficients k and n are constants. Meyer found that the value of n for most conventional metals ranged from 2 to 2.5. The value of k for a given material is equivalent to a reference indentation load at which the projected area's diameter is equal to 1.0. Interestingly this provides a form of similarity such that the value of d/D, where d is as before and D is the diameter of the indenter, will provide the same hardness using the Meyer technique or the Brinell method.

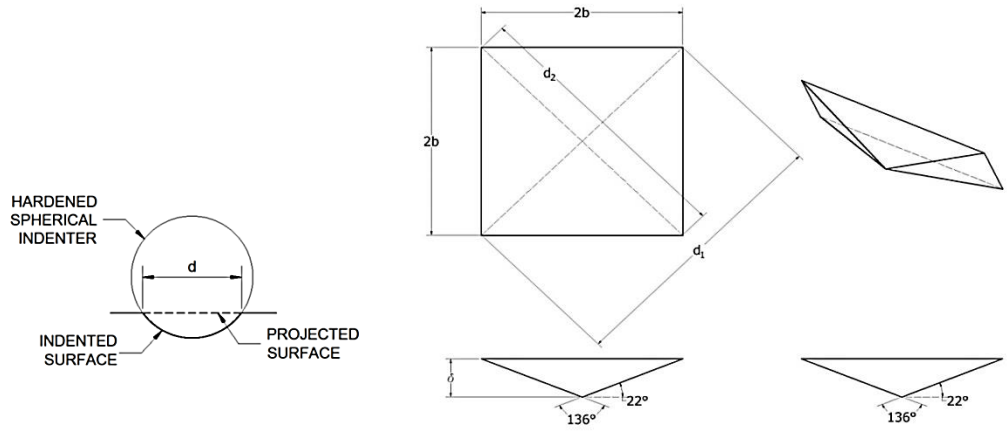

Figure 1-2 (a) Meyer's Indenter (b) Square Pyramid Cross Section (Vicker's Indenter)

Pyramidal diamond indentation testing, commonly referred to as the Vicker's Indentation test was first introduced by Smith and Sandland [29]. Their research focused on ways to improve the accuracy of the results generated from a standard Brinell hardness test. Through empirical testing they developed a Modified Ball Hardness test that increased the accuracy of the standard Brinell test. The only drawback was that as the hardness of the tested material increased the accuracy decreased. This limited accurate testing of metals to hardness values below the Brinell Hardness Number of 535 or Modified Brinell Hardness of 550. They concluded that this was primarily due to the deformation of the steel indenter ball as it is pressed into the test specimen thus skewing the recorded force and potentially distorting the indented cavity. Shore [30] also found this to be true and proposed the use of a spherical diamond indenter in place of the steel ball.

This was deemed a promising and effective change but the technical difficulty in shaping a diamond into a sphere proved to be problematic. Instead Smith and Sandland proposed using a natural, uncut pyramidal diamond. The proposed use of a diamond pyramid had the advantage that it was accurate over a wider range of metals than the steel ball method used in the Brinell test and did not require special shaping as the spherical diamond did. This proposed method was later more fully developed by Messrs. Vickers-Armstrong, Ltd. This new hardness test, is now more commonly known as the Vicker's hardness test. The hardness value is determined by dividing the measured load by the contact surface made during indentation. Unfortunately, it was found that the contact surface was difficult to measure during the actual indentation test. This can lead to error. However since the indenter used is a square pyramid (Figure 1-2b), with an angle between opposite faces of 136 degrees, there is a direct correlation between the contact area and the area of the base of the pyramid at the contact surface, with the area at the contact surface much easier to measure and calculate.

Examining the geometry of the square pyramid, the following relationship holds:

Area of the Base of the Pyramid = 0.9272 * Total Contact Surface Area.

Therefore, by using this relationship, and knowing the area of the base of the pyramid at specimen surface, the hardness can be determined. The area of the base is calculated by using the diametric opposites (Figure 1-2b) and averaging them such that the area of the pyramid at the contact surface is:

$$Area_{pyramid\ base} = \frac{d^2}{2} = \frac{\left(\frac{d_1+d_2}{2}\right)^2}{2} \qquad \textbf{(1. 7)}$$

Which then provides the following hardness value:

$$\text{Vickers Hardness } = \frac{Indenter\ Force}{Contact\ Surface\ Area} = \frac{0.927\ P}{\frac{d^2}{2}} \qquad \textbf{(1. 8)}$$

Another important feature of the square pyramid indenter is that the measured diagonal (d) is equal to seven times the total depth of indentation penetration into the specimen (δ);

$$d = 7.0006\ \delta \qquad \textbf{(1. 9)}$$

Therefore, if the depth can be measured accurately and using the relationships above, the Vicker's Hardness value can be directly calculated.

In the 1920's S. R. Rockwell [31] introduced a method for measuring the hardness of metals that built on the work of Brinell and Meyer. The initial load used to create the indention and to prepare the surface, is applied using a steady force of 10 kg. This is held for a few seconds, with the indentation depth then reset to zero. An additional load is then applied, either 90 kg or 140 kg. This again is held until full deformation is completed and then the load is removed, returning to the initial 10 kg load. The indentation depth is read directly and used to determine the Rockwell Hardness (Fig. 1-3a):

$$l = \frac{D}{2} - \delta, and\ d = 2a \quad \textbf{(1. 10)}$$

$$\left(\frac{D}{2}\right)^2 = a^2 + l^2\ then\ expanding: \quad \textbf{(1. 11)}$$

$$\left(\frac{\boldsymbol{D}}{\boldsymbol{2}}\right)^{\boldsymbol{2}} = a^2 + \left(\frac{D}{2} - \delta\right)^2 \quad \textbf{(1. 12)}$$

Then if δ<<D then

$$\delta = \frac{a^2}{D} = \frac{d^2}{4D} \quad \textbf{(1. 13)}$$

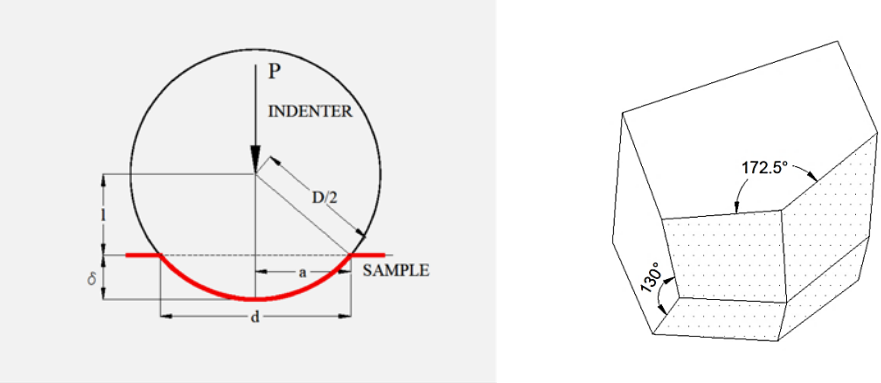

(a) (b)

Figure 1-3 (a) Rockwell Indenter, (b) Knoop Indenter.

With this term, Rockwell showed that the indentation depth is proportional to the projected surface area of the deformed section, which in turn is directly related to the Brinell or Meyer Hardness. From the Meyer Hardness:

$$Meyer\ Hardness = P_{mean}\ (mean\ pressure) = \frac{Force_{Indenter}}{\pi D \delta} \quad \textbf{(1. 14)}$$

With this relationship, we see that the Hardness is inversely proportional to the depth of penetration (δ). Rockwell, wanting a relationship that described an increasing hardness value as the hardness increased (while keeping the load fixed) proposed a modified relationship as shown:

For soft materials the Rockwell 'B' test is performed which uses a spherical indenter. –

$$Rockwell\ Hardness\ 'B' = 130 - \frac{\delta}{0.002} \qquad \textbf{(1. 15)}$$

For harder materials a conical indenter is used, with a hemispherical tip. The conical test is known as the Rockwell 'C' test.

$$Rockwell\ Hardness\ 'C' = 100 - \frac{\delta}{0.002} \qquad \textbf{(1. 16)}$$

By effectively removing the need to determine the diameter of the permanently deformed impression, Rockwell thus removed the need to use a precision microscope to measure the diameter of the permanently deformed impression.

In 1939, Frederick Knoop, Chauncey G. Peters, and Walter B. Emerson [32] proposed a method for determining the hardness of brittle and/or small thin specimens that could not be determined by other standard methods used in this time period which typically required a relatively deep penetration of the indenter into the test specimen. This method became known as the Knoop Hardness test. Another advantage of the Knoop Hardness test is that because of the shallow

indentation depths used, only the surface of a material is examined, which would specifically be important if one wanted to examine metals which have had a surface treatment applied, or hardened by a heat-treating process. It incorporated a diamond indenter in the shape of a rhombus (Figure 1-3b).

As they determined in a series of tests to optimize the angles of the rhombus, they found that during all of the individual tests, both elastic and plastic deformation took place. The angles chosen ultimately corresponded to a much longer diagonal than the opposite diagonal by a ratio of approximately 7:1. In preparation for the test the surface of the specimen is highly polished to allow for an accurate reading of the diagonal by a microscope. Knoop, et al found that after testing and subsequent indenter removal, some elastic recovery or contraction did occur in the surface. However, they found that when measuring the surface diagonals the transverse direction rather than the longitudinal direction measurably changed. This allowed them to then simply use the length of the long diagonal in determining the contact area. The hardness was then calculated by dividing the applied indentation load, in kilograms, by the unrecovered projected surface area in millimeters.

$$Knoop\ Hardness = \frac{P_{indenter}}{Area_{projected}} = \frac{P_{indenter}}{0.0703(l_d^2)} \qquad \textbf{(1. 17)}$$

where $P_{indenter}$ = load applied to the indenter in kilograms, l_d = the length of the longest diagonal in millimeters, and 0.0703 is a constant based on the diamond pyramid with face angles of 172.5 and 130 degrees respectively.

1.4 Hardness Testing and Modern Depth Sensing Techniques

Hardness testing of materials has become more important with the introduction of new materials and technologies such as electronics, multi-layered MEMS, and bio-mechanical work such as advances in both dental and bone research. Along with these emerging technologies, hardness testing has also advanced, primarily with the establishment of precision nano-indentation depth measuring equipment. This equipment has the ability to measure very accurately both the indenter load as well as its displacement as it is pressed into a test material [33-35] opening up the possibilities of examining materials at the micro and nano scales. Vickers and Berkovich indenters are commonly used to measure hardness at these length scales. As before, Vickers is a 4-sided pyramidal indenter with opposite face angle measurements of 136 degrees and a nominal hardness based on the following (Fig. 1-2b):

$$\text{Vickers Hardness Number} = \frac{Indenter\ Force}{Contact\ Surface\ Area} = \frac{1.854\,P}{d^2} \qquad \textbf{(1. 18)}$$

where d is the averaged diagonal measurement of the indenter impression taken at the sample surface. Recall that this measurement of d is 7.0006 times the

measured indentation depth (δ). Thus the Vickers Hardness in terms of indenter load and depth is:

$$\text{Vickers Hardness Number (VHN)} = \frac{1.854\,P}{(7.0006\,\delta)^2} \qquad \textbf{(1. 19)}$$

$$\text{Vickers Hardness Number (VHN)} = 0.0378\,\frac{P}{\delta^2} \qquad \textbf{(1. 20)}$$

And the projected area is

$$A_p = \frac{d^2}{2} = \frac{(7.0006\,\delta)^2}{2} = 24.5042\,(\delta)^2 \qquad \textbf{(1. 21)}$$

The Berkovich indenter [36] can be used for very small-scale materials and has the added benefit over the Vickers tester in that the indenter is a 3-sided indenter rather than the Vickers 4 sided square pyramidal indenter. The three faced indenter naturally converges to a single point thus making it much easier and less costly to make. However, because of the use of micro-scale and nano-scale specimens, the contact surface area from the indentation is very difficult to determine and typically requires a precision measuring device, such as an electron microscope. In order to overcome this difficulty a specific Berkovich indenter angle was chosen so as to mimic the Vickers four-sided indenter that has a face angle of 68 degrees. The optimum included angle of the Berkovich indenter was determined to be 65.3 degrees from the perpendicular to face (Fig. 1-4).

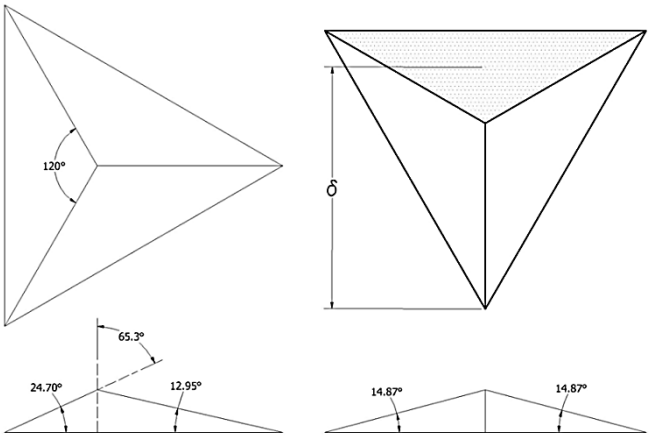

Figure 1-4 Berkovich Indenter

This leads to a projected area equal to:

$$A_p = \frac{d^2}{2} = 24.56\,(\delta) \qquad \textbf{(1. 22)}$$

By directly relating the indentation depth to the projected contact area this easily measured depth then provides an alternative to measuring the contact surface using sophisticated and costly devices such as microscopes. Because of this relationship, hardness and other engineering properties can be determined directly from the recorded load-depth data take from an indentation test.

Doerner and Nix [37] as well as Oliver and Pharr [38] examined the relationship between indentation load-depth sensing and the determination of material Elastic Modulus and Hardness. While there were slight differences in how to determine

the projected contact area from an indentation test, the general idea of how to interpret the results was the same and is the basis for present day indentation research and testing.

In order to understand the phenomena and power of the load-displacement measurements of an indentation test, early work by Bulychev, Alekhin, Shorshorov, et al [39] found that the plotted load-displacement data for an elastic-plastic material is similar to Figure 1-5.

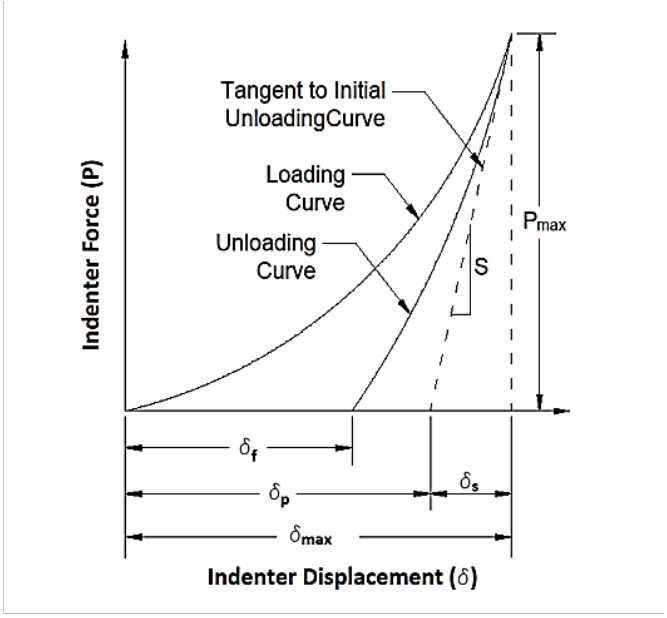

Figure 1-5 Load Displacement Plot - Elastic-Plastic Material [38, 40].

They also proposed that the slope, S (dP/dδ), of the initial unloading curve could be represented by the following:

$$S = \frac{dP}{d\delta} = \frac{2}{\sqrt{\pi}} E_r \sqrt{A_p} \quad \textbf{(1. 23)}$$

A_p is the projected contact surface area of the indented material from the test, and E_r is a reduced Elastic Modulus. This reduced Elastic Modulus accounts for the potential compliance contribution of the indentation test equipment, such that,

$$\frac{1}{E_r} = \frac{(1-\nu^2)}{E} + \frac{(1-\nu_i^2)}{E_i} \quad \textbf{(1. 24)}$$

Here E and ν are the Elastic Modulus and Poisson's Ratio for the test material and E_i and ν_i are the corresponding indenter Modulus and Poisson's Ratio. Bulychev, et al suggested that their relationship holds for conical, spherical, and cylindrical indenters [39, 40]. Pharr, Oliver, and Brotzen further proved that this relationship also holds for all types of indenters including pyramidal shapes [41].

However, while equation 1.23 provided a relationship between load-displacement data and material properties, there was still a need to accurately calculate the contact surface area, A_p. This became more urgent as modern day indentation research done in the 1980's and later provided an accurate method for investigating very thin films [33, 42-47] and surfaces. A means to measure this contact area at very small scales was required. This was initially done by optical means which unfortunately proved to be time consuming and expensive [38]. Researchers looked to the possibility of relating the indenter geometry to the contact surface area. While this proved to be a potential solution, the first question that needed answering was whether the surface area was best described

or more accurately described by using the contact area at peak load or whether it was more accurate to use the contact area measured at the indenter's final depth. Oliver, et al [48], through extensive testing, found that the contact area at final indentation depth provided a more accurate estimate.

Doerner and Nix [37] proposed using the unloading portion of the load-displacement curve to predict both the elastic modulus as well as the hardness of a material that experiences both elastic as well as plastic deformation during the test. Stilwell and Tabor [47] determined that if instead of using the unloading curve, the final depth was used, overestimating of the hardness would occur. Doerner and Nix proposed to separate out the plastic and elastic parts of the indentation load-displacement curve. In effect, they found that the initial unloading portion of the curve for materials that they had tested had a shape that could be described as linear elastic. This initial linear slope could then be represented by a flat cylindrical punch indenter (Figure 1-6) with a linear P-δ representation similar to, $P=k\delta^1$.

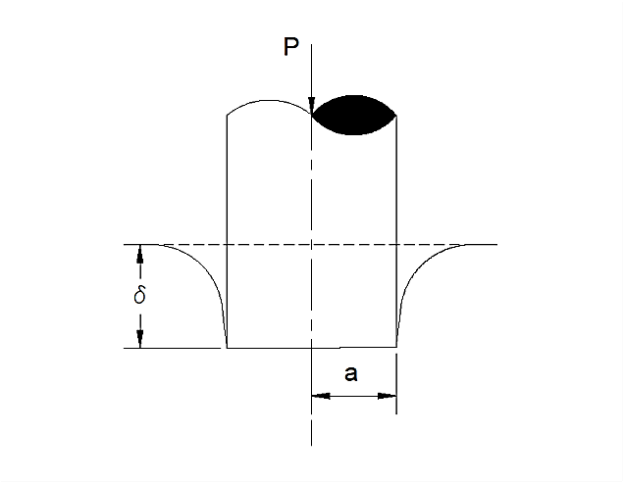

Figure 1-6 Flat Cylindrical Punch

Loubet, et al. [42] proved this hypothesis using a Vickers type indenter and invoking the general solution produced by Sneddon [16]. Their solution, specific to a Vickers indenter took the form:

$$S = \frac{dP}{d\delta} = \frac{\sqrt{2}}{\sqrt{\pi}}\ E_r\, d \qquad \textbf{(1. 25)}$$

where d is as described as before, the average measured distance of the diagonal of the Vickers indenter projected at the contact surface. This equation is consistent with equation (1.23) from above. Simplifying this equation in terms of the depth we get:

$$S = \frac{dP}{d\delta} = \frac{\sqrt{2}}{\sqrt{\pi}}\ \left(7\delta_p\right)E_r \qquad \textbf{(1. 26)}$$

with δ_p being the indentation depth (as shown in Fig. 1-5). What Doerner and Nix proposed was that this depth, δ_p, was most accurately described as the plastic depth (Figure 1-5). The plastic depth is determined by assuming a linear

tangential fit of the initial portion of the unloading curve and extrapolating this tangent to the x axis. The distance from the origin to this point on the x axis is the plastic depth. It is in using this, that Doerner and Nix then arrived at a relationship that could be used to determine the elastic modulus of the material and hardness. Thus, a solution is obtained by assuming a linear extrapolation of the unloading curve, equating this to that produced as Sneddon calculated by an elastic loading/unloading of a flat cylindrical punch.

However, Oliver and Pharr [38] proposed a slightly different method for determining the material elastic modulus as well as material hardness. While they generally agreed with the work done by Doerner and Nix, they found differences in the slopes of the unloading curves of various materials most of which turned out to be non-linear which would tend to invalidate the Doerner and Nix proposal of applying the flat cylindrical punch solution. As Oliver and Pharr noted, Sneddon [18] in his landmark paper derived the general relationships between load and penetration for an axisymmetric punch pushed into an elastic material. Sneddon [18] solved the classical Boussinesq problem using various indenters with different profiles [11, 49] assuming the indenter is as an axisymmetric solid of revolution that can be described by a continuous function [14]. Under elastic conditions he proposed the following relationship for indentation load in terms of indenter displacement,

$$P = n\delta^m \qquad \textbf{(1. 27)}$$

In this equation P is the recorded force of the indenter, δ is the associated displacement of the indenter normal to the contact surface at the load P, and n and m are constants. He found values of m for various indenters, with m=1 for a flat cylindrical indenter, m=2 for a conical indenter, m=1.5 for a spherical indenter (under small displacements) and m=1.5 for paraboloids of revolution. These results were based on an elastic analysis. However Oliver and Pharr [38] point out that examining indentation with material plasticity is far more complex. This is because the constitutive mechanics equations are non-linear. Due to this complexity, with the exception of very basic problems, studying indentation under plastic conditions can only be done experimentally or by finite element analysis. Tabor also examined such types of loading and proposed that in performing an experimental analysis, problems due to residual plasticity could be present and therefore suggested that multiple cycles of load and unloading of the indenter be done to remove these residual effects. Both Tabor [50] and Tabor and Stilwell [47] proposed that the shape of the unloading curve could in effect be used to understand both the hardness, through determining the elastic contact area, and elastic modulus of the material for spherical and conical indenters. They found that the material's linear elastic as well as plastic characteristics had an effect on the P-δ data. They proposed that in order to first remove all of the effects due to plasticity; multiple reversals of loading and unloading needed to occur. Secondly, due to time-dependent plastic effects, holding final maximum loading before unloading was also suggested.

Through extensive material testing Oliver and Pharr [38] found that the unloading curve was rarely represented as a linear elastic model suggested by Doerner and Nix. Instead these curves typically were shaped in a concave upward fashion. And what they found was that the unloading data fit more closely to a power-law function than a linear representation, with the exponent dependent on the material. From the materials that they tested, they found these values for the exponent ranged from 1.25 to 1.51, greater than our linear value of 1. In rewriting Eq. (1.23) they suggested that if a reasonably accurate representation of the unloading slope can be made, the reduced elastic modulus can be calculated;

$$E_r = \frac{\sqrt{\pi}}{2}\frac{S}{\sqrt{A_p}} = \frac{\sqrt{\pi}}{2\sqrt{A_p}}\frac{dP}{d\delta} \qquad \textbf{(1. 28)}$$

The two terms that need to be determined are $dP/d\delta$ and A_p, which is the projected contact area. For determining the contact area, Oliver and Pharr proposed that the area of the indenter could be represented by a function, $A_p = g(\delta_c)$. δ_c is the contact depth and is equal to the vertical component of the contact surface developed by the indenter during loading (Fig. 1-7a and 1-7b). They did caution that this function must be validated experimentally in order to ensure accuracy. If the contact depth, δ_c can be determined, then the contact area can be computed. The contact depth is calculated from the relationship $\delta = \delta_c + \delta_s$ again as noted in Figure 1-7a and b.

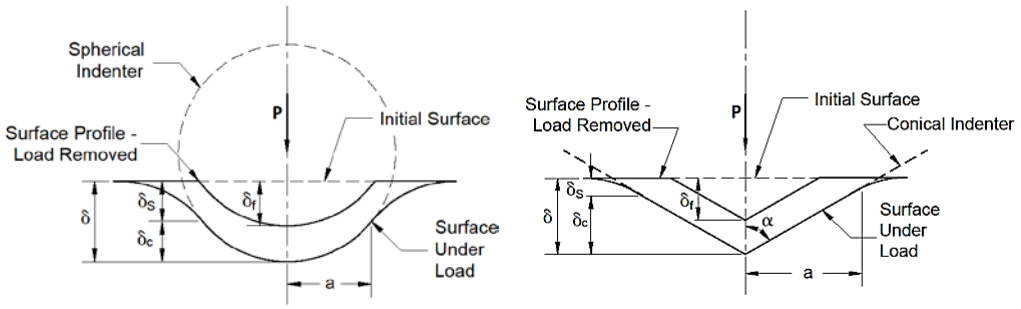

Figure 1-7 Elastic-plastic material (a) spherical indenter (b) conical indenter

From Figure 1-7a and b we see that δ_s is the distance from the initial un-indented surface of the material being tested to the start of the contact surface. From Sneddon for a conical indenter, δ_s (Figure 1-7b) is:

$$\delta_s = \frac{(\pi-2)}{\pi}(\delta - \delta_f) \qquad \textbf{(1. 29)}$$

Sneddon uses δ-δ_f because his results apply to only the elastic problem. Sneddon also determined that δ-δ_f is related to the load-displacement relationship for a conical indenter by the following:

$$(\delta - \delta_f) = 2\frac{P}{S} \qquad \textbf{(1. 30)}$$

With P as before, the indentation force, and S the stiffness (slope) of the loading/unloading curve (recall since Sneddon's analysis is for an elastic condition the loading/unloading curves are in fact the same). From these two relationships Oliver and Pharr proposed the following general term for δ_s:

$$\delta_s = \beta\frac{P_{max}}{S} \qquad \textbf{(1. 31)}$$

For a conical indenter they determined that β is:

$$\beta = \frac{2}{\pi}(\pi - 2) = 0.72 \quad \textbf{(1. 32)}$$

For other indenters they found that β = 1.0 for a flat indenter and β = 0.75 for an indenter that had a shape that could be represented by a paraboloid of revolution. With β = 1.0 for a flat punch the results from Oliver and Pharr are consistent with the results from Doerner and Nix for a similar type of indenter. Oliver and Pharr performed a number of experimental indentations of various materials and found that the unloading curves could all be represented by a simple power-law function, with exponent m. They found from these experiments that m varied from 1.25 to 1.51. The mean value was calculated to be 1.40. Oliver and Pharr then compared this value with the values noted in Table 1-1 in order to determine the best fit for a general relationship. They concluded that the best general value based on the mean value of m for β is 0.75.

Table 1-1 Oliver and Pharr Indenter Comparisons found from experiment

Punch Geometry	β	m
Flat	1.0	1.0
Paraboloid	0.75	1.5
Conical	0.72	2.0

For a generalized paraboloid fit we get the following for δ_s:

$$\delta_s = 0.75\frac{P_{max}}{S} \quad \textbf{(1. 33)}$$

In examining the unloading curve, Doerner and Nix suggested that the slope could be determined based on their work that showed that either most of or at least 1/3

of the initial unloading slope would be linear. However, Oliver and Pharr determined that this was somewhat inaccurate because the unloading was actually non-linear. Therefore drawing a tangent to the initial unloading curve was not a sufficient representation of the elastic contribution. Oliver and Pharr proposed that since all of the unloading curves from their research followed a power-law type of function the following term would provide a more accurate estimate of the unloading slope:

$$P = M\,(\delta - \delta_f)^m \qquad \textbf{(1. 34)}$$

They proposed that from the measured indentation data a least squares fit could be used to determine the coefficients M, m (note m is not the same as denoted in equation 1.27), and δ_f. Then by differentiating the above term with respect to δ the slope is determined. If the slope term is then solved at the point where the indenter has reached the maximum depth and force, the slope at the beginning of the unloading curve can be calculated. And once having this we can determine both the elastic modulus of the test material and its hardness:

$$E_r = \frac{\sqrt{\pi}}{2}\frac{S}{\sqrt{A_p}} = \frac{\sqrt{\pi}}{2\sqrt{A_p}}\frac{dP}{d\delta} \qquad \textbf{(1. 35)}$$

and

$$Hardness = H = \frac{P_{max}}{A_p} \qquad \textbf{(1. 36)}$$

Oliver and Pharr also posit that in referring to Sneddon's functions, they must hold for both an indenter just making contact with the test material surface that is flat and semi-infinite, as well as for a surface already deformed. As discussed in

the literature, with the exception of some minor differences this can be considered to hold for all modern day indenters being pushed into a test specimen [41].

In a later paper Oliver and Pharr [51] discussed the advances they have made in this solution technique they developed. Their method has become a primary tool for determining hardness and elastic modulus, and has been validated by many sources [52-65]. In this later paper they discuss effects due to pile-up and the determination of the area function as well as a discussion of the special term, load divided by the stiffness squared. This last topic introduces a new concept that the authors suggest is a measurable quantity that allows the solution for Hardness and Elastic Modulus without needing to calculate the contact area [66]. In this paper they also provide the solution using their technique, and extending the method to spherical indentation. Further work on spherical indentation has also been done by Fischer-Cripps [67], Field and Swain [68], Francis [69], and others [70, 71]. Field and Swain in their 1993 paper [72] also proposed an alternate solution to the Oliver and Pharr method described above.

Along with more accurate testing methods, recent work has also used indentation technology to determine the yield strength and power-law coefficients for elastic-plastic materials. This extends the knowledge of materials from a somewhat abstract value of hardness to continuum properties of tested materials. Other present day indentation research also examines creep effects in materials [73-75],

viscoelastic materials [76-79], fracture [80], and multi-layer models. An emerging field of indentation showing much promise is in the study of biomaterials [81-83].

1.5 Similarity, Dimensional Analysis, and the ∏-Theorem

In order to gain insight into the mechanics of indentation we first need to examine some of the fundamental principles. The first of these principles is the theory of similarity.

1.5.1 Galileo

Galileo discussed in his book, The Two New Sciences (see paper by Peterson [84]), the mechanics of scaling of the geometric properties of objects such as beams and ships. What he concluded was that geometrically similar objects would not necessarily be equally strong, and for a beam, would be dependent on the cross sectional area and inversely proportional to its length. Based on his work we arrive at the conclusion that similarity and dimension will play a role in the analysis of materials and the determination of mechanical properties.

1.5.2 Dimensional Analysis

A fundamental premise in describing the mechanical relationships of objects is that when developing a function that relates physical laws, the units within the function have to be the same. Cheng and Cheng [85] define this as generalized

homogeneity; in effect, each additive term in an equation must have the same units or the same dimension [86]. This is an important statement because if we are careful with the choice of units or dimensions we can significantly simplify a relationship. This concept led to the Pi or ∏-Theorem [87-98] for Dimensional Analysis. Tan discusses this in his text Dimensional Analysis [99]. He defines dimension as the essential nature of a quantity. He postulates that there are two types of quantities that may represent an object or physical property. These are dimensional and dimensionless properties. The former requiring specific magnitudes that relate units; for example time, mass, force and length are all dimensions that can be used to describe a given property. However, for dimensionless properties that may also be used to describe an object there is no such requirement. They are in effect normalized in some fashion such that the actual magnitude of such a singular term is not a requirement. A common approach for example would be to take a length unit and normalize it by diving by another length unit, effectively dividing one length dimension by another. Therefore what is important in an expression such as this is the ratio value of the two terms. Tan also defines the two terms: fundamental properties and derived properties. Fundamental properties are those terms which are mutually independent of one another. For example length and time are independent terms. Derived properties can be any number of terms that are used to describe an object or phenomenon where the dimensions of these terms are not independent but instead depend on, and can be fully described by the fundamental terms defined in

a problem. For example if our fundamental properties chosen are length, mass, and time then velocity can be described by the length divided by time. He further states that the essential principles in dimensional analysis relate to two specific principles. The first states that only magnitudes of quantities of similar dimensions can be used in developing a relationship that describes an object or phenomenon. The second principle states that for dimensional analysis, the physical phenomena and physical laws do not depend on the units selected to represent that phenomena as long as they are consistent. For example if we were examining a problem with a corresponding length scale, the units of the length scale if in millimeters requires that the normalizing factor also of length scale, be in millimeters. These important features will help us in formulating the ∏-Theorem and in turn will help in performing detailed numerical studies of indentation problems. In our problem and in general Newtonian Mechanics the fundamental units used are length (L), mass (M), and time (T). These terms are by definition dimensionally independent. From these units all other units can be defined. An example of this is the description of engineering acceleration where the fundamental units for dimension are length and time squared.

As a precursor to the review of the definition of the ∏-Theorem, Maxwell [100] proposed that a mechanical object or problem could be described by a simple power law monomial formula. Thus,

$$[X]= L^{\alpha}M^{\beta}T^{\gamma} \qquad \textbf{(1. 37)}$$

where the exponents listed are all real numbers and related to [X]. This is an important term when analyzing numerical simulations of indentation problems. As an example of [X] consider the term for acceleration, shown as $L^1T^{-1}T^{-1}$. If the exponents α, β, and γ are all zero then the term is defined as dimensionless and shown using the above example then $[X]= L^0M^0T^0=1$

It is also important to note that a dimensionless number cannot be described by using a dimensionally independent set of values. The $\prod$-Theorem was first introduced by Buckingham in 1914 [101-103]. His theorem in short, establishes that a physical phenomenon or object can be described by a set of dimensionless parameters. In doing so, the number of unknown terms can be reduced thus making the problem easier to solve.

A problem in engineering mechanics can be described by a general relationship such as the following:

$$b = f(b_1, b_2, b_3,\dots ,b_s, b_{s+1}, b_{s+2},\dots,b_n) \qquad \textbf{(1. 38)}$$

where b is a physical quantity with dimension of [b]. b_i values are independent with respect to b (dependent variable). If there are s fundamental quantities of these then there is also s number of independent dimensions. Therefore, there are (n-s) derived values that additionally describe b.

From the above description then b_1 to b_s are independent variables that have defined dimensions B_1, B_2,… ,B_s respectively. The remaining (n-s) variables are derived variables from these such that their dimensions are:

$$[b_{s+1}] = B_1^{q_1} B_2^{q_2} \dots B_s^{q_s} \quad \textbf{(1. 39)}$$

$$[b_{s+2}] = B_1^{r_1} B_2^{r_2} \dots B_s^{r_s} \quad \textbf{(1. 40)}$$

$$\vdots$$

$$to\ n-s\ where\ [b_n] = B_1^{u_1} B_2^{u_2} \dots B_s^{u_s} \quad \textbf{(1. 41)}$$

If the dependent variable's dimension is then a derived quantity shown with respect to a set of independent power values such that

$$[b] = B_1^{v_1} B_2^{v_2} \dots B_s^{v_s} \quad \textbf{(1. 42)}$$

then

$$\frac{b}{b_1^{v_1} b_2^{v_2} \dots b_s^{v_s}} = 1,1,1 \dots 1;\ \frac{b_{s+1}}{b_1^{q_1} b_2^{q_2} \dots b_s^{q_s}}, \frac{b_{s+2}}{b_1^{r_1} b_2^{r_2} \dots b_s^{r_s}} \dots \frac{b_n}{b_1^{u_1} b_2^{u_2} \dots b_s^{u_s}} \quad \textbf{(1. 43)}$$

With $\frac{b}{b_1^{v_1} b_2^{v_2} \dots b_s^{v_s}}$ the dependent variable and denoted as Π, we then get

$$\Pi_1 = \frac{b_{s+1}}{b_1^{q_1} b_2^{q_2} \dots b_s^{q_s}} \text{ and } \Pi_2 = \frac{b_{s+2}}{b_1^{r_1} b_2^{r_2} \dots b_s^{r_s}} \text{ and } \Pi_{n-s} = \frac{b_n}{b_1^{u_1} b_2^{u_2} \dots b_s^{u_s}} \quad \textbf{(1. 44)}$$

Then in general terms Π can be represented by $\Pi = f(\Pi_1, \Pi_2, \dots \Pi_{n-s})$ where the variables $\Pi_1, \Pi_2, \dots \Pi_{n-s}$ are mutually independent and are dimensionless numbers. This relationship has also effectively reduced the number of variables in a problem by the value s.

A physical object, phenomena, or problem can be defined by its dimension. As an example the motion of a particle can be described by the dimension velocity. The value associated with velocity is typically in terms of its units, ft./sec. km/h etc. These are derived from the fundamental dimensions of length (L) and time (T). The third fundamental dimension is mass (M). A unit value is used to compare dimensions that are the same.

An example of how the ∏-Theorem can be applied to indentation is the examination of a bulk volume that exhibits the properties of a power law work hardening material [104-108] under a conical indentation. This type of material can undergo both elastic and plastic deformation. The complete stress-strain relationship is shown as:

$$\sigma = E\varepsilon \text{ for } \varepsilon \leq \frac{\sigma_y}{E} \quad \textbf{(1. 45)}$$

and

$$\sigma = K\varepsilon^n \text{ for } \varepsilon \geq \frac{\sigma_y}{E} \quad \textbf{(1. 46)}$$

where σ_y is the yield stress of the material at initial yielding. The variable n is the work hardening exponent [107] and is unit-less. For metals n has a value that ranges between 0.1 and 0.5 [108]. E is the elastic modulus and K is the strength coefficient. Both E and K have the same units (force per unit area). In examining the above equations, continuity requires that:

$$K = \sigma_y \left(\frac{E}{\sigma_y}\right)^n \qquad \textbf{(1. 47)}$$

If n=0 we have a perfectly plastic condition, which can be represented by the stress strain curve in Figure 1-8a.

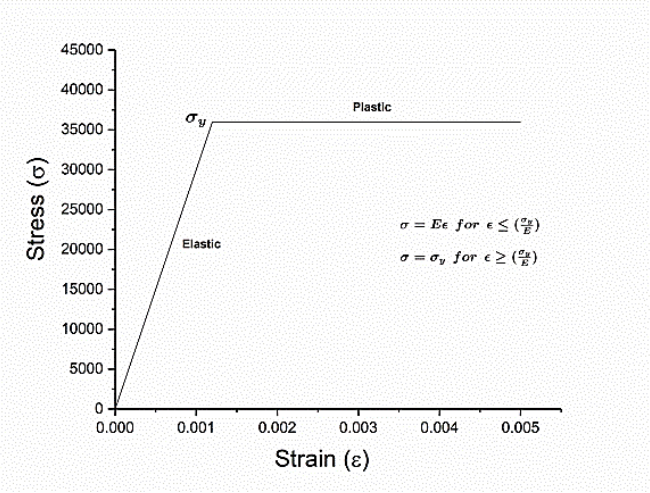

(a)

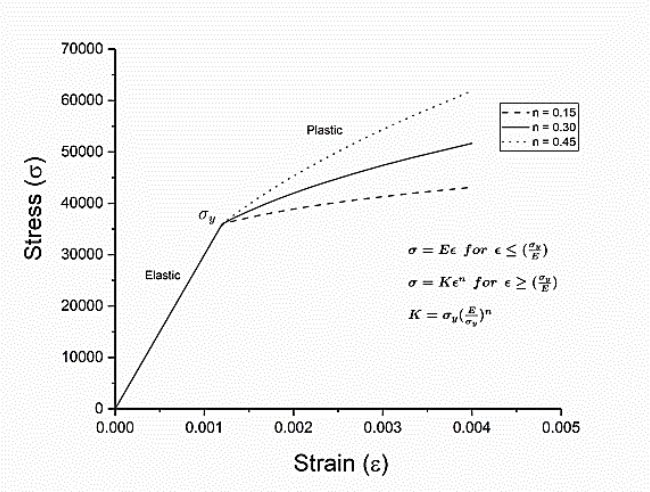

(b)

Figure 1-8 Plot of Stress, psi and Strain, in./in. (a) Elastic-Perfectly Plastic (b) Three Elastic-Plastic Materials with Work Hardening Coefficients of n=0.15, 0.30, 0.45.

Three elastic-plastic materials with work hardening values of 0.15, 0.3, and 0.45 are shown in Figure 1-8b.

Dimensional Analysis has many practical applications [105, 109-113] and for our example we use Dimensional Analysis and the Pi theorem in order to better understand the mechanics of a conical indentation test. Recall the following terms that make up the power law stress-strain relationship for an isotropic, elasto-plastic material:

$$\sigma, E, \varepsilon, n, \sigma_y$$

These terms play a role in the dimensional analysis and have to be considered in any equations developed for the conical indenter. For the indentation test, load, P, and displacement, δ are recorded and are terms that also must be considered. Finally the geometric properties of the conical indenter need to be represented. This can be done by denoting the angle of the cone by the half angle alpha, α (see Figure 1-7b).

There are other effects that may influence the indentation of a material and therefore potentially play a role in a dimensional analysis, but in general, things

like friction and the material surface condition can be neglected for this particular application. It has also been proven that Poisson's ratio (ν) can also be neglected [85].

With so many terms, it is important to denote what is the dependent and what are the independent variables. One possibility would be to make the indenter force as the dependent variable. It should be noted that other dependent variables could be chosen as well, such as material hardness, or possibly the stress or strain directly underneath the indenter. If the indenter force is chosen as the dependent variable then the mechanical properties, E, ν, n, and σ_y, could be considered independent parameters as well as the indentation displacement, δ. The geometric property for the indenter conical half angle alpha, α, would also be an independent parameter. The general expression then of the indenter force is given as:

$$P = f_{Loading}(E, \nu, \sigma_y, n, \delta, \alpha) \quad \textbf{(1. 48)}$$

The next step in Dimensional Analysis is to designate which terms have independent dimensions. An example would be to choose force per unit area as an independent parameter which would allow either E or σ_y to be considered independent. The length could also be chosen as an independent parameter, which in turn relates to the length dimension, δ, indentation depth. If force per unit area, and in particular the Elastic Modulus (E), and length as it relates to indentation depth (δ), are chosen as governing parameters then all other parameters in Equation (1.48) can be related to these. Then dimensionally for

Equation (1.48), $[\sigma_y]=[E]$, and $P=[E][\delta]^2$ where the brackets denote the dimension of the given parameter, with ν, n, and α dimensionless and can be shown as $[\nu] = [E]^0[\delta]^0$, $[n] = [E]^0[\delta]^0$, $[\alpha] = [E]^0[\delta]^0$. Applying the Pi Theorem in Dimensional Analysis then,

$$\prod_a = \prod_a(\prod_1, \nu, n, \alpha) \quad \textbf{(1. 49)}$$

where $\prod_1 = \frac{\sigma_y}{E}$ and $\prod_a = \frac{P}{E\delta^2}$

Then in terms of the indentation force,

$$P = E\delta^2 \prod_a(\frac{\sigma_y}{E}, \nu, n, \alpha) \quad \textbf{(1. 50)}$$

An important observation of Equation (1.50) is that the force, P, is directly proportional to the indentation depth squared, δ^2 [62]. Cheng and Cheng showed that this dependence also holds for conical indentation into an elastic perfectly-plastic material [113].

If hardness is a parameter that needs to be understood then the contact depth, δ_c (Figure 1-7b) may be a more important dependent parameter worth examining. The contact depth may be described by the following:

$$\delta_c = g_{Loading}(E, \nu, \sigma_y, n, \delta, \alpha) \quad \textbf{(1. 51)}$$

For contact depth the Pi Theorem can also be shown as,

$$\prod_b = \prod_b(\prod_1, \nu, n, \alpha) \text{ where } \prod_1 = \sigma_y/E \text{ and } \prod_b = \delta_c/\delta \quad \textbf{(1. 52)}$$

Then applying this to equation 1.52 for the contact depth we get,

$$\delta_c = \delta \prod_b(\frac{\sigma_y}{E}, \nu, n, \alpha) \quad \textbf{(1. 53)}$$

As seen from Eq. 1.53 the contact depth is directly proportional to the maximum depth. Knowing that the hardness of the material is represented by, Force and inversely proportional to the projected contact radius, then,

$$H = \frac{P}{\pi a^2} \quad \textbf{(1. 54)}$$

Also noting that $a = \delta_c \, tan \, \alpha$ then,

$$H = \frac{P}{\pi {\delta_c}^2 tan^2 \alpha} \quad \textbf{(1. 55)}$$

Because both P and δ_c are represented using dimensional analysis, hardness can also be represented in the same way.

A similar dimensional analysis can be performed for the unloading cycle of an indentation test. However under unloading conditions, δ_t, the maximum penetration depth (including the piling up or sinking-in of the material being tested) must also be included in the Pi Theorem. In this case,

$$\mathrm{P} = f_{Unloading}(\mathrm{E}, \nu, \sigma_y, n, \delta_t, \delta, \alpha) \quad \textbf{(1. 56)}$$

which can be expressed as,

$$P = E\delta^2 \Pi_\lambda (\frac{\sigma_y}{E}, \frac{\delta}{\delta_t}, \nu, n, \alpha) \quad \textbf{(1. 57)}$$

In the unloading cycle, P is no longer dependent on the indentation squared. There is now a component $\frac{\delta}{\delta_t}$ in the Π_λ function.

1.6 Motivation for this Research

In the early 1900's indentation analysis was an easy and cost effect method for examining the hardness of a material, in particular, metals. From hardness one could deduce the quality of the material produced as well as empirically relate the material hardness to other properties such as yield strength. This was important with the early development and manufacturing of different grades of alloy steels as the industrial boom flourished. It was here as well, where the study of contact and thereby the study of indentation took hold.

Now in the latter part of the 20^{th} century and into the early 21^{st} century new areas of research are once again calling on the use of indentation in order to examine the engineering properties of materials. From the introduction of MEMS, nanomaterials, advanced electronics, and bio-engineering where there is much interest in further examination and modelling of the human bone as well as subjects like the study of enamel of human teeth are now calling on indentation to help us understand the fundamental material properties as was once done in the early 1900's.

However, indentation is a complex, non-linear type of contact problem. While studied extensively over the last one hundred years there has been great difficulty in analytically solving this type of problem and only the very basic types of indentation problems have been solved. Hertz, Brinell, Tabor, Sneddon, Mindlin,

and Johnson are a few of the researchers that have successfully been able to do so. A viable alternative then was to study indentation empirically. Years ago this would have meant undertaking the elaborate process of setting up and then performing multiple indentation experiments, recording measured load and displacement, and then carefully examining the indented surface area after the indenter was retracted. With this data a correlation would then be made to the mechanical properties we wish to study such as hardness. However this testing could turn out to be quite costly and time consuming. Luckily, an alternate method to performing these indentation tests was introduced in the latter part of the 20 century in the form of simulations and in particular in the use of the Finite Element Method (FEM). By using finite element analysis, generating large amounts of data could be done efficiently and relatively quickly. It is now commonly used and forms the basis for the research presented in this thesis.

There have been tremendous advances in the specific area of indentation of elastic films on substrates. This is of particular interest to the electronics industry but other examples also exist of this type of application such as the paint affixed onto a steel car body or an optical coating that has been applied to a pair of reading glasses. For this type of problem we are able to accurately simulate the interaction between indenter, film, and substrate by using FEM.

For indentation into multi-layered materials it was generally felt that testing should be done at shallow depths in order to remove any effect from the substrate [58, 59]. Unfortunately, indentation at shallow depths introduces other harmful effects such as an enhanced strain gradient under the indenter which becomes more prominent at these shallower depths, as well as localized surface interaction that is dependent on the surface roughness of the film. These issues tend to complicate taking data and potentially cause errors in a shallow indentation test. An alternative method to this would be to carefully remove the film from the substrate and then place it into a tensile testing machine and perform a standard tensile test [114]. Two other methods that could be used in order to extract film properties is the bulge test [115, 116] and the cantilever beam test [117]. But at small scales handling and placement as well as the accuracy of the test is problematic. Another possibility is to use indentation at moderate depths where the substrate actually affects the load-data generated. Under these circumstances it is possible to then learn about the properties of the substrate as well. Therefore the primary focus of this research, and the basis of this thesis, is to extend the level of knowledge of the penetration of a spherical indenter into a film substrate system to moderate depth. Through the innovation of invoking the non-self-similarity characteristics of a spherical indenter, a unique pair of relationships shall be developed utilizing a single indentation test. Then a determination can be made for two unknown material properties of either the film or the substrate, especially and most importantly the mechanical properties of the substrate.

An in-depth study by Kurapati, Lu, and Yang [118] examined the load-displacement relationship for a film on substrate composite material under a spherical indentation test. The authors proposed a unique power law relationship that allowed for the direct solution of the film elastic modulus, but only if the substrate modulus was known a priori along with other restrictions. However, what if the substrate modulus was not known? What if the substrate modulus was known but the film thickness was unknown? Under these conditions it appears to this author's best knowledge there is no identifiable literature that addresses such a problem. The following research will attempt to fill this void.

In Chapter 2 a different method of measuring the mechanical properties of a film affixed to a substrate will be proposed. In particular we will show that in pushing a spherical indenter into an elastic film and substrate to a moderate depth can yield interesting mechanical properties of both the film and substrate while also reducing problematic surface effects or strain-gradient effects that may be present from a shallow indentation. An examination will be done on a broad spectrum of values of material properties, incorporating Dimensional Analysis and Similarity in order to simplify the problem. Through Dimensional Analysis we will be able to create an Elastic Modulus Ratio (EMR) which will relate the film elastic modulus to the substrate modulus by the non-dimensional ratio E_f/E_s. This will simplify and reduce the number of variables needed for solution. For the model

system of an elastic film deposited on an elastic substrate, we will establish the general approach of spherical indentation, focusing on the substrate property determination. The general approach is depicted as a flow chart shown in Figure 1-9. Indentation data is taken from different indentation depths, which reflects different degrees of film and substrate interaction. An effective reverse analysis algorithm is established such that, from an indentation test if either the film modulus or film thickness is known, the other variable can be determined along with the substrate modulus. Error sensitivity of the proposed formulation will then be analyzed in a systematic way.

Chapter 3 will examine a problem typical in today's manufacturing world; an elastic film affixed to a substrate, with the film under an equi-biaxial stress state that is independent from the substrate. A method will be proposed for the solution of both the mechanical properties of the substrate as well as the induced stress in the film. It is the goal of this chapter to develop the role that the prestress of the film plays on a two-layer composite. We establish through spherical indentation a framework to characterize the material properties of the substrate and film as well as a method to determine the prestress of the film. The general approach is depicted as a flow chart shown in Figure 1-10. It is proposed that through an initial forward analysis a set of equations can be developed. From a single spherical indentation test, the measurement of the indentation force at two prescribed depths can be made, and with this data two relationships are developed

from the forward analysis where the material properties of both the film and substrate as well as the film prestress can be determined. A generalized systematic error sensitivity analysis of this formulation is also performed.

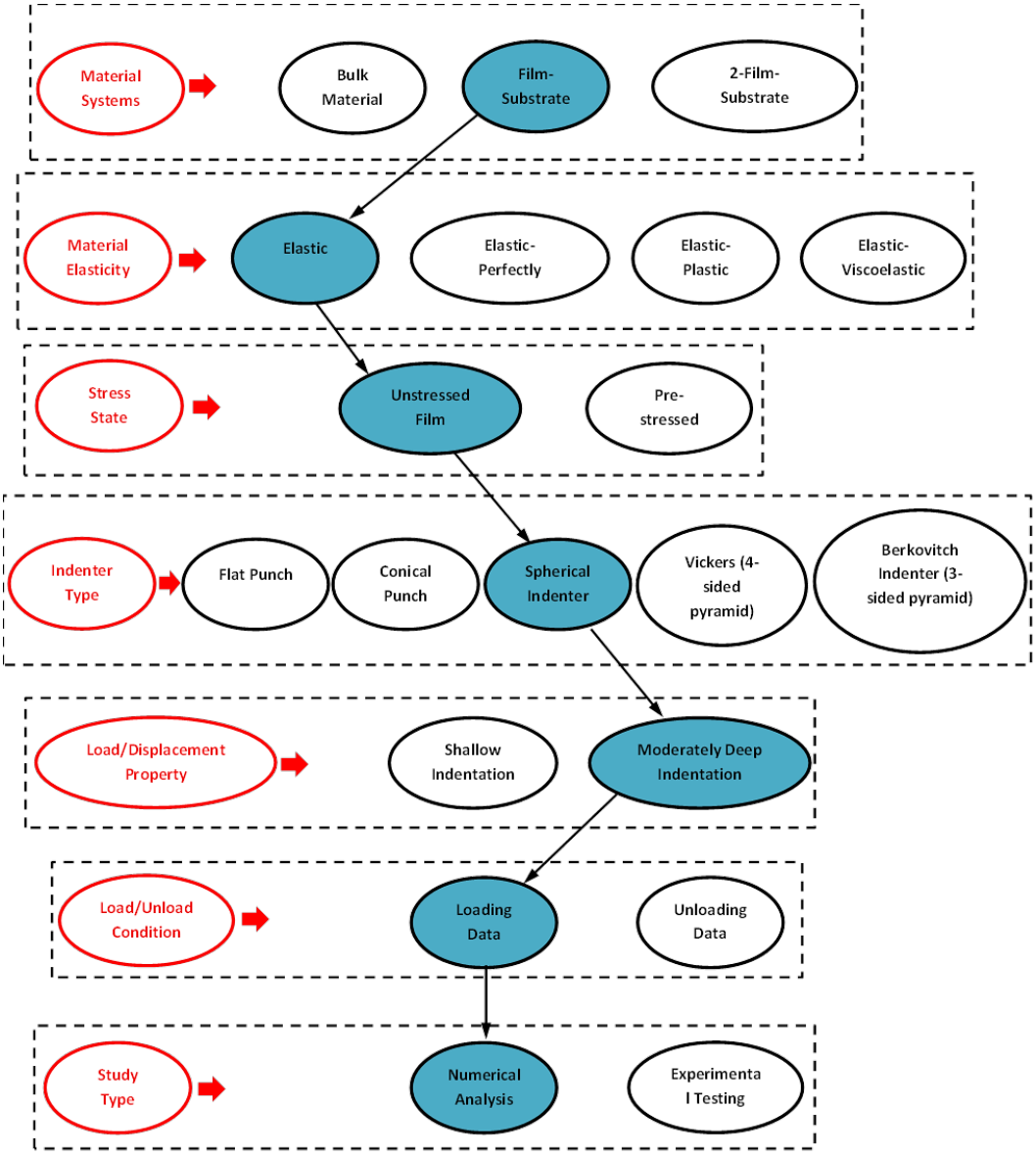

Figure 1-9 Chapter 2 Indentation analysis decision tree.

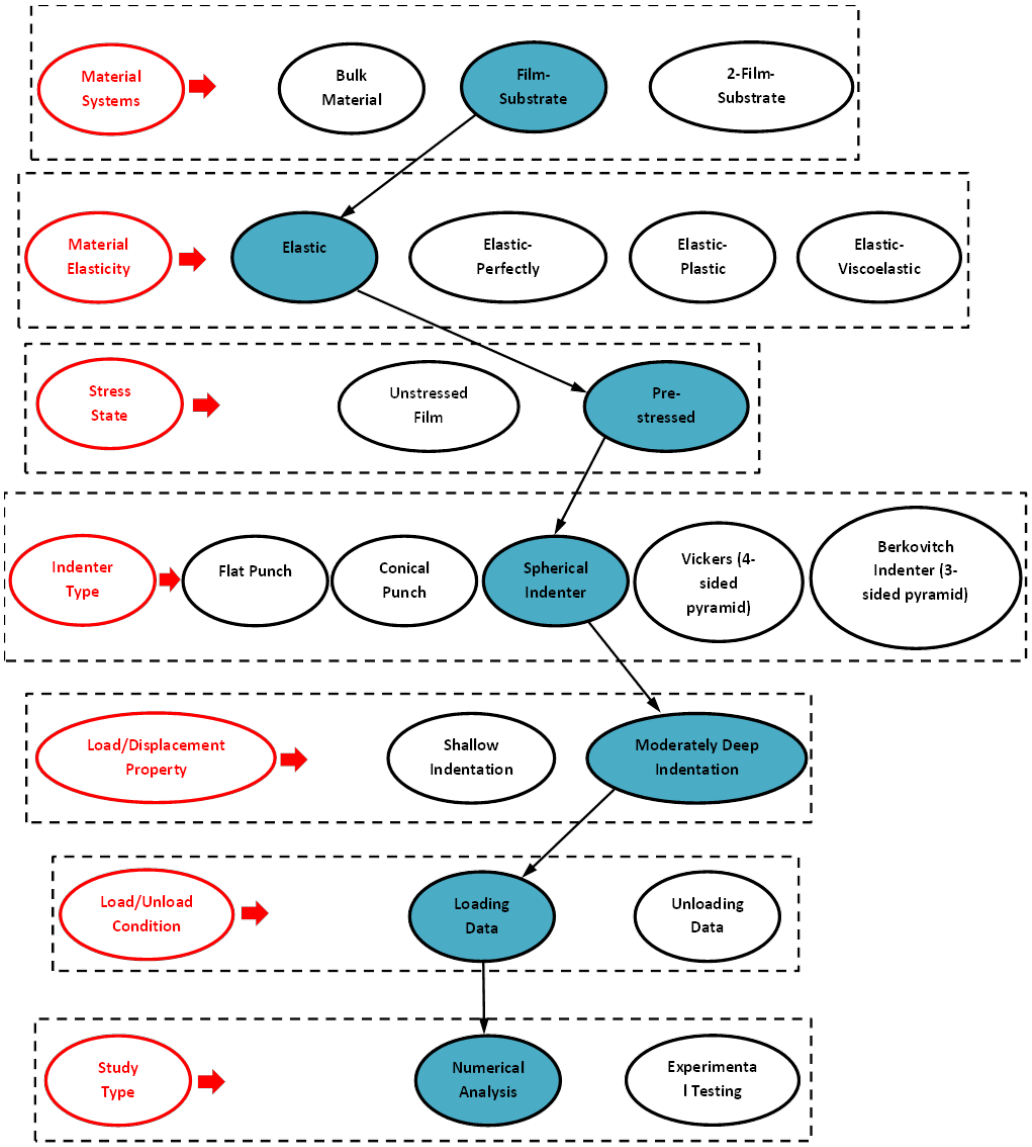

Figure 1-10 Chapter 3 Indentation analysis decision tree.

In Chapter 4 a further examination of the film on substrate problem will be performed but instead of limiting the analysis to a single film on a substrate, we will deduce the properties of the film and an intermediate layer of material that is

part of a multilayer system. This type of problem can be found in the optical engineering field where multiple coatings are affixed to a base material, such as plastic or glass. We may also find this type of application in the automobile industry where multiple layers of paint may be applied to an automobile.

Another practical application of how indentation may help increase the understanding of nature is in the 3-layered base-membrane-algae interaction of a reverse osmosis water filtration system. In this chapter we will perform a set of simulations that specifically examines this three layered system, in particular film (algae) thickness and film (algae) material properties, such as elastic modulus while at the same time embracing the effects from the substrate (polyamide) and sub-base (polysulfone) and their relationship to the film. It is the goal therefore in this chapter to establish the framework and understanding of indenting a film (algae) on a substrate (polyamide) and sub-base material (polysulfone), while varying the film to substrate elastic modulus ratio and also varying the film thickness. This analysis will be performed using spherical indentation, which in going to moderate indentation depths should prevent penetrating damage to the film while providing a unique solution to the proposed problem. The general approach is depicted as a flow chart shown in Figure 1-11.

Chapter 5 will conclude this work by summarizing the research performed in two and 3-layered composite systems undergoing contact and indentation, utilizing

finite element simulations and invoking Dimensional Analysis in order to reduce the number of variables required for solution. As part of this chapter a brief discussion of future work will be proposed that can extend this research into new areas of study and which are also of particular interest to the author.

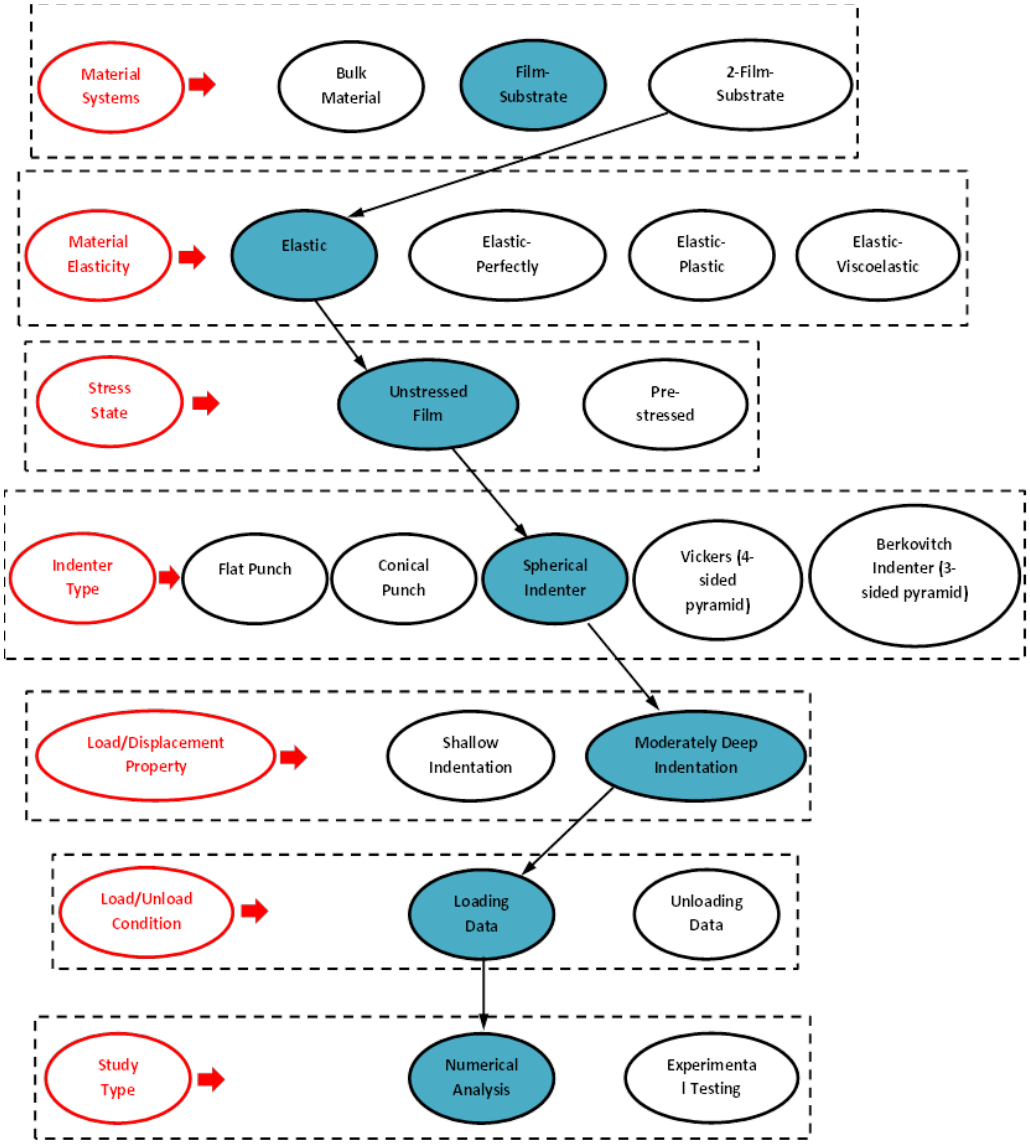

Figure 1-11 Chapter 4 Indentation analysis decision tree.

2 Spherical indentation on an elastic coating and substrate system

2.1 Introduction and Motivation

Thin film/substrate systems play important roles in almost every aspect of engineering. In microelectronics, one or more layers of thin films (metallic, semiconductor, or dielectric) are deposited onto a substrate of another material (typically Si); in biomedical engineering, skin acts as a protective and sensing layer above the tissue substrate. In optical engineering, precision eyeglass, camera, and telescope lenses can often be covered with a scratch resistant coating, or an ultraviolet coating treatment, or an antireflective coating, all of which directly affects the quality of the optical system. In power engineering, photovoltaic film-on-substrate materials are becoming one of the emerging alternative resources of clean energy; and in almost every consumer product, paint not only enhances appearance but also protects the system from oxidation, corrosion, or wear, etc. Note that in these illustrative examples, a fully functional system requires the film to stay on top of, and affixed to the substrate. Thus an evaluation of the physical properties of the substrate often requires the presence of the film/coating.

When it comes to the evaluation of the mechanical integrity of the system, both film and substrate properties are important. More specific examples can also be

found in mechanical and civil engineering, including the cladding of façade/roof materials, polyurethane (waterproof) coating of a steel structure, and thermal barrier coating on a turbine blade. In these cases, the cladded facade, coated roofing material, waterproof coating, and thermal barrier coating, as well as their substrates (often metal-based), face deterioration and wear during service. The first step of evaluating the mechanical integrity is to measure the mechanical characteristics of the coating and substrate, such as elastic properties, plastic properties, fracture toughness, etc. During the conventional inspection of a turbine engine for example, one would have to break the blade in order to expose the cross-section, such that the substrate property and coating thickness/property can be examined. Such a conventional process is quite inconvenient and expensive. It may be more desirable to develop an in-situ field test without having to remove the coating from its substrate, enabling the measurement of both the coating thickness/property and substrate property.

Among various techniques, micro and nanoindentation is arguably the simplest approach for measuring the mechanical properties of small material structures including thin films [53, 119]. It involves minimum sample preparation and can be carried out without removing the film from its substrate. In an indentation test, a diamond (or nearly rigid) indenter is pressed into a film/substrate composite material (Fig. 2-1) and the indentation load (P) and indentation depth (δ) are continuously measured with high accuracy.

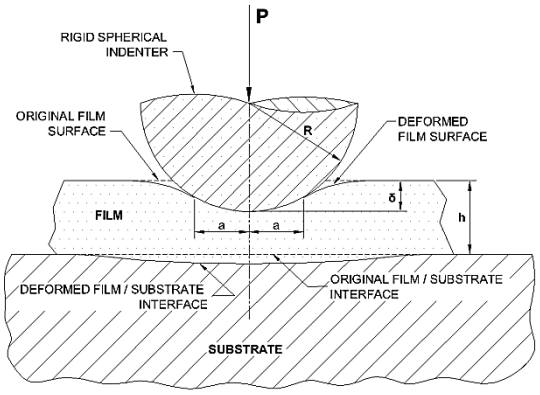

Figure 2-1 Schematic of spherical indentation on a homogeneous, isotropic film attached to a homogeneous, isotropic substrate.

If the system is elastic, the loading and unloading curves coincide. Due to the complicated stress and strain fields resulting from the finite deformation and nonlinear contact [120, 121], the $P-\delta$ curve is implicitly related with the film and substrate properties as well as the material/system structure (e.g. the presence of substrate in a film/substrate system). A functional relationship needs to be established such that through a reverse analysis, the most important and essential material parameters of the system may be derived from the experimental data [85].

In the vast majority of indentation studies on thin film/substrate systems, the focus was on determining the mechanical properties of the film [37, 85, 122, 123].

In this regard, the conventional approach assumes that the contact depth should be less than 10-20% of the film thickness (*h*) [59], such that the substrate effect may be avoided and the measured indentation response ($P-\delta$ curve) will be related only to the film [85]. Such an assumption, however, is not true in some cases where the substrate effect is not negligible at very shallow indentation [119]. Besides, there are many experimental issues that potentially generate measurement errors at very low indentation depths [124, 125], such as indenter tip-film surface adhesion, specimen surface roughness, indenter tip bluntness, and strain gradient effects, among others. These effects make it difficult to accurately measure $P-\delta$ curves and/or obtain intrinsic film properties. An alternative approach to circumvent these problems is to make δ moderately deep and to explore the film properties based on an understanding of the substrate effect, using well-developed continuum mechanics [119, 126, 127]. Once the substrate effect is subtracted off from the indentation measurement, intrinsic film properties may be obtained providing results that agree well with experiments [127]. The moderately deep indentation test on film is also shown to produce a unique solution to the indentation measurement [128, 129].

However, in many technologically significant systems, the substrate property is equally important and oftentimes the substrate is beneath a protective layer that cannot be removed. For instance, consider the tissue below the skin, the turbine blade below a thermal barrier coating, the lens glass beneath the antireflective

coating, and the material below a protective layer of paint. To take advantage of indentation, an in-situ test on these systems requires that the indentation test be directly carried out on the top coat with the goal of extracting the substrate properties from the indentation response (which is a mixture of both film and substrate properties).

To effectively do so, indentation must be performed at a moderate depth such that the substrate effect is significant. Such a technique also allows for good signal to noise resolution and will reduce the effects inherent with shallow testing. At different indentation depths, the variation in this substrate effect allows for the determination of substrate and other system properties. As a first step of such an approach, in this paper, we focus on the simplest model system of an elastic film deposited on a semi-infinite elastic substrate (since we only focus on elastic properties in this paper, in what follows, the material property or mechanical property refers to the elastic modulus unless otherwise noted); such an assumption is valid, for example, for a skin/tissue system where the stiffness measurement of the tissue can often indicate critical health/disease symptoms. In order to not damage the top coat or cause cracking, a spherical indenter is used. The goal is to first develop a plausible framework for measuring substrate mechanical properties (in the presence of a top coat) and coating thickness or coating elastic properties (where needed) via indentation. Later such a framework can be expanded to more

complex material systems by considering plastic deformation and other types of microstructure/material details.

In what follows, we first present a model and computational method as described in the section; Model and Computational Method. Then, we illustrate the general forward-reverse analysis algorithms using a fixed indenter radius to film thickness ratio of one (R/h=1), for the determination of film and substrate elastic moduli (Formulation for a Fixed Indenter Radius). We then expand the analysis incorporating a variable R/h (General Formulation with Variable Indenter Radius), and propose a set of reverse analysis algorithms to effectively measure the film thickness and/or film/substrate properties from a single spherical indentation test. A comprehensive error sensitivity analysis is also provided in this chapter. The results in this section may be useful for further understanding the substrate effect and utilize the results to measure the substrate properties in the presence of a protective coating. The proposed method may effectively determine the elastic properties of a film/substrate that may not easily be determined otherwise.

2.2 Model and Computation Method: Model

The model under consideration is given in (Fig. 2-1), where a rigid spherical indenter (with radius R) is penetrating a film of uniform thickness (h) deposited on a semi-infinite substrate. The film modulus is E_f and substrate modulus is E_s

(both homogeneous and isotropic); they remain bonded at all times. The Poisson's ratio is defined as ν_f, and ν_s, for both the film and substrate but are usually less important factors during indentation analysis [85]; for most materials the Poisson's ratio can be approximated as 0.3. Among the three key variables, (E_f, E_s, h), we wish to be able to determine any two of them simultaneously from the experimental $P-\delta$ data if the other one is known *a priori*. From dimensional analysis, the indentation load and depth follow the relationship:

$$\frac{P}{E_f \delta^2} = \Pi\left(\frac{E_f}{E_s}, \frac{R}{h}, \frac{\delta}{h}\right) \quad \textbf{(2. 1)}$$

where Π is a dimensionless function that can be determined by performing extensive finite element analyses (also known as the forward analysis). By reversely solving such an equation (reverse analysis), the desired material properties can be determined.

During loading of a bulk material in a conical indentation test, the normalized indentation loading curvature, $C = P/\delta^2$, is a depth-independent constant for a given material [85]. Because the loading curve is quadratic, only one material parameter can be determined at a time for an elastic bulk material when sharp indentation is used. However, for a thin film deposited on a different substrate material, the indentation stress field varies with respect to the substrate effect, and the normalized loading curve is not a constant during penetration [126, 127, 130], and the similar situation holds for spherical indentation as well [126, 128].

Therefore, the loading curvature is varying with indentation depth during spherical indentation on a film/substrate system. In order to take advantage of the substrate effect so as to measure the substrate property, in this paper, the normalized loading curvatures are examined at $\delta_1=h/2$ and $\delta_2=h/4$. These two prescribed depths are chosen such that (1) δ_2 is sufficiently large such that substrate effects can be invoked, and the aforementioned experimental noise at very small depth is absent; (2) δ_1 is not too deep otherwise delamination may occur in a practical experiment; (3) within a large range of material parameters investigated in this study, δ_1 and δ_2 are sufficiently different such that the film and substrate effects are distinct at these two depths, yielding two independent dimensionless functions f_1 and f_2:

$$\frac{P_1}{E_f\delta_1^2} = f_1\left(\frac{E_f}{E_s},\frac{R}{h}\right) \qquad \delta_1=h/2 \qquad \textbf{(2.2)}$$

$$\frac{P_2}{E_f\delta_2^2} = f_2\left(\frac{E_f}{E_s},\frac{R}{h}\right) \qquad \delta_2=h/4 \qquad \textbf{(2.3)}$$

The independent film and substrate effects at these two depths enable us to determine two unknown parameters among E_f, E_s, and h. Note that during an experiment the maximum indentation depth does not have to be exactly half of the film thickness, as long as it is sufficiently deep (and at least half of the film thickness).

2.3 Model and Computation Method: Numerical analysis

The formulation of contact finite element analysis is described in a number of papers by Taylor, Sackman, Hughes, et. al. [131-133] . This research was based on the impact-contact problem associated with the study of topics related to brain trauma for example. Their research examined compressible, near-incompressible, and incompressible bodies. Elements were adopted to fit both large motion/small strain (head injury) and large elastic strain (collisions and impact with materials like foam pads). The constitutive equations developed in this work are the basis for present day contact problems in common FEA codes such as ABAQUS [134].

The forward analysis was performed for 27 different elastic modulus ratios (EMR, E_f/E_s), ranging from 0.04 to 25.00; in addition, R/h was varied from 0.5 to 3.0. For each combination, a numerical indentation experiment was performed using the finite element method (FEM) with software ABAQUS [134]. The indenter was taken to be rigid and frictionless contact was assumed (friction is also a minor factor during indentation analysis [85, 135] and lubrication may be applied during an experiment). The model as shown in (Fig. 2-2) was an axisymmetric solid with a 100 mm radius prescribing one boundary and 100 mm height the other; the substrate dimension is much larger than the maximum indentation depth, thus being able to simulate the indentation of a film on a semi-infinite substrate. The bottom of the model was simply supported. Eight-node bi-quadratic continuum elements with reduced integration were used for both the film and substrate. An

extensive study was performed in order to optimize the model and mesh. The final mesh used in these simulations (for both forward and reverse analyses) contained approximately 7,000 elements with 30,000 corresponding nodes.

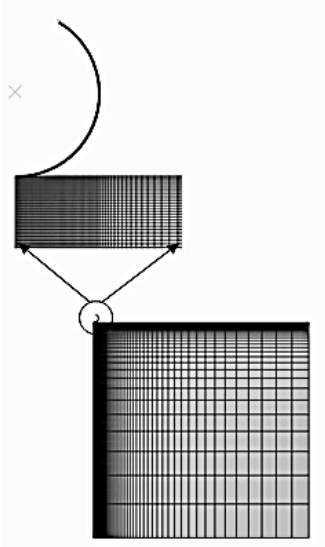

Figure 2-2 Axisymmetric FE Model of a rigid indenter in contact with an isotropic film attached to a homogeneous, isotropic substrate. The model is made up of 6,960 elements with 28,193 nodes.

2.4 Formulation for a Fixed Indenter Radius: Forward analysis

For $R/h=1$, representative results of the normalized load-displacement (P-δ) curves are given in (Fig. 2-3). Note that here the load is normalized by $E_f h^2$ instead of $E_f \delta^2$ in order to more clearly reveal the shapes of the P-δ curves. The indentation load varies with depth nonlinearly in part due to the substrate effect and in part due to the spherical indenter geometry. As δ increases, a stiff substrate

tends to enhance the loading curvature whereas the spherical constraint tends to decrease the curvature of the *P-δ* curve [128]. When E_f/E_s gets larger than about 25, indentation is analogous and approaches the limit of plate bending where the *P-δ* relationship takes a linear form. When E_f/E_s is smaller than about 0.02, the other limit (film on a rigid substrate) is approached.

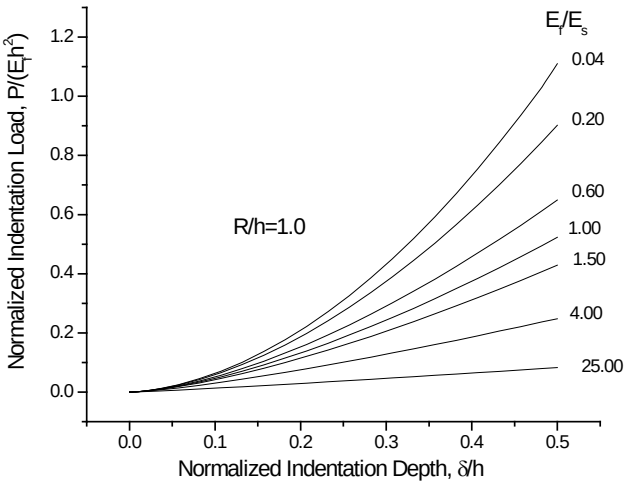

Figure 2-3 Normalized indentation load - penetration depth for various Elastic Modulus ratios (EMR), with *R/h*=1.0.

When E_f/E_s = 1.0 in (Fig. 2-3), the problem reduces to that of Hertzian contact between a rigid sphere and a semi-infinite elastic body. The comparison with the Hertzian solution [136] in (Fig. 2-4) shows good agreement (the small difference is due to the fact that the Hertzian solution is only valid at small deformation whereas the strain at δ/R = 0.5 is quite large).

By taking data from $\delta_1 = h/2$ and $\delta_2 = h/4$, the relationships between the normalized indentation load and EMR were obtained from FEM simulations and shown as symbols in (Fig. 2-5). The following relationships can be fitted (which are shown as lines in Fig. 2-5) to the data generated:

$$\frac{P_i}{E_f \delta_i^2} = A_i \left(\frac{E_f}{E_s} - B_i\right)^{C_i} \quad \textbf{(2.4)}$$

where i=1 and 2 with the right hand side of Eq. (2.4) representing the functional forms f_1 and f_2 in Eqs. (2.2) and (2.3), respectively (specified for R/h=1); P_i is the indenter load at δ_i, and A_i, B_i, and C_i are coefficients summarized in Table 2-1.

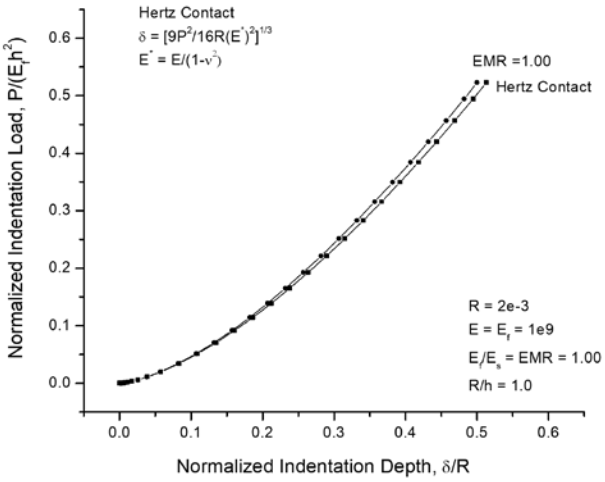

Figure 2-4 Normalized indentation load - penetration depth for Elastic Modulus ratio (EMR=1.0) and Hertz Contact Relationship, with *R/h*=1.0.

Table 2-1 Coefficients with respect to Eq. (2.4)

i	*δ/h*	*A*	*B*	*C*
1	0.50	2.580	-0.392	-0.643
2	0.25	3.887	-0.613	-0.574

The difference between the two curves in Fig. 2-5 shows that the film effect and substrate effect are indeed different at these two prescribed depths, and therefore the two independent functions (i=1,2 in Eq. 2.4) allow for the simultaneous solution of two useful mechanical properties.

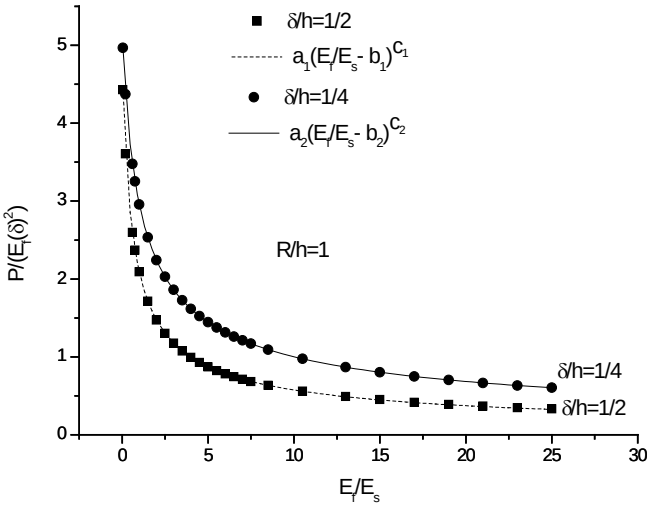

Figure 2-5 Normalized indentation load – elastic modulus ratio (E_f/E_s) relationship with R/h=1

2.5 Formulation for a Fixed Indenter Radius: Reverse analysis for identifying film and substrate properties

We first assume that the film thickness h is known and one could choose a spherical indenter whose radius is exactly equal to h. For an elastic film/substrate system (with identifiable moduli), a numerical indentation test with these input values is performed, such that the indentation parameters δ_1, δ_2, P_1, and P_2 can be measured. In the numerical reverse analysis, different combinations of E_f and E_s are iterated and substituted into Eq. (2.4) such that, the total error of the two equations in Eq. (2.4) is the smallest, at which a pair of film/substrate properties is identified (i.e. effectively measured). In effect the reverse analysis is a method for determining the unknown variables of the problem, using the P-δ data from an actual indentation test (or data from an indentation simulation). Fig. 2-6 presents the results of a set of reverse analyses, where the data is shown as error vectors with respect to our calculated (identified through reverse analysis, tip of arrow) vs. actual elastic moduli (input value, end of arrow). It should be noted that in these numerical examples, the input values were randomly chosen and were not used during the establishment of Eq. (2-4) in the forward analysis.

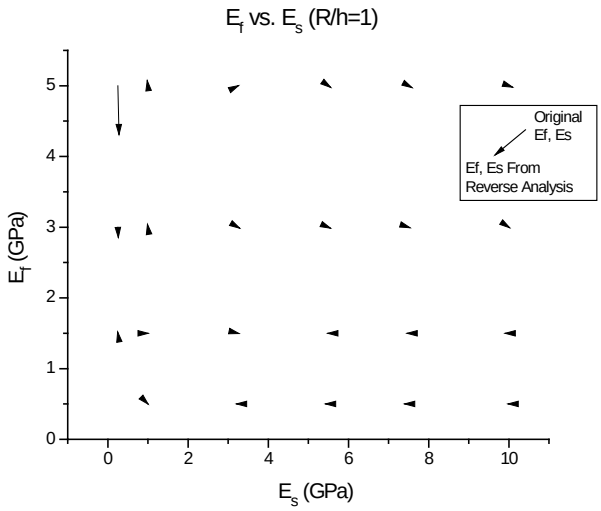

Figure 2-6 Comparison of actual (input) material parameters, elastic moduli of film and substrate, versus material properties determined from reverse analysis with *R/h*=1. The arrow end reflects the value from original data, and the tip denotes the value generated from the reverse analysis.

In Fig. 2-6, within a large parameter space of E_f and E_s, it is readily seen that the proposed method is quite accurate; the error between the identified and original material properties is smaller than 2.0% in most cases, with the only exception being at large EMR values. In fact, according to Fig. 2-5, the slopes of the functions f_1 and f_2 are close when E_f / E_s is large, and that would be prone to numerical error. To improve numerical accuracy of the reverse analysis at large EMR, instead of using E_f / E_s as the variable in Eq. (2.4), the $\log\left(E_f / E_s\right)$ can be employed and the corresponding revision to Fig. 2-5 would have more distinct slopes between the two curves when EMR is large. This method, however, would

sacrifice accuracy at small EMR values and it is only recommended when E_f / E_s >14 or so.

2.6 General Formulation with Variable Indenter Radius: Forward analysis

When *R/h* is allowed to vary, the results of Eqs. (2.2) and (2.3) can be expressed as surfaces. From FEM simulations with varying *R/h*, functions similar to Eq. (2.4) were established. This implies that the coefficients in Eq. (2.4) are thus functions of *R/h*, and fitting of the results from these simulations lead to

$$A_i = a_i + b_i\left(\frac{R}{h}\right) + c_i\left(\frac{R}{h}\right)^2$$

$$B_i = d_i\left(\frac{R}{h} - e_i\right)^{f_i}$$

$$C_i = g_i + h_i\left(\frac{R}{h}\right) + i_i\left(\frac{R}{h}\right)^2 + j_i\left(\frac{R}{h}\right)^3 \qquad \textbf{(2.5)}$$

where *i*=1 and 2 represent functional forms corresponding to $\delta_1 = h/2$ and $\delta_2 = h/4$, respectively. The functional forms were first assumed (based on similarity) and the fitting coefficients a_i through j_i were found by performing extensive FE analyses (varying *R/h* values), and are as tabulated in Table 2-2. Each R/h value established different and distinct terms for A_i, B_i, C_i (*i*=1,2). With this data, plots of each variable were generated and the equations in (2.5) were thus determined [137], which have as their independent variable, *R/h*. When Eq. (2.5) is

substituted into Eq. (2.4) and letting i=1 and 2, the functions f_1 or f_2 are obtained, respectively. With respect to equations (2.2) and (2.3), the data-points and their surface representations are shown in Fig. 2-7(a) and (b).

Table 2-2 Corresponding values for constants *a* through *j* for Eq. (5).

	***i*=1**	***i*=2**
a	1.224846156	1.917634150
b	1.566823980	2.292621556
c	-0.220780141	-0.332342895
d	-0.339258530	-0.569811105
e	0.250993541	0.131676841
f	-0.502857850	-0.536523089
g	-0.443972545	-0.408903108
h	-0.305585325	-0.250474345
i	0.131695246	0.104549024
j	-0.024207613	-0.019555639

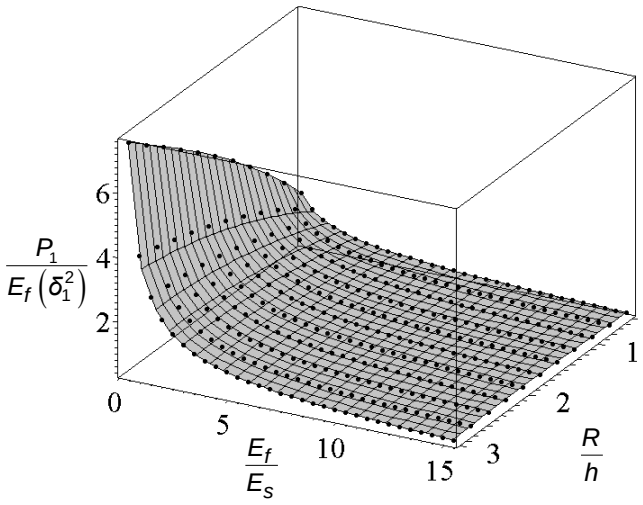

(a)

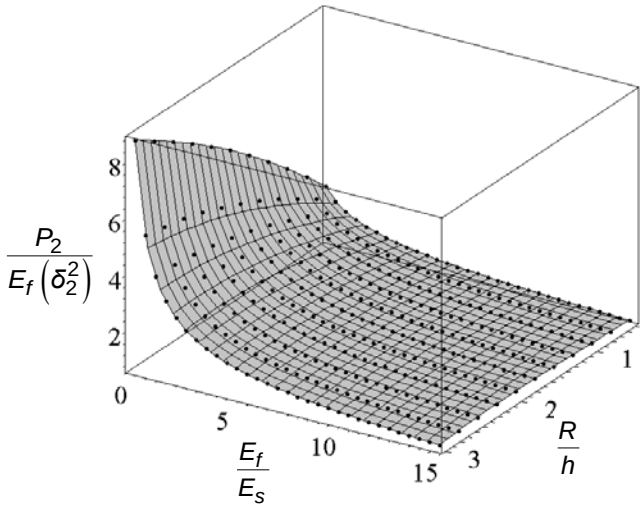

(b)

Figure 2-7(a) and (b) Fitted surface plot of generated data as calculated for varying R/h values with data points (a) (δ_1=h/2) and (b) (δ_2=h/4).

2.7 General Formulation with Variable Indenter Radius: Reverse analysis

Numerical indentation experiments (with spherical indenter of known radius *R*) were carried out on film/substrate systems with specified input parameters E_f, E_s, and *h*; each indentation test performed was sufficiently deep. Based on the relevant indentation parameters measured from the *P*-δ curve, the reverse analysis was carried out to identify two parameters among E_f, E_s, or *h* assuming the other (third) one was known.

First, it was assumed h was known *a priori*. The reverse analysis was then straightforward, similar to the method described above, except now R/h took different values and the corresponding coefficients were different. A simple algorithm was developed in order to determine a solution. Known values for the analysis were h, $\delta_1 = h/2$, $P(\delta_1)$, $\delta_2 = h/4$, $P(\delta_2)$, and R. Using R/h and Eq. (2.5) the variables A_i, B_i, C_i (i=1,2) were determined. Substituting these values into Eq. (2.4) we have two equations for solving the two unknowns E_f and E_s. The solution was found from an iterative procedure. The results are presented in Fig. 2-8a where different and arbitrary values of R and h are explored. There is an excellent match between the identified (measured) film/substrate elastic properties and the input values (true solutions).

In order to solve for the two unknowns; substrate modulus, E_s and film thickness, h, where film modulus, E_f and indenter radius, R are known *a priori*, an indentation test was performed (note that we can exchange E_f for E_s in this analysis). An arbitrary maximum indenter penetration depth, δ_{total} was chosen with the only constraint that it has to be larger than one-half the actual film thickness, $\delta_{total} \geq h_{actual}/2$. Recall from the fitting curves shown in Fig. 2-7 that $\delta_1 = h/2$ and $\delta_2 = h/4$. The force-displacement data was taken over a number of incremental or intermediate steps (k) from 0 to δ_{total}.

The iterative solution procedure began by assuming a small value for E_s. Using this value, along with the penetration depth, $\delta(n)$ and corresponding load, $P(n)$, the value $P(n)/E_f\left[\delta(n)\right]^2$ was determined. This was performed for k steps from n = 1 to k. The value of $f_1(n)\{(E_f/E_s, R/h_1)\}$ was also determined and subtracted from $P(n)/E_f[\delta(n)]^2$. These calculations for each incremental step were performed using a film thickness of $h_1 = 2\delta(n)$. Each data point n was examined to see whether $\left[P(n)/E_f\left[\delta(n)\right]^2 - f_1(n)\left\{E_f/E_s, R/h_1\right\}\right]_1$ was minimized or approached zero. This in turn led to a potential solution for film thickness, h. The same analysis was performed for the function $f_2(n)\left\{\left(E_f/E_s, R/h_2\right)\right\}$ and $\left[P(n)/Ef\left[\delta(n)\right]^2 - f_2(n)\left\{\left(E_f/E_s, R/h_2\right)\right\}\right]_2$ with $h_2 = 4\delta(n)$.

The procedure continued, incrementally increasing the value for E_s, while repeatedly rewinding and reading the P-δ data. The solution was found when the two values of E_s deduced from the approaches based on h_1 and h_2 were equal, and where the corresponding thicknesses converged. Sample results of determining the variables $E_f - h$ and $E_s - h$ from the reverse analysis are presented in Figs. 2-8b and 2-8c, respectively.

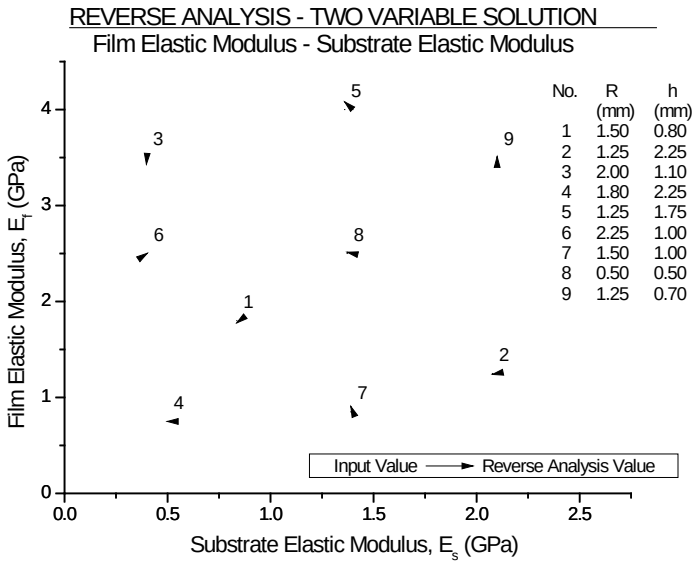
REVERSE ANALYSIS - TWO VARIABLE SOLUTION
Film Elastic Modulus - Substrate Elastic Modulus
Film Elastic Modulus, E_f (GPa)
Substrate Elastic Modulus, E_s (GPa)
No. R (mm) h (mm)
1 1.50 0.80
2 1.25 2.25
3 2.00 1.10
4 1.80 2.25
5 1.25 1.75
6 2.25 1.00
7 1.50 1.00
8 0.50 0.50
9 1.25 0.70
Input Value
Reverse Analysis Value

(a)

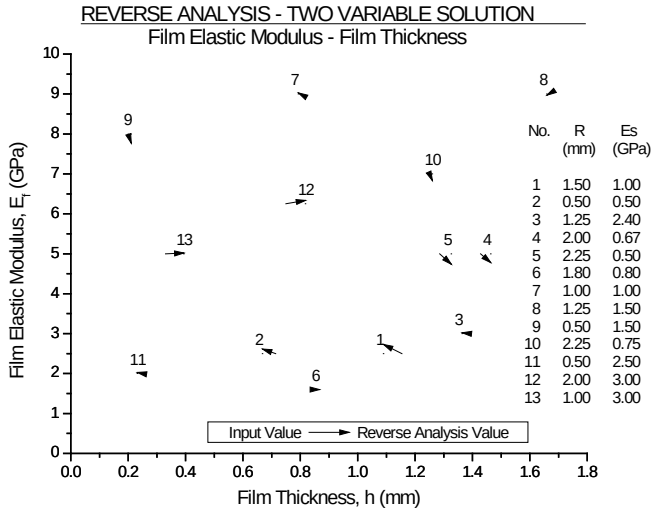
REVERSE ANALYSIS - TWO VARIABLE SOLUTION
Film Elastic Modulus - Film Thickness
Film Elastic Modulus, E_f (GPa)
Film Thickness, h (mm)
No. R (mm) Es (GPa)
1 1.50 1.00
2 0.50 0.50
3 1.25 2.40
4 2.00 0.67
5 2.25 0.50
6 1.80 0.80
7 1.00 1.00
8 1.25 1.50
9 0.50 1.50
10 2.25 0.75
11 0.50 2.50
12 2.00 3.00
13 1.00 3.00
Input Value
Reverse Analysis Value

(b)

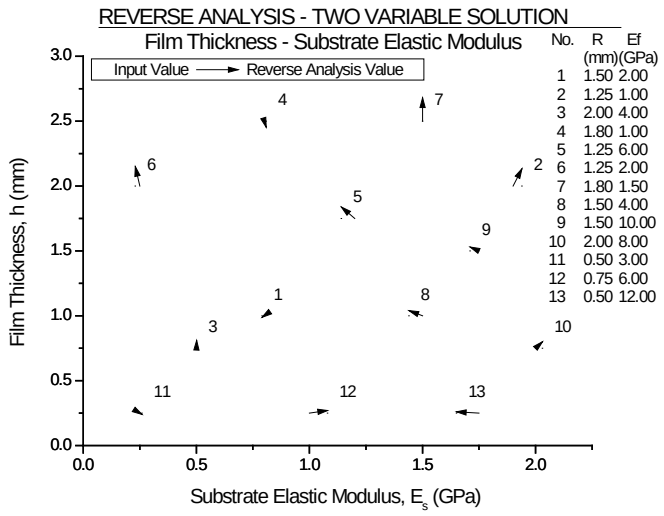

(c)

Figure 2-8 (a) Film and substrate moduli deduced from the reverse analysis (with random film thickness and indenter radius), compared to actual (input) values. (b) Film modulus and film thickness deduced from the reverse analysis (with random indenter radius and substrate modulus), compared to actual (input) values. (c)Film thickness and substrate modulus deduced from the reverse analysis (with random indenter radius and film modulus), compared to actual (input) values.

Again in all reverse analyses examples, the input parameters used were randomly selected and not used in the forward analysis. While there were no clear trends with regard to the reverse analyses, the error for the examined cases was less than 8% -- such small error holds for other material combinations as long as E_f / E_s is less than about 14 (by referring to Fig. 2-5, when E_f / E_s is very large, the slope of the curve tends to approach zero, which leads to larger error sensitivity). Likewise, when $R/h<0.5$ or $R/h>3.0$, convergence starts to become an issue. Therefore, our proposed method is expected to work well when $0.04<E_f/E_s<14.0$

and $0.5 < R/h < 3.0$). Overall the good match between the identified and original values of material/system parameters has validated the effectiveness of the proposed technique.

2.8 General Formulation with Variable Indenter Radius: Reverse analysis of TiN film on silicon substrate

An additional reverse analysis test was performed using indentation data taken from experiments performed by Shiwa, Weppelmann, et al [138] for a spherical indenter pushed into a film/substrate to moderate depth. The 2.7 μm film material tested was Titanium-Nitride (TiN) and the substrate that the film was bonded to was silicon. The modulus of elasticity of the TiN is well known and considered to be 251 GPa while the range of the silicon modulus is 62 GPa to 202 GPa [139-144]. It is not clear, based on the author's published paper, as to the exact value of the elastic modulus of the silicon that was used in the indentation test. Reference was made however in discussion, that the elastic modulus ratio between the film and substrate plays a role in understanding the stresses in and around the contact site. The question of the silicon elastic modulus then warrants the application of the reverse analysis technique as outlined in this chapter to help in understanding this important parameter.

From the generated P-δ input data in Shiwa, Weppelmann, et al, Figure 2-9 was created. Using this data along with the measured loads at $\delta_1 = h/2$ and $\delta_2 = h/4$

under the condition that the film thickness is known a priori, two different sets of reverse analysis calculations utilizing equations 2.4 and 2.5 were made. Note that for when the film thickness is not known, an iterative computer algorithm was developed that converges on an acceptable solution to the problem. The following results were determined from these analyses.

1. If E_f and E_s are the engineering properties that are unknown, the results from the reverse analysis provide respectively, solutions of E_f = 266.7 GPa, and E_s = 76.6 GPa. This corresponds to a calculated error of the film modulus of 6.25%.

2. If instead of E_f and E_s the unknown properties are E_s and h, the film thickness, then again through the reverse analysis we get a substrate modulus of 81.5 GPa and film thickness of 2.76 μm. This leads to an error in calculated film thickness of 2.2%.

However, caution in interpreting these results is important to note. There are a number of potential fabrication and testing variables that could affect the results and possibly introduce errors in the data and therefore the analysis. For example, fabrication of the film on substrate composite material was performed using a filtered arc physical vapor deposition system. The temperature at which the deposition occurred was approximately 350º C. Given the difference in the

coefficients of thermal expansion between the TiN and silicon, with TiN having roughly a factor of 3 higher thermal expansion coefficient as compared to silicon, suggests that after cooling to room temperature there was likely the development of generated internal stresses between the film/substrate system. However the fabrication process temperature of 350C is still lower than some methods of fabrication such as DC reactive magnetron sputtering which may deposit TiN onto silicon at temperatures as high as 600C. At the lower temperature of fabrication (350C), thermal stresses are minimized, though still present.

There are other potential effects to the data recorded from this test that need to be considered. For example, by using the unloading portion of the test data instead of the loading portion, effects such as thermal drift and load oscillation at the start of unloading are present. When the testing reaches its maximum depth and unloading starts to occur, the material has reached a point where the strain from indentation is at its maximum. Also when the change from loading to unloading occur slight oscillations in load can potentially occur. Since the depth for δ_1 and δ_2 fall below the maximum indentation depth of 1400 nm oscillation of the data and drift is not as pronounced; thereby suggesting that using the loading data may be more attractive. It is also well known that the unloading data is more strongly affected by the compliance of the indentation equipment than the loading portion of the data again making the use of the loading curve more attractive in reducing errors in the P-δ data [38]. However there is still an effect from tester compliance

on the indentation loading since the compliance is defined as the deflection of the testing machine divided by the indentation load [145]. This deflection can be attributed to the stiffness of the test frame, indenter shaft, or test sample fixture.

Other potential errors come in the form of cold working of the surface of the film due to specimen preparation. Polishing of the film surface can create residual stresses within the film that must be accounted for. However, in the absence of preparing the surface by polishing the specimen another potential error is introduced that may affect the data. This is created by using an unpolished film, which could have a surface roughness significant enough that it may create friction between the indenter and specimen and also significant abnormalities in the surface may directly affect the accuracy of the measured depth.

Also discussed by Shiwa, Weppelmann, et al in this study, is the observation that there was a linear and completely reversible phase during the indentation test that ranged from a force of 0 to approximately 100 mN. However, beyond this point, through acoustic emission sensing done simultaneously with the indentation test, the authors noted probable cracking in both the film and substrate. This cracking could lessen any buildup of internal stresses in the test material due to the indentation and cause errors in the data taken. Also through the use of a scanning electron microscope indications of some cracks observed beyond 650 mN suggest that some plastic deformation did occur. However, because this plastic

deformation occurs only at higher loads may indicate that elastic behavior dominates (which is typically true for very high strength materials). Because of this dominance, it is proposed that effects due to cracking or plastic deformation may be cancelled out by the dominance of the strongly elastic property of the film. It may very well be that most of the considered errors in the indentation test are self-cancelling because of these material properties and conditions noted which could additionally validate the results obtained by our reverse analysis.

It should also be noted that the use of a diamond spherical indenter instead of a sharp three-sided Berkovich indenter greatly reduces the locally high stress concentrations directly under the indenter, reducing the potential for cracking of the film and substrate during indentation, thereby minimizing potential errors in the data taken. With sharp indenters the risk of creating very high strain gradients directly under the tip is possible. These strain gradients can create dislocations in the test material which in turn increases the effective yield strength, thus changing the hardness and therefore the P-δ data [145].

Using the above analysis and examining the separate calculations for two different unknown properties E_f and E_s and E_s and h, we independently arrived at similar results for the silicon substrate elastic modulus. It can therefore be suggested that through this reverse analysis we can conclude that the silicon has an elastic modulus used in this test approximating a value of 80 GPa.

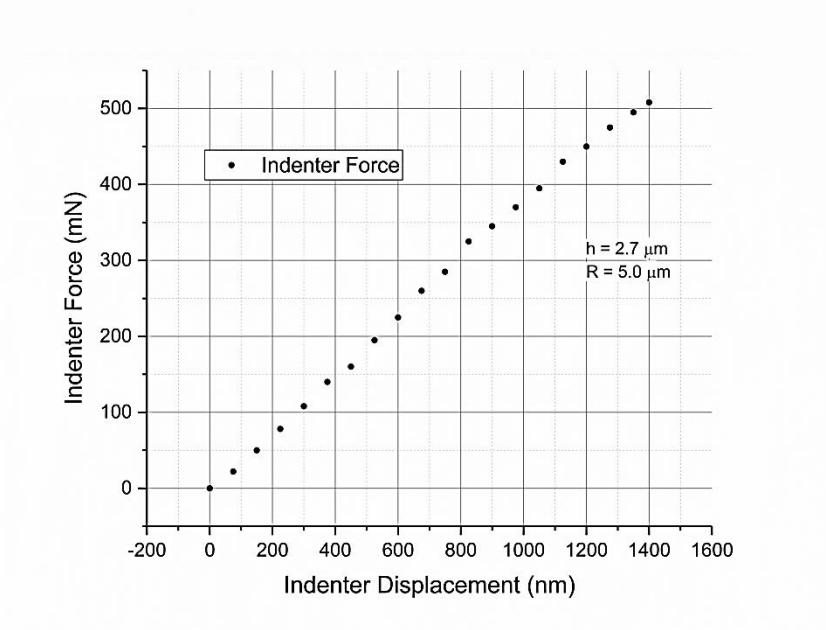

Figure 2-9 Indenter Load (P) – displacement (δ) data for TiN-Silicon film substrate. TiN film thickness (h) is 2.7 μm [138].

2.9 General Formulation with Variable Indenter Radius: Error sensitivity

In the reverse analyses above, the indentation parameters δ_1, δ_2, P_1, and P_2 are measured directly from the numerical indentation experiment, and they are "exact" in this regard. However, during actual lab experiments, the error in measurements of the indentation loads P_1 and P_2 or depths δ_1 and δ_2 is inevitable (e.g. due to calibration errors, misalignment of the sample or indenter, noise, etc.), and thus the error sensitivity of the film/substrate properties determined from the reverse analysis must be investigated.

By differentiating the dimensionless functions Eq. (2.2) and Eq. (2.3) term by term we get:

$$\frac{dP_1}{E_f\delta_1^2}-\frac{P_1dE_f}{E_f^2\delta_1^2}-\frac{2P_1d\delta_1}{E_f\delta_1^3}=\frac{\partial[f_1(\frac{E_f}{E_s},\frac{R}{h})]}{\partial(\frac{E_f}{E_s})}d(\frac{E_f}{E_s})+\frac{\partial[f_1(\frac{E_f}{E_s},\frac{R}{h})]}{\partial(\frac{R}{h})}d(\frac{R}{h}) \qquad \textbf{(2.6)}$$

$$\frac{dP_2}{E_f\delta_2^2}-\frac{P_2dE_f}{E_f^2\delta_2^2}-\frac{2P_2d\delta_2}{E_f\delta_2^3}=\frac{\partial[f_2(\frac{E_f}{E_s},\frac{R}{h})]}{\partial(\frac{E_f}{E_s})}d(\frac{E_f}{E_s})+\frac{\partial[f_2(\frac{E_f}{E_s},\frac{R}{h})]}{\partial(\frac{R}{h})}d(\frac{R}{h}) \qquad \textbf{(2.7)}$$

The above equations can be reorganized, such that the perturbation of material properties, dE_s/E_s, dE_f/E_f, and dh/h, can be expressed as functions of the perturbations of indentation parameters, dP_1/P_1, dP_2/P_2, $d\delta_1/\delta_1$, and $d\delta_2/\delta_2$. Due to the relative simplicity of the functional forms f_1 and f_2 adopted in this study, the solution can be represented in closed-form.

For instance, assume *R* and E_f are known precisely, then their differentiated terms would drop out; $dR\to 0$ and $dE_f\to 0$. In effect this means there is no potential error associated with these terms and after rearranging Eq. (2.6) and Eq. (2.7) the following relationships for dE_s/E_s and dh/h can be shown:

$$\frac{dE_s}{E_s}=\alpha_1\frac{dP_1}{P_1}+\alpha_2\frac{d\delta_1}{\delta_1}+\alpha_3\frac{dP_2}{P_2}+\alpha_4\frac{d\delta_2}{\delta_2} \qquad \textbf{(2.8)}$$

$$\frac{dh}{h} = \beta_1 \frac{dP_1}{P_1} + \beta_2 \frac{d\delta_1}{\delta_1} + \beta_3 \frac{dP_2}{P_2} + \beta_4 \frac{d\delta_2}{\delta_2} \qquad \textbf{(2.9)}$$

where α_j and β_j (*j*=1-4) are *error sensitivity coefficients* and are functions of R/h and E_f / E_s. This will allow for the examination of the effect from differential changes in load and displacement. For example, if all other indentation parameters are measured precisely but only P_2 has a 1% error (perturbation), the resulting perturbation on the measured E_s would be α_3% and the resulting error on the identified *h* would be β_3%. The smaller these error sensitivity coefficients, the less sensitive the algorithm is to certain measurement perturbations. In the above equations, values for α_j and β_j are:

$$\alpha_1 = W\frac{Q_4}{f_2}, \quad \alpha_2 = -2W\frac{Q_4}{f_2}, \quad \alpha_3 = -W\frac{Q_2}{f_1}, \quad \alpha_4 = 2W\frac{Q_2}{f_1}$$

$$\beta_1 = -\frac{h}{r}\left[\frac{f_1}{Q_2} + \frac{Q_1}{Q_2}\frac{E_f}{E_s}\left(\frac{WQ_4}{f_2}\right)\right], \quad \beta_2 = \frac{h}{r}\left[\frac{2f_1}{Q_2} + \frac{Q_1}{Q_2}\frac{E_f}{E_s}\left(\frac{2WQ_4}{f_2}\right)\right],$$

$$\beta_3 = \frac{h}{r}\left[\frac{Q_1}{Q_2}\frac{E_f}{E_s}\left(\frac{WQ_2}{f_1}\right)\right], \quad \beta_4 = -\frac{h}{r}\left[\frac{Q_1}{Q_2}\frac{E_f}{E_s}\left(\frac{2WQ_2}{f_1}\right)\right]$$

where

$$Q_1 = A_1 C_1 \left(\frac{E_f}{E_s} - B_1\right)^{C_1 - 1}$$

$$Q_2 = (\frac{E_f}{E_s} - B_1)^{C_1} \langle b_1 + 2c_1\left(\frac{R}{h}\right) - A_1C_1\frac{\left\{f_1d_1(\frac{R}{h} - e_1)^{f_1-1}\right\}}{\left(\frac{E_f}{E_s} - B_1\right)}$$

$$+ A_1\left[\ln(\frac{E_f}{E_s} - B_1)\right]\left[h_1 + 2i_1\left(\frac{R}{h}\right) + 3j_1\left(\frac{R}{h}\right)^2\right]\rangle$$

$$Q_3 = A_2C_2(\frac{E_f}{E_s} - B_2)^{C_2-1}$$

$$Q_4 = (\frac{E_f}{E_s} - B_2)^{C_2} \langle b_2 + 2c_2\left(\frac{R}{h}\right) - A_2C_2\frac{\left\{f_2d_2(\frac{R}{h} - e_2)^{f_2-1}\right\}}{\left(\frac{E_f}{E_s} - B_2\right)}$$

$$+ A_2\left[\ln(\frac{E_f}{E_s} - B_2)\right]\left[h_2 + 2i_2\left(\frac{R}{h}\right) + 3j_2\left(\frac{R}{h}\right)^2\right]\rangle$$

Coefficients A_i-C_i are shown in Eqs. (2.5) and a_i-h_i values are listed in Table 2-2. Likewise, when solving Eq. (2.6) and Eq. (2.7) with respect to E_f and h (assuming that the substrate modulus, E_s, and R are known):

$$\frac{dE_f}{E_f} = \zeta_1\frac{dP_1}{P_1} + \zeta_2\frac{d\delta_1}{\delta_1} + \zeta_3\frac{dP_2}{P_2} + \zeta_4\frac{d\delta_2}{\delta_2} \quad \textbf{(2.10)}$$

$$\frac{dh}{h} = \omega_1\frac{dP_1}{P_1} + \omega_2\frac{d\delta_1}{\delta_1} + \omega_3\frac{dP_2}{P_2} + \omega_4\frac{d\delta_2}{\delta_2} \quad \textbf{(2.11)}$$

with the corresponding error sensitivity coefficients:

$$\zeta_1 = (X)\left(\frac{Q_4 R}{f_2 h}\right), \quad \zeta_2 = (-2X)\left(\frac{Q_4 R}{f_2 h}\right), \quad \zeta_3 = (-X)\left(\frac{Q_2 R}{f_1 h}\right), \quad \zeta_4 = (2X)\left(\frac{Q_2 R}{f_1 h}\right)$$

$$\omega_1 = (X)\left(1+\frac{Q_3 E_f}{f_2 E_s}\right), \quad \omega_2 = (-2X)\left(1+\frac{Q_3 E_f}{f_2 E_s}\right), \quad \omega_3 = (-X)\left(1+\frac{Q_1 E_f}{f_1 E_s}\right), \quad \omega_4 = (2X)\left(1+\frac{Q_1 E_f}{f_1 E_s}\right)$$

where

$$X = \frac{1}{\left[\left(\frac{Q_4 R}{f_2 h}\right)\left(1+\frac{Q_1 E_f}{f_1 E_s}\right)-\left(\frac{Q_2 R}{f_1 h}\right)\left(1+\frac{Q_3 E_f}{f_2 E_s}\right)\right]}$$ with Q_i (i=1-4) as noted above

In terms of the perturbations of E_f and E_s (assuming that the film thickness and R are known):

$$\frac{dE_f}{E_f} = \eta_1 \frac{dP_1}{P_1} + \eta_2 \frac{d\delta_1}{\delta_1} + \eta_3 \frac{dP_2}{P_2} + \eta_4 \frac{d\delta_2}{\delta_2} \qquad \textbf{(2.12)}$$

$$\frac{dE_s}{E_f} = \varepsilon_1 \frac{dP_1}{P_1} + \varepsilon_2 \frac{d\delta_1}{\delta_1} + \varepsilon_3 \frac{dP_2}{P_2} + \varepsilon_4 \frac{d\delta_2}{\delta_2} \qquad \textbf{(2.13)}$$

with the corresponding error sensitivity coefficients:

$$\eta_1 = \frac{Q_3}{f_2\left(\frac{Q_3}{f_2}-\frac{Q_1}{f_1}\right)}, \quad \eta_2 = \frac{-2Q_3}{f_2\left(\frac{Q_3}{f_2}-\frac{Q_1}{f_1}\right)}, \quad \eta_3 = \frac{-Q_1}{f_1\left(\frac{Q_3}{f_2}-\frac{Q_1}{f_1}\right)}, \quad \eta_4 = \frac{2Q_1}{f_1\left(\frac{Q_3}{f_2}-\frac{Q_1}{f_1}\right)}$$

$$\varepsilon_1 = \frac{\left(\frac{E_s}{E_f}+\frac{Q_3}{f_2}\right)}{\left(\frac{Q_3}{f_2}-\frac{Q_1}{f_1}\right)}, \quad \varepsilon_2 = \frac{-2\left(\frac{E_s}{E_f}+\frac{Q_3}{f_2}\right)}{\left(\frac{Q_3}{f_2}-\frac{Q_1}{f_1}\right)}, \quad \varepsilon_3 = -\frac{\left(\frac{E_s}{E_f}+\frac{Q_1}{f_1}\right)}{\left(\frac{Q_3}{f_2}-\frac{Q_1}{f_1}\right)}, \quad \varepsilon_4 = \frac{2\left(\frac{E_s}{E_f}+\frac{Q_1}{f_1}\right)}{\left(\frac{Q_3}{f_2}-\frac{Q_1}{f_1}\right)}$$

The 24 error sensitivity coefficients can be plotted as functions of R/h and E_f / E_s. We illustrate the results through α_i and β_i, since they correspond to the measurement of substrate modulus and film thickness (and therefore dE_s / E_s and dh / h), which is a new aspect of the present study. Recall that miscalibration and misalignment are likely to cause systematic errors, i.e. in practice we would expect dP_1 / P_1 and dP_2 / P_2 to be of same order of magnitude, and $d\delta_1 / \delta_1$ and $d\delta_2 / \delta_2$ with similarly close values, therefore, in Figs. 2-10 (a) - 2-10 (d), we plot $\alpha_1 + \alpha_3$, $\alpha_2 + \alpha_4$, $\beta_1 + \beta_3$, and $\beta_2 + \beta_4$, respectively, which represent the perturbation of substrate modulus due to force measurement error, the perturbation of substrate modulus due to depth measurement error, the perturbation of film thickness due to force measurement error, and the perturbation of film thickness due to depth measurement error. It can be seen that the error sensitivity is relatively small for most space of R/h and E_f/E_s. However, there is one region where the error sensitivity is high especially when both R/h and E_f / E_s are large (which is consistent with Fig. 2-7). Thus, the measured substrate property and film thickness are more sensitive to perturbations of the indentation parameters if the film is thin and stiff; on the other hand, such an error-sensitive region may be avoided in an experiment by employing different indenter radii. Moreover, it appears that the error sensitivity to indentation depth perturbation $(\alpha_2 + \alpha_4, \beta_2 + \beta_4)$ are higher than that to indentation force

perturbation ($\alpha_1+\alpha_3$, $\beta_1+\beta_3$), and the measurement of film thickness ($\beta_1+\beta_3$, $\beta_2+\beta_4$) is more prone to errors than the measurement of substrate modulus ($\alpha_1+\alpha_3$, $\alpha_2+\alpha_4$).

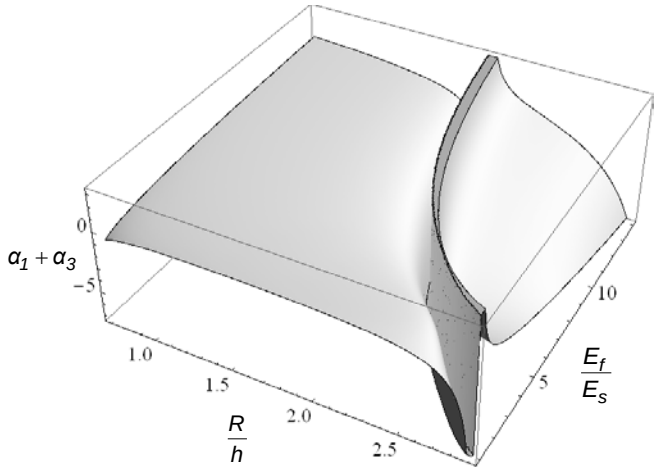

(a)

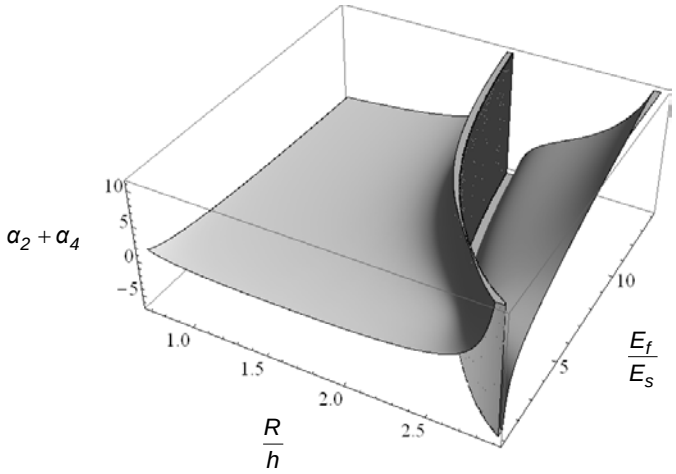

(b)

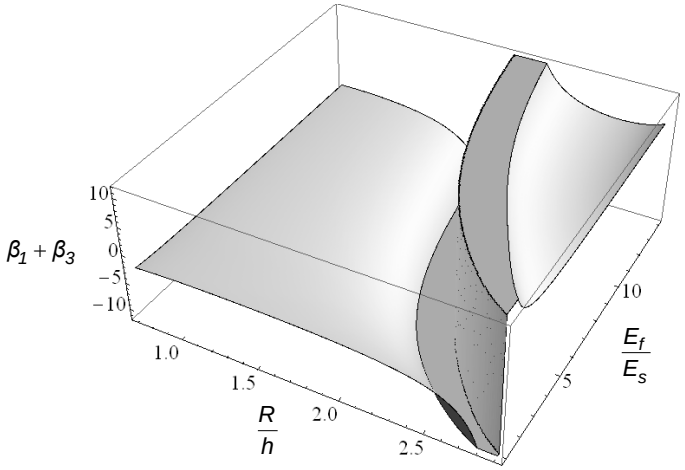

(c)

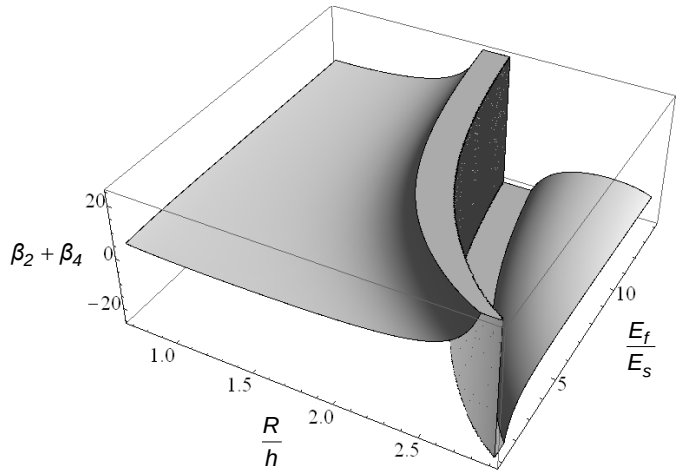

(d)

Figure 2-10 (a)-(d) Combination of coefficients for error sensitivity associated with the perturbations of E_s and h. (a) $\alpha_1 + \alpha_3$, (b) $\alpha_2 + \alpha_4$, (c) $\beta_1 + \beta_3$, and (d) $\beta_2 + \beta_4$.

When the measurement of E_f and h, or the measurement of E_f and E_s are of concern, the error sensitivities are much smaller (the plots are not shown but they

may be easily drawn according to the equations above). For example, the corresponding $\zeta_j + \zeta_{j+2}$ and $\omega_j + \omega_{j+2}$ (j=1,2) are about half of their counterparts of α_i and β_i, although there is also a region (where R/h is close to 2) where the error sensitivity becomes large. Whereas, $\eta_1 + \eta_3 \approx \varepsilon_1 + \varepsilon_3 \approx 1$, and $\eta_2 + \eta_4 \approx \varepsilon_2 + \varepsilon_4 \approx -2$, throughout the entire space of R/h and E_f / E_s explored. This implies that if the film thickness is known precisely, the proposed method has high accuracy and is also quite robust (insensitive to errors). When the film thickness is not known, it would impact the error sensitivity in particular when the substrate property is also unknown.

When two of the three variables are known *a priori*, the third can be estimated with very good accuracy. The errors of E_f and E_s are quite low throughout the range of *R/h* and EMR combinations studied, and they are lower than the values as derived above. However, as before, when *h* is unknown, there is a region on the *R/h*-EMR surface where larger errors may occur. As expected this is predominantly true at high *R/h* and EMR values.

2.10 Chapter Summary

The vast majority of indentation studies on film/substrate systems assume that both the film thickness and substrate properties are known a priori. However this is often not the case in practice especially when the substrate is protected by a

non-removable coating. In this case, the indentation response is a mixture of film/substrate properties and the relevant substrate contributions need to be understood. This is necessary in order to extract the intrinsic substrate properties and/or film thickness and film properties.

For a model system of elastic film on an elastic substrate, a framework has been established to close such a gap. Spherical indentation was used since it is suggested that it may avoid damaging the protective film. The formulation was established incorporating indentation force-depth data at two particular depths, one-half and one-quarter of the film thickness. The substrate effects are distinct at these two depths, allowing the establishment of two independent functions which enables the solution of two parameters among the three variables, film modulus, substrate modulus, and film thickness, if the other one is known. An effective reverse analysis algorithm was established and the identified properties agreed well with the input values used in numerical indentation experiments, which proves its accuracy and effectiveness. In addition, a systematic error sensitivity analysis was carried out, where it was found that the uncertainty of film thickness would contribute the most to the perturbation of measured material parameters, especially when R/h fell within a particular region. Thus, during an experiment, it is suggested to employ an indenter radius R such that R/h is clearly well away from the dangerous zone. Such selection of R can be obtained from iterations during an experiment, that is, several indenter radii can be chosen and the

proposed process is repeated until the determined properties converge. If the film thickness is known, the proposed technique is quite robust and insensitive to measurement errors, regardless of the indenter size one uses.

This analysis was a first step toward the goal of measuring substrate properties in a film/substrate system, using the substrate effect at moderate indentation depths.

3 Examination of Prestressed Coating/substrate Systems Using Spherical Indentation - Determination of Film Prestress, Film Modulus and Substrate Modulus.

3.1 General Introduction and Problem Statement

Film on substrate sandwich materials are commonly found in the electronics, optical, manufactured painted products, transportation and the general building industry [146-148]. In the electronics industry we find electronic circuits embedded onto different types of substrate boards, providing many of today's electronic high-tech products. Another example of this type of engineered system is a multi-layered optical lens. One could find an antireflective coating, or a scratch-resistant coating, or a UV protective coating, or any combination of the three affixed to a typical optical lens. A unique but common film-substrate system is the human body's outer skin system. The body's skin is made up of multiple layers all of which have functional roles in providing a protective layer for the body or providing a mechanism to dissipate heat or releasing moisture from the body. In the automotive, building, and consumer product industry paint provides a protective coating and also may provide an enhanced visual appearance. This

paint is often applied in multiple layers along with an outer layer of wax or surface protection material.

As is often the case the film and substrate each have unique mechanical or physical properties such as thickness and elastic modulus. It is assumed that during any type of normal operation the two materials remain fully bonded and act together to form a well-engineered system. However, in order to try to understand the performance of this system, the material properties of both the film and substrate need to be well understood. And of course over the long term operation of such a system it is important to know how these material and geometric properties may be changing. This is very important in helping to determine the service life of equipment such as turbine blades. A turbine blade might well have a thermal coating applied to it. However, through sustained usage this thermal coating could wear or break off. If this occurs, the normal operation of the turbine blade may be impaired and catastrophic failure may occur. However, as with many operating systems, only destructive methods can be used to determine the present condition of such materials. For the turbine blade, cutting the blade to expose the blade cross section and analyzing it may be the only appropriate way of determining turbine service life. A potential option to cutting the blade is to use an indentation test to determine mechanical properties. It could be done in the lab or possibly in-situ, creating no physical permanent damage to an existing blade, and yet provide the necessary mechanical

information needed to try and forecast continued service life for the turbine. The film does not have to be separated or removed from the base and arguably may be the simplest method to measuring the mechanical properties of small-scale structures, e.g. thin films on elastic substrates [53, 119, 149-152]. The primary advantage in adopting this approach is that it does not require the separation between the film and the substrate base. The indentation test as proposed in this research is conducted with a diamond-tipped spherical indenter, pushed into the film-substrate structure as shown (Fig. 3-1). During the indentation process, the load, P, to push the indenter tip into the surface of a material is measured along with the indentation depth (δ). The stress fields resulted from the large deformation and non-linear contact in the indentation process are relatively complicated. However the P-δ data is able to indirectly relate the elastoplastic properties of the film [121, 153]. Using the P-δ data along with the functional relationship derived in the forward analysis, the material and structural properties can be determined with a reverse analysis [85].

Because common film/substrate systems function in a state where the film is under an equibiaxial stress state, it is the intent of this present research to determine the material/structural properties of both the film and substrate under this stress condition. This stress state can be attributed to the thermal mismatch of the film and substrate either through fabrication or during the normal operation of the system. It can come from the forming process due to heat treatment or

through a peening process of the material. This biaxial stress state can even lead to premature failure of the system [154, 155]. As proposed by Suresh and Giannakopoulos [156] sharp indenters can be used to evaluate the residual stress levels of thin films on elastic substrates as well as bulk materials. However, a drawback to this method is that it requires indentation testing of multiple (and identical) prestressed film/substrate systems. This method also requires an indentation test performed on a reference sample of an identical film/substrate system under zero biaxial stress (unstressed condition). This method using the sharp indentation technique requires multiple tests and comparison, which can be costly and sometimes impractical to achieve.

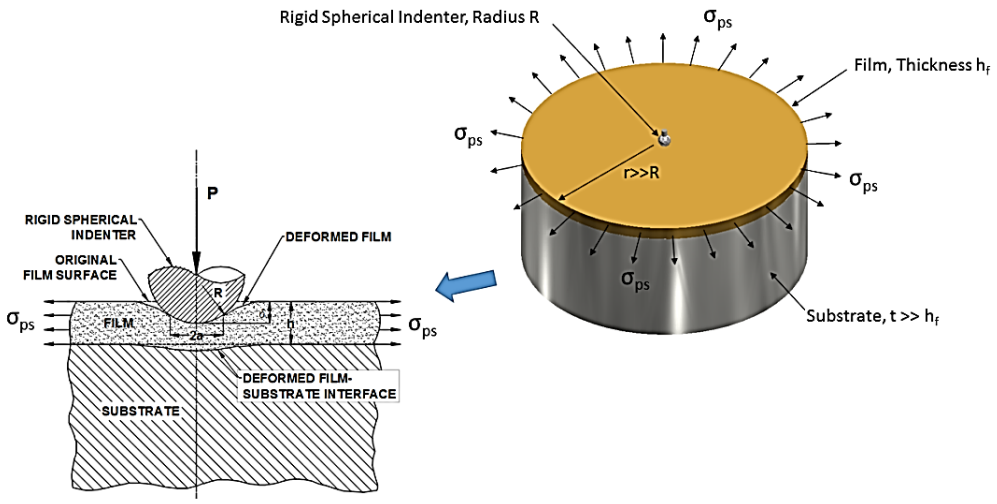

Figure 3-1 Indenter/Film/Substrate Model.

One of the physical characteristics related to the overall performance of a film/substrate composite material is the ability for a system to remain structurally intact. This means typically, that the region between the film and substrate, the bonded surface denoting the demarcation between the two, remain attached and structurally continuous. For example, if a coated turbine blade that, through extreme conditions or aged service length, has the film (protective coating) delaminate from the substrate (blade) it could potentially introduce extremely high temperatures to the turbine blade. The effect of this could be a premature failure of the blade structure, with potentially catastrophic consequences. Hence, the ability to predict the conditions necessary for a film to delaminate from the substrate is a very important necessity in understanding the service life of such a system. The beginning of a crack between the film and substrate typically occurs when the Strain Energy Release Rate (G) exceeds a critical value (G_c).

There are several methods that are used to determine the Strain Energy Release Rate [37]. Mechanical methods seem to be the most appropriate since the testing can be performed on actual fabricated film/substrate systems. These can be further broken up into “strength based” tests or “fracture based” tests. The strength based test, alternately called adhesion strength or bond strength testing is a mechanical test that measures the induced stress from peeling the coating or film off the substrate. The stress measured just prior to the initiation of film-substrate separation is then called the strength of the film-substrate joint.

However, the drawback to performing a peel test is that it is typically only accurate for tough and flexible coatings. In effect then, brittle type coatings do not lend themselves to this type of test.

Fracture mechanics is an alternate form of mechanical testing [122, 123]. This type of testing is used to determine the "fracture toughness" of the film/substrate joint. Types of fracture testing are the Double Cantilever Beam test method, Four Point Bend Test, Brazil-Nut Test and indentation testing. All of these tests with the exception of indentation testing requires fairly elaborate preparation and/or test set-up in order to provide sound, reasonably accurate test results. In addition, presently all testing, including some types of indentation testing requires an elaborate examination of the cracked joint.

However, indentation does provide a straightforward and easy way to perform a film/substrate bond test, requiring minimal preparation and straightforward data taking in the form of recording indenter load and displacement values [124, 157]. In addition, Drory and Hutchinson [158] developed a relationship for the Strain Energy Release Rate:

$$G = \frac{\left(1 - {v_f}^2\right)h}{2E_f}\ \sigma_r(R^*)^2$$

where v_f is Poisson's Ratio of the film, E_f is the elastic modulus of the film, R* is the circular interface crack, and h is the film thickness. Also, $\sigma_r(R) = \sigma_0 +$

$\sigma_r^I(R^*)$, with σ_0 representing the residual stress in the film and $\sigma_r^I(R^*)$ representing the stress due to indentation. As stated by Evans and Hutchinson [154] and Hu and Evans [159] residual stress plays a role in the delamination and spalling of many thin film on substrate systems. Residual stress can be developed in a thin film from vapor deposition, sputtering, machining, and differential cooling from forming processes. The present paper suggests a proposed solution for determining the prestress level in a film substrate system that may help in further understanding the delamination or spallation failure process.

When an indentation is performed it is primarily used to determine the film properties of a system such as elastic modulus or hardness. What is usually overlooked is the substrate material and therefore substrate mechanical properties. In fact many of the common indentation test methods directly neglect the substrate effect [85, 126-128, 130]. This is done by minimizing the depth of indentation penetration to less than approximately 10% of the thickness of film (h) [85, 160]. However, there are problems associated with conducting tests at shallow depths [119, 161, 162]. For instance, the recorded data from a test can be influenced by initial frictional drag of the indenter as it makes contact with the test specimen. At shallow depths localized material roughness and changes in indenter tip geometry could affect the P-δ data recorded. Also, in many problems, substrate properties could be as important if not more important than the film properties. For example the mechanical properties of an in-service helicopter

rotor blade may be of more importance than any coating used to protect the rotor from sand, moisture, or heat.

Understanding the properties of a substrate may be accomplished by pushing an indenter moderately deeply into a test specimen [119, 158, 163, 164]. Knowing that the substrate will now play a role in the development of the P-δ data we may be able to develop a relationship that accounts for this effect and through a reverse analysis be able to extract these properties, such as substrate elastic modulus directly [159]. It is the intent of this study then to develop the appropriate relationships as applicable to a semi-infinite film/substrate system under moderately deep loading of a spherical indenter, and then determine the mechanical properties of both the film and substrate but also be able to determine any pre-stressed state on the film that may exist. By doing so through this technique, we are not bound to the requirement that the specimen has to be in a nominal stress-free state in order to perform an indentation test.

Through a wide-ranging set of finite element simulations incorporating changing both material parameters as well as different levels of pre-stress, a set of general functional relationships are established (forward analysis). The data generated will be at two distinct and consistent indentation depths. By doing so, two unique relationships can be developed providing the ability to solve directly for two unknown material/mechanical properties (elastic modulus of the film and

substrate or film pre-stress) as long as one of the three is known a priori. This study is then further extended to consider variable indenter radii and variable film thickness. A rigorous error sensitivity analysis will also be discussed.

3.2 Model and Method

The model used in this study is comprised of a thin film that is fully bonded to a semi-infinite substrate and a rigid spherical indenter. The film has an applied equibiaxial presetress, denoted as σ_{ps}. The indenter is placed in contact with the film and moved in a direction that is normal to the film surface. The film has an elastic modulus denoted as E_f and Poisson's ratio of v_f. The elastic modulus of the substrate is denoted as E_s and the corresponding Poisson's ratio is denoted as v_s. v_f and v_s are kept the same with a value of 0.25. The Poisson's ratio, is considered a minor contributor to the P- δ data and therefore removed from the derivation in the forward analysis [106]. The film and the substrate are both considered homogeneous, isotropic elastic materials.

This study is mainly focused in developing the relationships that can be used to determine two of three variables; E_f, E_s, and σ_{ps}. However, one of these three must always be known a priori. By conducting the dimensional analysis, the following functional relationship is developed and will need to be used in the forward analysis:

$$\frac{P}{E_f \delta^2} = \prod \left(\frac{E_f}{E_s}, \frac{R}{h}, \frac{\sigma_{ps}}{E_f}, \frac{\delta}{h} \right) \quad \textbf{(3.1)}$$

To make use of the substrate effect [126, 158, 159, 164] the indentation load should be taken at two indentation depths $\delta_x = h/2$, and $\delta_y = h/4$, where h is the thickness of the film [165], from which two independent relationships from (3.1) are deduced:

$$\frac{P_x}{E_f \delta_x^2} = f_x \left(\frac{E_f}{E_s}, \frac{R}{h}, \frac{\sigma_{ps}}{E_f} \right) \quad \textbf{(3.2)}$$

$$\frac{P_y}{E_f \delta_y^2} = f_y \left(\frac{E_f}{E_s}, \frac{R}{h}, \frac{\sigma_{ps}}{E_f} \right) \quad \textbf{(3.3)}$$

Subscripts x and y denote the functional relationships in Eqs. (3.2 and 3.3) at the two prescribed depths, δ_x and δ_y. It should be noted that in actual practice the maximum value of the depth of indentation can exceed the prescribed h/2 value and in effect can take any value as long as it is greater than h/2.

In the first phase of this study, we assume that the film thickness (h) is known as well as the indenter radius (R) providing a constant relationship for R/h. The value for R/h will be changed in a later section of this study (see Section 3.4). However, in keeping R/h constant we get the following:

$$\frac{P_x}{E_f \delta_x^2} = f_x\left(\frac{E_f}{E_s}, \frac{\sigma_{ps}}{E_f}\right), \text{with } \frac{R}{h} = 1.0 \qquad \textbf{(3.4)}$$

$$\frac{P_y}{E_f \delta_y^2} = f_y\left(\frac{E_f}{E_s}, \frac{\sigma_{ps}}{E_f}\right), \text{with } \frac{R}{h} = 1.0 \qquad \textbf{(3.5)}$$

Using a range of variables for E_f/E_s and σ_{ps}/E_f in the forward analysis the functional forms f_x and f_y can be determined. Using Eqs. (3.4) and (3.5) along with f_x and f_y two of the three unknowns E_s, E_f, or σ_{ps} can be determined (again with the third being known a priori).

The film and substrate are axisymmetric with the substrate modeled with a semi–infinite material thickness. All numerical indentation simulations were performed with ABAQUS [166]. The film/substrate regions were modeled with 4-node bilinear axisymmetric, reduced integration elements (CAX4R). Approximately 180,000 elements (Fig. 3-2) were used in the model. The film is equibiaxially prestressed to a desired level before the start of indentation. We assume that the contact is frictionless which is again considered a minor factor in this study [85, 135].

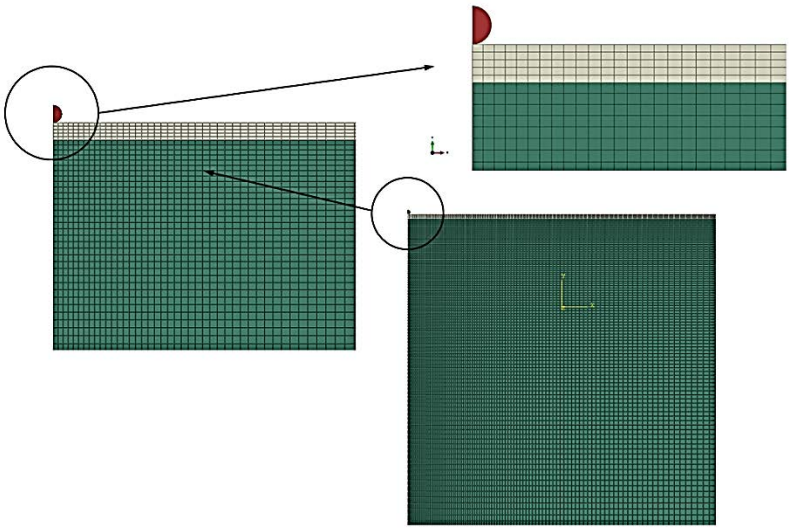

Figure 3-2 Model of the spherical indentation on a prestressed elastic film/substrate system.

The elastic modulus ratio (EMR) along with the normalized film prestress (K) need to be varied in order to provide a good cross section of material properties and nominal stress values. However, it has been verified that even under the highest compressive stress buckling of the film does not occur. The elastic modulus ratio is denoted as EMR= $\frac{E_f}{E_s}$. Its range in this analysis is $0.25 \leq \text{EMR} \leq 15.00$. The film prestress, K=$\frac{\sigma_{ps}}{E_f}$ also changes based on the following, $-0.10 \leq K \leq 0.10$, where the negative value denotes a compressive stress.

In the text, "Hardness of Metals," by Tabor [21] as well as Doerner and Nix [37] in their paper, "A method for interpreting the data from depth-sensing indentation instruments" the authors propose along with Quinn, Patel, and Lloyd [167], in

their paper "Effect of Loading Rate Upon Conventional Ceramic Microindentation Hardness," that the rate of indentation does have an effect on hardness (and therefore measured force-depth data). While there are standards established for maximum indenter velocity in indentation testing, for example ASTM Standard E-384 [168], which will minimize the effect of indenter rate on force-displacement data, the authors of this paper do not explicitly address this issue in both the forward and reverse analysis simulations performed. But the authors have followed Tabor's suggestion; "It is thus evident that for satisfactory static hardness measurements the load must be applied very slowly and steadily." Therefore incremental, slow movement of the indenter into the substrate was performed during the forward and reverse analyses. These incremental movements of the indenter were based on a normalized maximum indentation depth equal to 1.0. In all simulations performed the starting normalized increment was 1.0e-12, with no one normalized incremental movement of indenter larger than 0.003 (0.3% of total indentation movement).

3.3 Formulation of a Fixed Indenter Radius

3.3.1 Forward analysis

From a set of indentation simulations, the normalized load-depth relationships as shown in Figure 3-3 are decidedly non-linear. This is due primarily to the effect of the substrate from pushing the indenter moderately deep into the film, as well as the spherical geometric shape of the indenter [129]. In comparing the

curvatures for the scenario of EMR=0.25 in Figure 3-4(a) and EMR = 15.0 in Figure 3-4(b), as the substrate becomes more flexible, the plots take on a more linear form. This is a result of the loss in substrate effect (softer substrate) and with the corresponding indentation behavior becoming dominated by the effect of film bending.

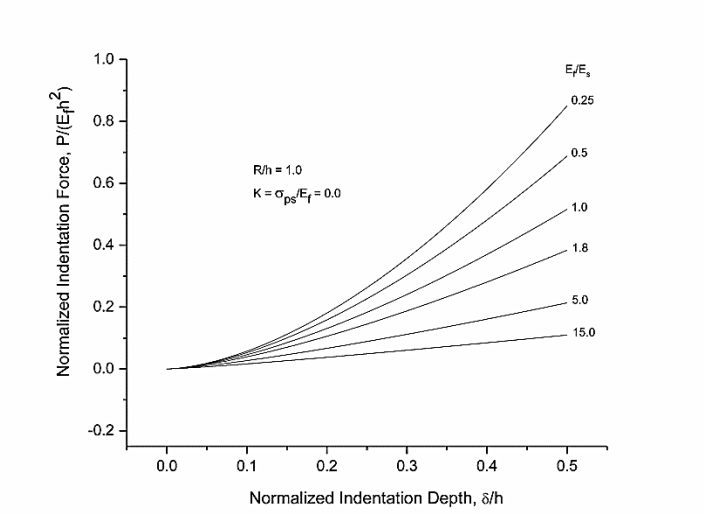

Figure 3-3 Normalized load - penetration depth for different Elastic Modulus ratios, with *R/h*=1.0, K=0.

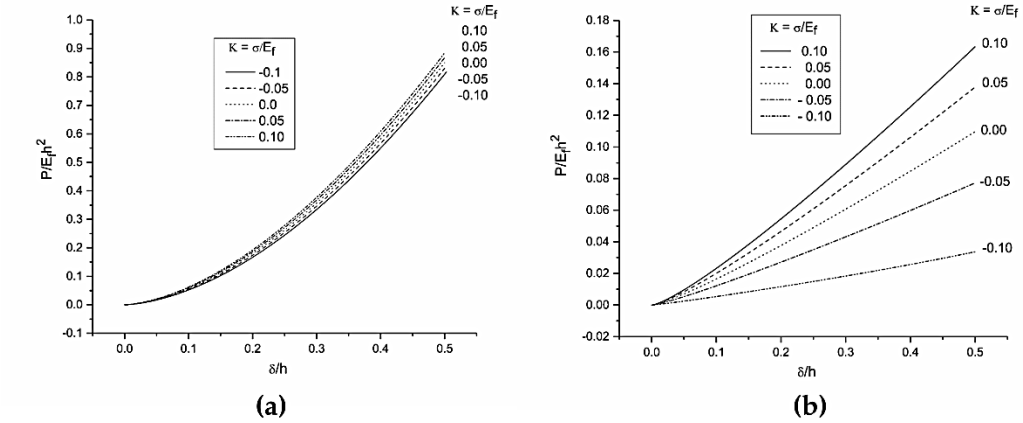

Figure 3-4 Normalized P-δ Data for Various K Values at EMR of (a**) Ef/Es=0.25 and (**b**) Ef/Es=15.0.**

Prestressing of the film of a composite structure will affect the force required to indent the specimen. This is because the indenter now has to exceed the surface tension created in the film by the induced prestress. Changes in substrate stiffness will also affect the force/prestess interaction. Extensive simulations were performed, modelling the system at two prescribed indentation depths: $\delta_x = h/2$ and $\delta_y = h/4$. From this analysis and fitting of the data from Eqs. (3.4) and (3.5) a set of generalized functions, f_x and f_y have been developed and shown in Eq. (3.6):

$$\frac{P_i}{E_f \delta_i^2} = f_i\left(\frac{E_f}{E_s}, \frac{\sigma_{ps}}{E_f}\right) = A_i\left(\frac{E_f}{E_s} - B_i\right)^{C_i} + D_i\left(\frac{E_f}{E_s}\right)^2 + E_i\left(\frac{E_f}{E_s}\right) + F_i \qquad \textbf{(3.6)}$$

$$with \quad i = x, y \text{ for } \delta_x = \frac{h}{2} \text{ and } \delta_y = \frac{h}{4}$$

And with:

$$A_i = a_{0_i} + a_{1_i}\,\mathrm{K} + a_{2_i}\,\mathrm{K}^2 + a_{3_i}\,\mathrm{K}^3 + a_{4_i}\,\mathrm{K}^4$$

$$B_i = b_{0_i} + b_{1_i}\,\mathrm{K} + b_{2_i}\,\mathrm{K}^2 + b_{3_i}\,\mathrm{K}^3 + b_{4_i}\,\mathrm{K}^4$$

$$C_i = c_{1_i}\left(c_{2_i} - \mathrm{K}\right)^{c_{3_i}}$$

$$D_i = d_{0_i} + d_{1_i}\,\mathrm{K} + d_{2_i}\,\mathrm{K}^2 + d_{3_i}\,\mathrm{K}^3 + d_{4_i}\,\mathrm{K}^4$$

$$E_i = e_{0_i} + e_{1_i}\,\mathrm{K} + e_{2_i}\,\mathrm{K}^2 + e_{3_i}\,\mathrm{K}^3 + e_{4_i}\,\mathrm{K}^4$$

$$F_i = constant$$

where coefficients $a_{ni}, b_{ni}, c_{ki}, d_{ni}, e_{ni}$ (i=x,y, and x=1, y=2, n=0-4, k=1-3) are fitted constants (see Table 3-1).

A comparison of f_x and f_y from Eq. (3.6) at corresponding δ_x and δ_y with the input parameter used in the forward analysis are shown in Figure 3-5a and 3.5b. As represented, the functions align nicely with actual forward analysis input parameters.

Table 3-1 General Coefficients for EMR-K Fitting Function

F_1	-0.138142626	F_2	-0.27345413
a_{01}	2.674281604	a_{02}	4.034252118
a_{11}	0.802831035	a_{12}	1.147974895
a_{21}	1.971999573	a_{22}	5.222286008
a_{31}	-8.544787918	a_{32}	-29.25982734
a_{41}	44.46597133	a_{42}	131.1351472
b_{01}	-0.383265786	b_{02}	-0.568865038
b_{11}	0.549111802	b_{12}	0.763772049
b_{21}	-1.29341713	b_{22}	-2.600832556
b_{31}	3.373917099	b_{32}	10.53364711

b_{41}	-24.85527757	b_{42}	-60.95042138
c_{11}	-0.35865278	c_{12}	-0.29205364
c_{21}	-0.434558478	c_{22}	-0.295299789
c_{31}	-0.63882907	c_{32}	-0.470757762
d_{01}	-0.000225813	d_{02}	-0.000201266
d_{11}	-0.003103271	d_{12}	-0.003870197
d_{21}	0.003580859	d_{22}	-0.00153943
d_{31}	0.102776788	d_{32}	0.277177385
d_{41}	-0.877371942	d_{42}	-2.443837931
e_{01}	0.008209149	e_{02}	0.008712058
e_{11}	0.110259779	e_{12}	0.157132416
e_{21}	-0.24475966	e_{22}	-0.276338029
e_{31}	-0.115013816	e_{32}	-1.035169875
e_{41}	3.664067224	e_{42}	13.69568226

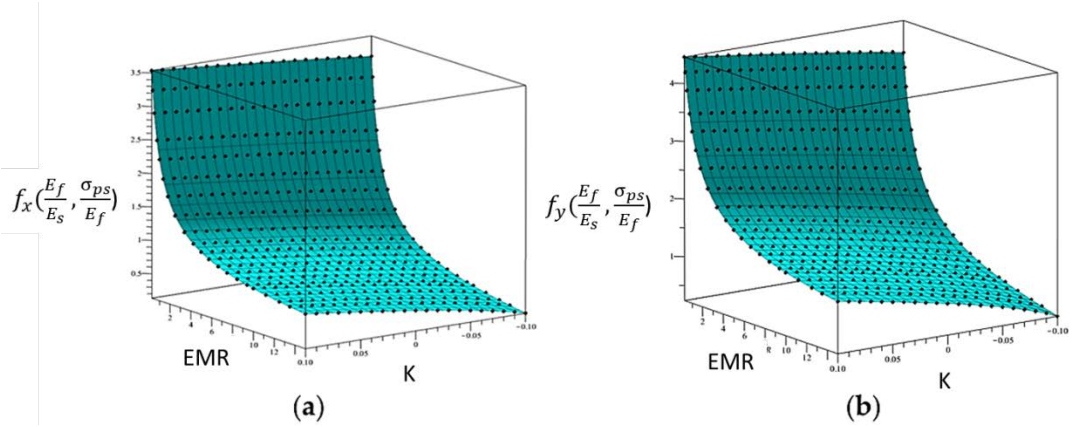

Figure 3-5 Data points from forward analysis overlaid with surface plots, f_x and f_y at (a) δ_x=h/2 and (b) δ_y=h/4.

3.3.2 Reverse analysis

Various reverse analysis (RA) simulations were performed in order to confirm the results developed in the forward analysis. Values were varied, providing a thorough test across a large range of elastic modulus and film prestress parameters. These RA parameters were a stand-alone set of values independent

from those used in the forward analysis. As noted earlier, the equations in Eq. (3.6) provide the ability to solve for any two variables, E_s, E_f, or σ_{ps} as long as one of the three is known. Accurate results were obtained by employing an error minimization algorithm for recorded *P-δ* data [165]. Figure 3-6 shows the error in percent from the reverse analysis for various combinations of unknowns. For all three different combinations, the error range is between -6% and 8%. In further analysis of the error as plotted, maximums tend to occur at higher normalized prestress and in particular, at compressive values. This compressive stress probably creates instabilities in the generation of the *P-δ* data. However, because the error is generally low throughout all EMR and K parameters, the results prove to be an acceptable method in determining any two of the three variables.

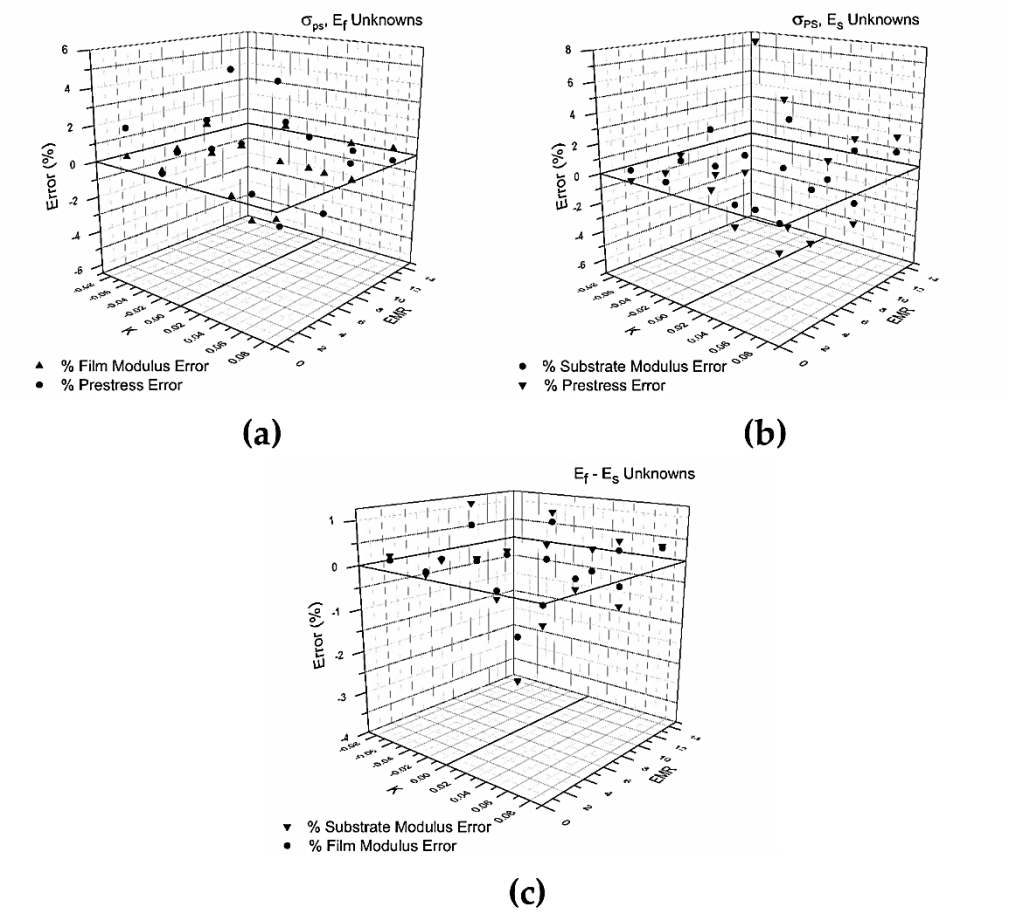

Figure 3-6 Reverse Analysis Error (a) with E_s and σ_{ps} as unknowns; (b) with E_f and σ_{ps} as unknowns; (c) with E_f and E_s as unknowns.

3.4 General Formulation with Variable Film Thickness

3.4.1 Forward analysis

In section 3.2 of this paper, the parameters used for an initial forward analysis included a fixed film thickness and indenter radius, with a corresponding R/h ratio of 1.0. However, in many practical problems, the film thickness may be unknown. In instances such as this additional work must be done to extend the

present results to the problem of variable film thickness, such that there are now four parameters to address in a forward analysis: E_f, E_s, h, and σ_{ps}. This section develops an initial formulation for this type of problem. It is a proof-of-principle analysis to show that this work can be extended to such a problem, essentially solving for two unknowns with the other two parameters known a priori. In order to prove this an EMR of 2.5 is chosen and remains fixed while the normalized prestress and normalized film thickness parameters are modified. The values chosen for this part of this research are $-0.10 \leq K \leq 0.10$ and R/h of 0.5, 0.75, 1.0, 2.0, 5.0, and 10.0, establishing a range of $0.5 \leq R/h \leq 10.0$. Recall that $K=\frac{\sigma_{ps}}{E_f}$. Values for the normalized indentation force versus normalized prestress are shown in Figure 3.7 for two prescribed indentation depths of $\boldsymbol{\delta}_x$=h/2 and $\boldsymbol{\delta}_y$=h/4. As can be seen, these plots show discreet independent curves for the various R/h values chosen and provide confidence that the forward analysis will deliver a set of independent relationships. These relationships are shown in Equation (3.7) with the corresponding values for constants shown in Table3- 2.

$$\frac{P_j}{E_f \delta_j^2} = M_j + N_j K + Q_j K^2 \; for \; j = x, y \; and$$

$$\delta_x = \frac{h}{2} and \; \delta_y = \frac{h}{4}$$

$$with \; M_j = m_{1_j} e^{[(R/h)/t_{x_j}]} + m_{2_j} e^{[(R/h)/t_{2_j}]} + y_{0_j} \qquad \textbf{(3.7)}$$

$$and \; N_j = n_{1_j} e^{[(R/h)/t_{3_j}]} + n_{2_j} e^{[(R/h)/t_{4_j}]} + y_{1_j}$$

$$and\ Q_j = q_{1_j} + q_{2_j}(R/h) + q_{3_j} q_{4_j}^{(R/h)}$$

M_j, N_j, and Q_j are coefficients and shown in Table 3-2, with j = x,y and x=1, y=2.

Table 3-2 Coefficients for R/h-K Fitting Function.

M_j			
Y_{01}	4.29294	Y_{02}	6.17453
m_{11}	-3.15663	m_{21}	-4.35566
m_{21}	-0.64938	m_{22}	-1.03513
t_{11}	-10.7228	t_{12}	-9.85780
t_{21}	-0.63728	t_{22}	-0.67550
N_j			
Y_{11}	4.16337	Y_{12}	7.74763
n_{11}	-1.43510	n_{12}	-2.01002
n_{21}	-2.19215	n_{22}	-4.76786
t_{31}	-0.59133	t_{32}	-0.66103
t_{41}	-4.20076	t_{42}	-5.08646
Q_j			
q_{11}	-1.70805	q_{12}	-3.39752
q_{21}	0.01899	q_{22}	-0.00069
q_{31}	0.80714	q_{32}	2.10207
q_{41}	0.47556	q_{42}	0.58296

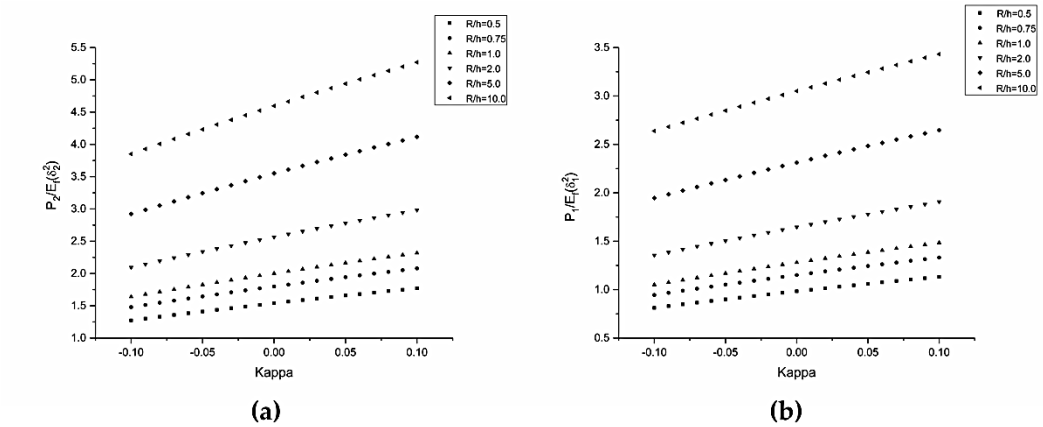

Figure 3-7 Normalized Indentation Force as a function of $K=\sigma_{ps}/E_f$, at $0.5 \leq R/h \leq 10.0$, (a) $\delta_x=h/2$. (b) $\delta_y=h/4$.

3.4.2 Reverse analysis

Incorporating the equations from Eq. (3.7) a reverse analysis was performed for various normalized film thickness and normalized prestress values. The plotted errors for the reverse analysis are shown in Fig. 3-8. These results show reasonable errors for the various R/h and K values chosen. The range of errors are between -2% and 6%. As before, these results were obtained by incorporating a minimization, averaging algorithm shown in Fig. 3-9 and performing a single indentation test with a maximum depth of at least h/2. It should be stated again that this analysis at an Elastic Modulus Ratio of 2.5 is a proof-of-principle study to validate that the results from section 3.3 can be extended to other R/h values.

A search of existing published experimental indentation tests was made in order to find P-δ data that could be used in this reverse analysis. It was the intent of the author to verify this theory with actual experimental test data. Unfortunately no applicable data that fit within the material and film prestress parameters was found.

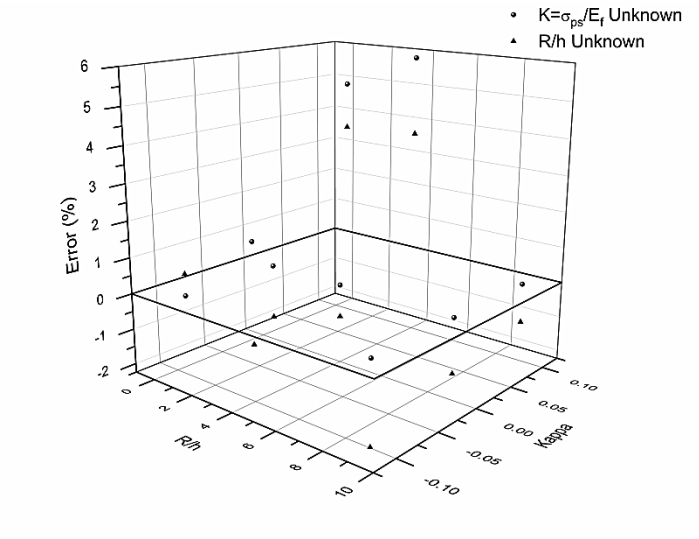

Figure 3-8 Error Plot of Reverse Analysis, -0.10 ≤ K ≤ 0.10, 0.5 ≤ R/h ≤ 10.0.

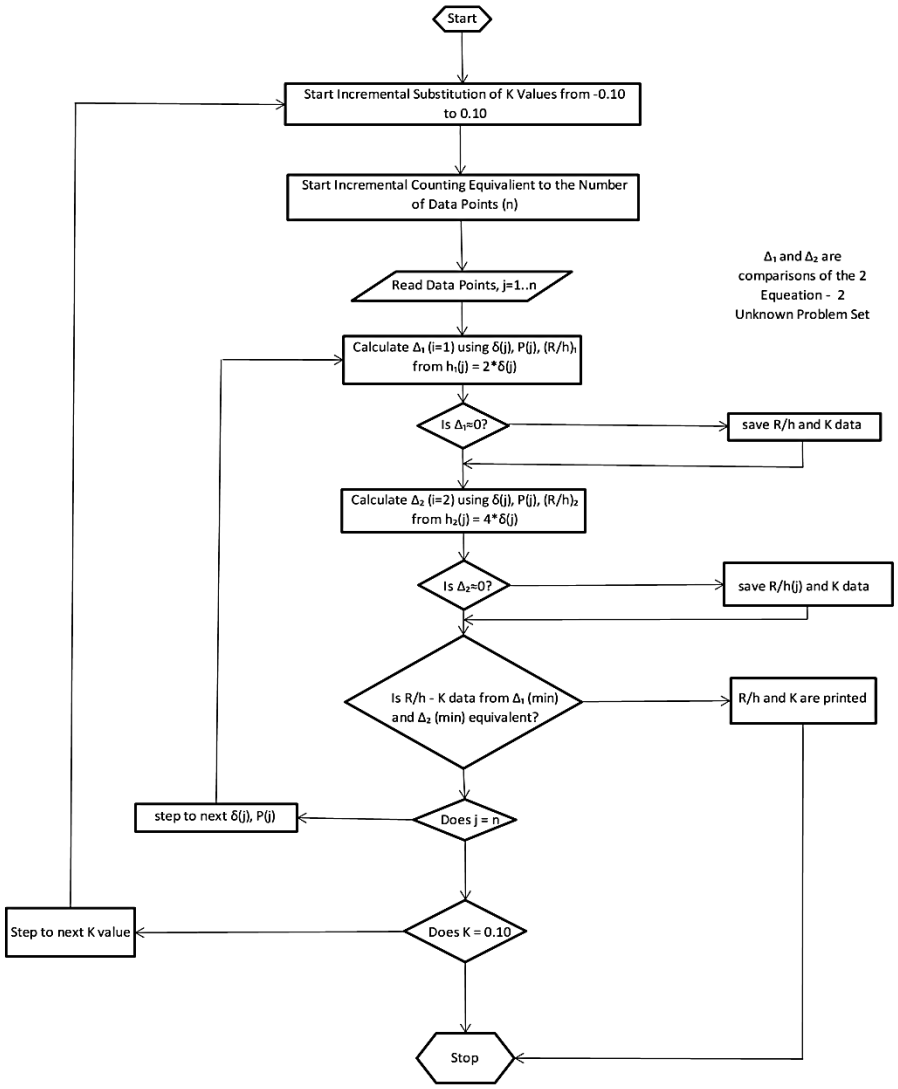

Figure 3-9 General Algorithm of Reverse analysis.

3.5 Error Formulation

Indentation tests require the simultaneous pushing of the indenter into the test material while at the same time recording the indenter force and displacement (P-δ data). The recorded data while assumed correct may have substantial errors

due to problems with measuring the force, indenter depth, or for other reasons. These errors easily affect the determination of the material properties of both film, substrate, as well as film prestress. This next section will examine the potential errors due to problems with measured indenter force and displacement and how each may affect the variables σ_{ps}, E_f, and E_s.

In this error analysis, the following relationships from Eqs. (3.4) and (3.5) are still applicable:

$$\frac{P_i}{E_f \delta_i^2} = f_i\left(\frac{E_f}{E_s}, \frac{\sigma_{ps}}{E_f}\right), \text{with } \frac{R}{h} = 1.0 \text{ and i} = \text{x, y}$$

This means that the thickness of the film (h) is known such that one may correspondingly match the radius of the indenter (R) exactly to this film thickness (therefore R/h is a constant and known). The indenter is assumed to be spherical and rigid. As part of this derivation, it is also assumed that v_s and v_f are fixed and known. The overall geometry is as before in relationship to film and substrate thickness, $h_f << h_s$, incorporating a fully axisymmetric geometry. The values for $P_i - \delta_i$ are as noted before in the forward analysis, indentation depths $\delta_x = h/2$, and $\delta_y = h/4$, are each based on h, the film thickness.

Differentiating the dimensionless functions from Eqs. (3.4) and (3.5) in a term-by-term manner, we get the following:

$$\frac{dP_i}{E_f\delta_i^2} - \frac{P_i dE_f}{E_f^2\delta_i^2} - \frac{2P_i d\delta_i}{E_f\delta_i^3} =$$

$$= \frac{\partial\left[f_i\left(\frac{E_f}{E_s}, \frac{\sigma_{ps}}{E_f}\right)\right]}{\partial\left(\frac{E_f}{E_s}\right)} d\left(\frac{E_f}{E_s}\right) \qquad \textbf{(3.8, 3.9)}$$

$$+ \frac{\partial\left[f_i\left(\frac{E_f}{E_s}, \frac{\sigma_{ps}}{E_f}\right)\right]}{\partial\left(\frac{\sigma_{ps}}{E_f}\right)} d\left(\frac{\sigma_{ps}}{E_f}\right),$$

$$with\ i = x, y$$

Errors that could affect indenter force and displacement ($\partial P_x/P_x$, $\partial P_y/P_y$, $\partial\delta_x/\delta_x$, $\partial\delta_y/\delta_y$) may result from measurement errors, recording errors, out of calibration equipment, the indenter not perfectly set normal to film face, noise in the instrumentation signal, surface effects, as well as others. Reorganizing these terms and combining them it can be seen that they can be related to the potential variation of unknowns, $\partial E_f/E_f$, $\partial E_s/E_s$, $\partial\sigma_{ps}/E_f$, which is the normalized film modulus, substrate modulus, and film prestress.

For example, if the modulus of the film is known then the perturbed term dE_f is zero. Therefore, the equations as shown in (3.8) and (3.9) can be computed as two independent relationships with two unknown variables. The film's equibiaxial

stress and substrate elastic modulus are solved in terms of the perturbation values as shown in (3.10):

$$\frac{d\sigma_{ps}}{E_f} = \alpha_1 \frac{dP_x}{P_x} + \alpha_2 \frac{d\delta_x}{\delta_x} + \alpha_3 \frac{dP_y}{P_y} + \alpha_4 \frac{d\delta_y}{\delta_y} \qquad \textbf{(3.10)}$$

where:

$$\alpha_1 = \frac{\Omega_x Q_y}{w},\ \alpha_2 = \frac{-2\Omega_x Q_y}{w},\ \alpha_3 = \frac{-\Omega_y Q_x}{w},\ \alpha_4 = \frac{2\Omega_y Q_x}{w}$$

with $w = \left(Q_y V_x - Q_x V_y\right)$

$$\frac{dE_s}{E_s} = \beta_1 \frac{dP_x}{P_x} + \beta_2 \frac{d\delta_x}{\delta_x} + \beta_3 \frac{dP_y}{P_y} + \beta_4 \frac{d\delta_y}{\delta_y}$$

and where $\beta_1 = \frac{\Omega_x V_y}{X},\ \beta_2 = \frac{-2\Omega_x V_y}{X},\ \beta_3 = \frac{-\Omega_y V_x}{X},\ \beta_4 = \frac{2\Omega_y V_x}{X}$

with $X = (E_f/E_s)(Q_y V_x - Q_x V_y)$ and $f_t(E_f/E_s, \sigma_{ps}/E_f)$, $\Omega_t = \frac{P_t}{E_f \delta_i^2} = f_t\left(\frac{E_f}{E_s}, \frac{\sigma_{ps}}{E_f}\right)$, for $t = x, y$ is as shown in Eq. (3.6). Q_t and V_t are as shown below:

$$Q_t = \frac{\partial\left[f_t\left(\frac{E_f}{E_s}, \frac{\sigma_{ps}}{E_f}\right)\right]}{\partial\left[\frac{E_f}{E_s}\right]} = A_t C_t \left(\frac{E_s}{E_f} - B_t\right)^{C_t} + 2D_t\left(\frac{E_s}{E_f}\right) + E_t \;\; with\; t = x, y \qquad \textbf{(3.11)}$$

$$V_t = \frac{\partial A_t}{\partial\left(\frac{\sigma_{ps}}{E_f}\right)}\left[\frac{E_f}{E_s} - B_t\right]^{C_t}$$

$$+ A_t \left\{ -C_t\left(\frac{E_f}{E_s} - B_t\right)^{C_t - 1} \frac{\partial B_t}{\partial\left(\frac{\sigma_{ps}}{E_f}\right)} \right.$$

$$\left. + \left(\frac{E_f}{E_s} - B_t\right)^{C_t - 1} ln\left(\frac{E_f}{E_s} - B_t\right) \frac{\partial C_t}{\partial\left(\frac{\sigma_{ps}}{E_f}\right)} \right\} + \left(\frac{E_f}{E_s}\right)^2 \frac{\partial D_t}{\partial\left(\frac{\sigma_{ps}}{E_f}\right)}$$

$$+ \left(\frac{E_f}{E_s}\right) \frac{\partial E_t}{\partial\left(\frac{\sigma_{ps}}{E_f}\right)} + \frac{\partial F_t}{\partial\left(\frac{\sigma_{ps}}{E_f}\right)} \quad with\; t = x, y$$

with A_t, B_t, C_t, D_t, E_t $(t = x, y)$as defined in Eq. (3.6) and

$$\frac{\partial A_t}{\partial\left(\frac{\sigma_{ps}}{E_f}\right)} = a_{1_t} + 2a_{2_t}\left(\frac{\sigma_{ps}}{E_f}\right) + 3a_{3_t}\left(\frac{\sigma_{ps}}{E_f}\right)^2 + 4a_{4_t}\left(\frac{\sigma_{ps}}{E_f}\right)^3$$

$$\frac{\partial B_t}{\partial\left(\frac{\sigma_{ps}}{E_f}\right)} = b_{1_t} + 2b_{2_t}\left(\frac{\sigma_{ps}}{E_f}\right) + 3b_{3_t}\left(\frac{\sigma_{ps}}{E_f}\right)^2 + 4b_{4_t}\left(\frac{\sigma_{ps}}{E_f}\right)^3$$

$$\frac{\partial C_t}{\partial\left(\frac{\sigma_{ps}}{E_f}\right)} = c_{1_t} c_{3_t}\left(\frac{\sigma_{ps}}{E_f} - c_{2_t}\right)^{c_{3_t} - 1}$$

$$\frac{\partial D_t}{\partial\left(\frac{\sigma_{ps}}{E_f}\right)} = d_{1_t} + 2d_{2_t}\left(\frac{\sigma_{ps}}{E_f}\right) + 3d_{3_t}\left(\frac{\sigma_{ps}}{E_f}\right)^2 + 4d_{4_t}\left(\frac{\sigma_{ps}}{E_f}\right)^3$$

$$\frac{\partial E_t}{\partial\left(\frac{\sigma_{ps}}{E_f}\right)} = e_{1_t} + 2e_{2_t}\left(\frac{\sigma_{ps}}{E_f}\right) + 3e_{3_t}\left(\frac{\sigma_{ps}}{E_f}\right)^2 + 4e_{4_t}\left(\frac{\sigma_{ps}}{E_f}\right)^3$$

$$\frac{\partial F_t}{\partial\left(\frac{\sigma_{ps}}{E_f}\right)} = 0$$

coefficients $t = x, y$ and $a_{r_t}, b_{r_t}, c_{q_t}, d_{r_t}, e_{r_t}$ $(with\ r = 0-4, q = 1-3, x = 1, y = 2)$ are listed in Table 3-1.

The relationships for $\alpha_{1\text{-}4}$ and $\beta_{1\text{-}4}$ are developed from equations in Eq. (3.10) and Eq. (3.11). The practical description of these terms are that they provide a sense of the level of magnitude associated with the different normalized potential errors derived, dP_i and $d\delta_i$ for (i=x,y). These values can give the tester insight into the accuracy of the measured P-δ data and therefore a level of confidence in the accuracy for the calculated variables, σ_{ps}, E_f, and E_s. For example if the error associated with the indenter force (P_x) at displacement δ_x is approximately 1% then the total error associated with dP_x/P_x is α_1%. This would contribute to the overall error in prestress. Thus the larger the perturbation error the larger the overall error. Also note that typically errors associated with both measured displacement and measured force occur simultaneously. In effect, errors for P_x and P_y would occur simultaneously and therefore both contribute to the error. The

same holds true with the indenter displacements, δ_x and δ_y. In order to understand the overall effect from force and displacement, the coefficients are grouped together and summed. This is shown in Fig. 3-10a and 3-10b, for the potential error in film prestress. The lower the combined value, then the lower the effect of measured displacement or measured force irregularities would have on the overall error associated with prestress. The same effect for substrate elastic modulus can be determined when examining values related to β_1 - β_4. The perturbations shown in the following error plots have proposed physical explanations as noted below. However, they may also come from instabilities that are inherent in the fitting functions chosen. A better fitting function may provide a more stable estimation of error.

In examining these error plots in Fig. 3-10, we can see that the error sensitivity is relatively low. Nevertheless, there are regions in which the potential error shown can be excessive. Multiple tests may be appropriate and then averaged. However, if two of the three variables are known (therefore only one unknown to be determined), the potential areas of high error sensitivity are no longer present.

An alternative example to understanding measurement error sensitivity is the scenario where the film modulus and film prestress are unknowns. In this case E_s is known and therefore $dE_s = 0$. Equations (3.8) and (3.9) can be solved directly for the perturbed normalized film modulus and prestress and are shown:

$$\frac{dE_f}{E_f} = \xi_1 \frac{dP_x}{P_x} + \xi_2 \frac{d\delta_x}{\delta_x} + \xi_3 \frac{dP_y}{P_y} + \xi_4 \frac{d\delta_y}{\delta_y} \quad \textbf{(3.12)}$$

where:

$$\xi_1 = \frac{\Omega_x V_y}{Y}, \xi_2 = \frac{-2\Omega_x V_y}{Y}, \xi_3 = \frac{-\Omega_y V_x}{Y}, \xi_4 = \frac{2\Omega_y V_x}{Y}$$

$$with\ Y = \left[\Omega_x V_y - Q_y V_x + \frac{E_f}{E_s}\left(V_y Q_x - V_x Q_y\right)\right]$$

$$\frac{d\sigma_{ps}}{E_f} = \varepsilon_1 \frac{dP_x}{P_x} + \varepsilon_2 \frac{d\delta_x}{\delta_x} + \varepsilon_3 \frac{dP_y}{P_y} + \varepsilon_4 \frac{d\delta_y}{\delta_y}$$

where:

$$\varepsilon_1 = \frac{X_y}{U_x}, \varepsilon_2 = \frac{-2X_y}{U_x}, \varepsilon_3 = \frac{-X_x}{U_x}, \varepsilon_4 = \frac{2X_x}{U_x}$$

$$with\ U_x = \frac{X_y V_x}{\Omega_x} - \frac{X_x V_y}{\Omega_y}, X_x = \left(1 + \frac{Q_x E_f}{\Omega_x E_s} - \frac{V_x \sigma_{ps}}{\Omega_x E_f}\right), X_y$$

$$= \left(1 + \frac{Q_y E_f}{\Omega_y E_s} - \frac{V_y \sigma_{ps}}{\Omega_y E_f}\right)$$

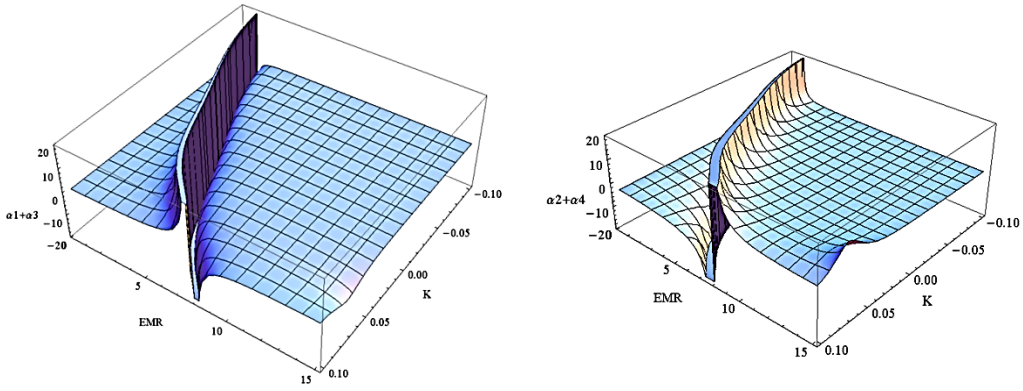

(a) (b)

Figure 3-10 Plots for dP (a) $\alpha_1 + \alpha_3$ and dδ (b) $\alpha_2 + \alpha_4$ as each affects the potential error in $d\sigma_{ps}/E_f$ over various $K=\sigma_{ps}/E_f$, $EMR=E_f/E_s$.

As a final instance of the potential errors associated with the measurement of indentation data with two unknowns, consider the case where only the film prestress is known. In this instance $d\sigma_{ps} = 0$ with $\frac{dE_f}{E_f}$ and $\frac{dE_S}{E_S}$ the terms that need to be evaluated. By knowing σ_{ps} then Equations (3.8 and 3.9) can be solved for the normalized perturbation of both the film and substrate moduli. This is shown in detail below:

$$\frac{dE_f}{E_f} = \tau_1 \frac{dP_x}{P_x} + \tau_2 \frac{d\delta_x}{\delta_x} + \tau_3 \frac{dP_y}{P_y} + \tau_4 \frac{d\delta_y}{\delta_y} \quad \textbf{(3.13)}$$

where:

$$\tau_1 = \frac{Q_y \Omega_x}{U_y}, \tau_2 = \frac{-2Q_y \Omega_x}{U_y}, \tau_3 = \frac{-Q_x \Omega_y}{U_y}, \tau_4 = \frac{2Q_x \Omega_y}{U_y}$$

$$with\ U_y = Q_y \left(\Omega_x - V_x \frac{\sigma_{PS}}{E_F}\right) - Q_x \left(\Omega_y - V_y \frac{\sigma_{PS}}{E_F}\right)$$

and $$\frac{dE_S}{E_S} = \eta_1 \frac{dP_x}{P_x} + \eta_2 \frac{d\delta_x}{\delta_x} + \eta_3 \frac{dP_y}{P_y} + \eta_4 \frac{d\delta_y}{\delta_y}$$

where:

$$\eta_1 = \frac{R_y}{\psi_x}, \eta_2 = \frac{-2R_y}{\psi_x}, \eta_3 = \frac{-R_x}{\psi_x}, \eta_4 = \frac{2R_x}{\psi_x}$$

$$with\ \psi_x = \frac{E_f}{E_s}\left(\frac{R_x Q_y}{\Omega_y} - \frac{R_y Q_x}{\Omega_x}\right), R_x = \left(1 + \frac{Q_x E_f}{\Omega_x E_s} - \frac{V_x \sigma_{ps}}{\Omega_x E_f}\right), R_y = \left(1 + \frac{Q_y E_f}{\Omega_y E_s} - \frac{V_y \sigma_{ps}}{\Omega_y E_f}\right)$$

In examining the potential errors associated with normalized film and substrate modulus or normalized prestress and film modulus, the results show large regions of stable and reasonable values providing good confidence in calculated results. However, there are small-localized regions where the error perturbations could be quite large. One of the areas where larger errors could occur are at locations where large compressive stress and stiff modulus (high EMR) exists. A practical explanation for this could be that the high compressive stress creates instabilities

in the measured displacement and force. Another case is shown at very low Elastic Modulus Ratios. Here the P- δ data is most likely dominated by the high stiffness of the substrate. The substrate at this extreme may cause problems with the derived algorithm. Further development of this derived relationship may be appropriate.

The above analysis assumes that there is only one known variable. Therefore, two unknown variables need to be determined. However in many occasions two of the variables are known such that only one unknown needs to be found. For example, if the moduli of both substrate and film are known, then the potential error in prestress with reference to perturbations for displacement and force can be shown as:

$$\frac{d\sigma_{ps}}{E_f} = \omega_x \frac{dP_x}{P_x} + \omega_y \frac{d\delta_x}{\delta_x} \qquad \textbf{(3.14)}$$

where

$$\omega_x = \frac{\Omega_x}{V_x}, \qquad \omega_y = -2\frac{\Omega_x}{V_x}$$

with Ω_x and V_x as noted before. Coefficients ω_x and ω_y are displayed in Figure 3-11 and show that the error sensitivity coefficients for the single unknown are found to be uniform and low, without the potentially troubling peaks noted in the two-variable error analysis described above. This analysis therefore provides

good confidence that indentation used to determine a single variable is an attractive method.

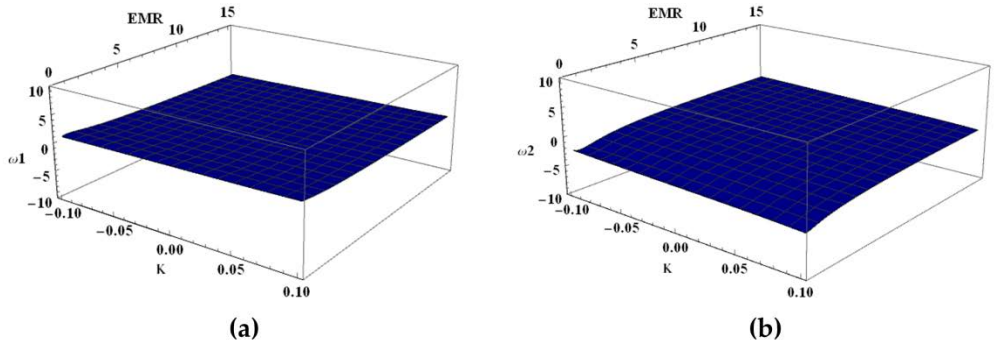

Figure 3-11 Perturbation Coefficient for Indenter (a) Force Measurement and (b) Displacement Measurement.

3.6 Chapter Summary

Understanding both the film and substrate material and mechanical properties are important for many practical applied systems. While most analysis examines just the film properties, it is proposed in this study that both film elastic modulus as well as substrate elastic modulus can be determined simultaneously. Stresses in the film can affect the overall performance and ultimate safety of a film/substrate system. Knowing this stress or determining the change in stress may be as important if not more important than knowing the elastic modulus properties. Through a comprehensive numerical study in the forward analysis an effective algorithm has been established to deduce through a single indentation test the elastic moduli and equi-biaxial prestress. Using a spherical indenter at moderate

depth, the effects from both the film and substrate provides an effective method in solving for two of the three variables E_f, E_s, and σ_{ps}.

An in depth error analysis was performed that highlights the need for precision measurements at areas of high instability. For example, when the film is under high compressive stress it is imperative that P-δ data be measured accurately. A suggested way to minimize measurement errors is to perform multiple tests and then average computed results. If two of the three variables are known precisely (E_f, E_s, σ_{ps}), then measurement of P-δ data is less sensitive to measurement errors and should provide a robust and accurate solution. The overall strategy described in this study can be extended to elastoplastic properties and also variable film thickness (as proved in this study).

Extensive simulations have been the basis for the proposed method of determining the unknowns, E_f, E_s, and σ_{ps}. The results as shown clearly need to be verified by performing a rigorous set of indentation tests on prestressed film/substrate samples. It is the intent of the author to address this in future work.

4 Spherical indentation on a Multi-layered System: determining Film Modulus and thickness from a single indentation test

4.1 Introduction

The typical thin film material that is firmly attached to a supporting substrate is a common engineered system in today's high technology world. What is equally as common are multi-layered systems made up of 2, 3, and more layers. We can find this combined material system in the building, automotive, aircraft, and optical industries. In the building industry, a film on substrate composite can be found in treated glazing system, or as a composite roofing system, or possibly as a coated siding façade. In the aircraft industry heat resistant films are commonly applied to jet engine turbine blades during the manufacturing process. Tinted aircraft windows can also be represented by a film/substrate model. Optical lenses are a case of multi-layered film systems in use. Lenses commonly have a combination of tinted or anti-reflective film coating, polarizing coating, and possibly a scratch resistant coating added to the base lens material.

In the broad area of electronics, common printed circuit boards are made up of a semiconductor film deposited on a silicon based substrate. In addition, one

cannot forget the paint that is applied to today's automobile, or almost any commonly manufactured material. This paint acts as an anticorrosion environmental film attached to or bonded to a substrate material often applied in multiple layers, with an outer coating of wax. One of the common concerns for almost all of these film/substrate systems is the importance that the materials remain fully bonded during the planned operational life of the system. With all multi-layered film-substrate systems, the potential effect of de-bonding of layers or the structural (elastic) breakdown of an individual layer could on many occasions cause failure of a system to fully operate under its desired plan of use or in extreme conditions cause a catastrophic failure of the system.

The film-substrate components as described above act as a complete structural system which requires that the mechanical properties be known in order to fully understand the successful operation, wear, and potential failure of the system. Properties usually required to be understood are the film elastic modulus (E_f), yield strength (σ_y), and even the film thickness (h). Film thickness in particular can provide an insightful understanding of the present condition or overall health of the system. As paint wears, it exposes the base material to harsh, wet environments. A turbine rotor blade whose heat resistant film starts to wear or thin may cause premature failure of the blade. The film elastic modulus, E_f is also a parameter that is necessary in order to fully understand system performance. Typically in order to determine these important properties of the film or substrate

the two materials would need to be mechanically separated from each other. This is required in order to perform a tensile test or to mechanically measure the film thickness. This is costly and difficult. An interesting method for non-destructively testing small-scale material systems is by the use of indentation [53, 119]. Indentation, at the nano or micro scale provides the ability to measure material performance without invasively modifying the test specimen. Nor does it require that the film be separated from the substrate. It is also a technique that may help us understand the engineering properties of the base material or substrate, which is sometimes overlooked when examining material performance. With a standard indentation test a hardened (diamond) tipped indenter is pushed into the material being tested while simultaneously recording indentation force versus indenter penetration depth. The force recorded, labeled P, and the measured elastic indentation depth, labeled $\boldsymbol{\delta}$, can be seen in general form in Figure 4-1. During indentation the stress fields developed during this large deformation and non-linear contact test are very complicated. However there have been a number of studies performed [120, 121] that show that from this P-$\boldsymbol{\delta}$ data the film elastic properties can easily be deduced. To be able to use this data one has to first develop a set of functional relationships that correlates the load displacement data to system mechanical properties. This is done through a series of simulations or tests which is called a forward analysis [85]. From this, one can determine a fitted function or set of functions that along with the P-$\boldsymbol{\delta}$ data can then help predict these important material properties [37, 85, 122, 123]. In

carefully developing these simulations in the forward analysis we might also be capable of determining the substrate mechanical properties, which when trying to understand the deteriorating mechanical performance of a structural system, the substrate properties could be just as important as the properties of the film. Unfortunately though, most conventional approaches used to understand the interaction of the film/substrate structural system oftentimes try to avoid this so-called substrate effect. The substrate effect is developed when an indenter is pushed into the test material beyond approximately 10% of the film thickness [59, 85]. However, it should also be noted that in performing indentation tests at shallow depths there are additional contributing factors which can reduce the effectiveness and accuracy of the test. These inherent problems have been investigated by a number of researchers [119, 124, 125]. For example understanding the effect from surface roughness of the tested material, or adjustments needed for worn indententor tips, or possible frictional effects as the indenter is pushed into the material, all can lead to errors in the data taken during a test.

And as stated above, there are instances where the substrate properties are of vital importance to the performance of the system. For example as a film starts to develop significant structural or geometric changes, it may be equally important to understand if there is any change in the mechanical properties of the substrate, especially if the substrate provides the structural backbone of the system.

Consider the composite rotor of a helicopter that is coated with a polymer-based erosion prevention coating (providing a resistance to the harmful effects from sand). While understanding the characteristics of the coating is and of itself an important topic, for the safety of the aircraft, understanding the rotor base material is of primary importance.

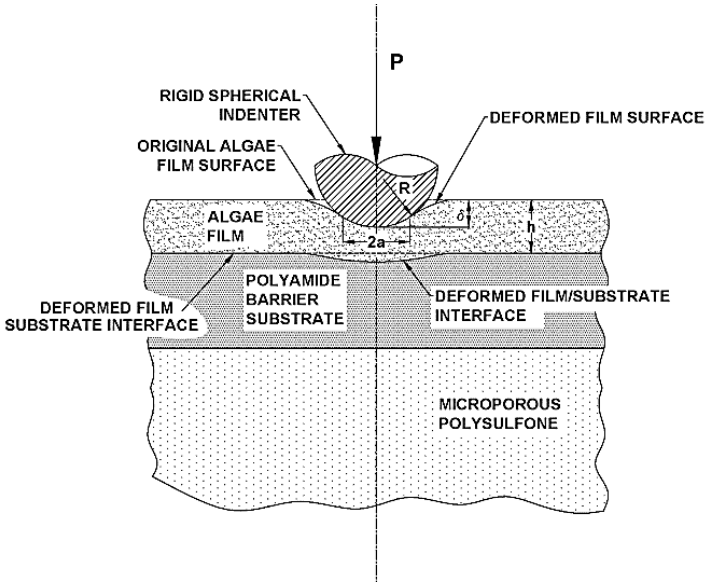

Figure 4-1 Indenter/Film/Substrate Model [169].

There has been however, a method proposed that incorporates a moderately deep indentation test that allows a full analysis of the film/substrate system [119, 126, 127, 129, 130]. By performing a moderately deep indentation test, the effect from the substrate then is fully reallized and through a reverse analysis [128] the test can provide useful information of both the film and substrate.

Reason to perform research

This present work started from a set of general discussions concerning multi-layered thin film systems and then extended to the current concern on the future availability of fresh drinking water throughout the world [170].

There are a number of papers that discuss the current state of making water potable (fit for drinking), as well as leveraging emerging technologies that propose to make the process cheaper. One method of desalination that is presently used takes advantage of the well-known process called reverse osmosis [171]. This promising technology could become an affordable method of desalination for the average consumer in less developed countries of the world.

The creation of drinking water using the technique of reverse osmosis utilizes the theory of osmotic transport of fluids through a membrane but instead uses the application in reverse format to remove suspended solids from brackish water or seawater [172]. The materials and technology used in this process is relatively inexpensive [173]. However the long term operation of reverse osmosis filtration causes fouling of the filter material from a buildup of algae that is generated as a byproduct from the process [174, 175].

Our present study examines at a fundamental level a three-tiered multi-layered film on substrates system with the practical application to how indentation may

help increase the understanding of the membrane-algae interaction and possibly provide a path forward towards optimizing the length of operation before the cleaning of a filter is required. It may also help lead to a better understanding of the methods required to thoroughly clean a membrane filter for possible future use. It is the author's plan to do this through the development of a set of simulation models that specifically examine this three layered system, in particular film (algae) thickness and film (algae) material properties, such as elastic modulus while at the same time embracing the effects from the substrate (polyamide) and sub-base (polysulfone) and their relationship to the film [169].

In summary the goal of this study is to establish the framework and understanding of indenting into a film (algae) on a substrate (polyamide) and sub-base material (polysulfone), while varying the film to substrate elastic modulus ratio and also varying the film thickness. This analysis will be performed using spherical indentation, which in going to moderate depths should prevent penetrating damage to the film while providing a unique solution to the proposed problem.

In the next section, the physical model will be discussed as well as the material parameters used in this study. Through the results of a single indentation test, measuring data at two different but consistent depths, the reverse analysis can effectively identify the two material film parameters in question. Also, a rigorous review of the error sensitivity in the proposed model is discussed.

4.2 Model and Computation Method

The properties chosen and the basis for our model for this study generally represent common filter materials used in today's reverse osmosis process [169, 176-179]. While most commercial membranes have proprietary material characteristics, the model chosen is representative of a typical membrane, shown in Figure 4-2. Figure 4-3 represents a cross section for such a material while Table 4-1 provides the parameters used in the forward analysis (FA) model and again forms the basis of this present study.

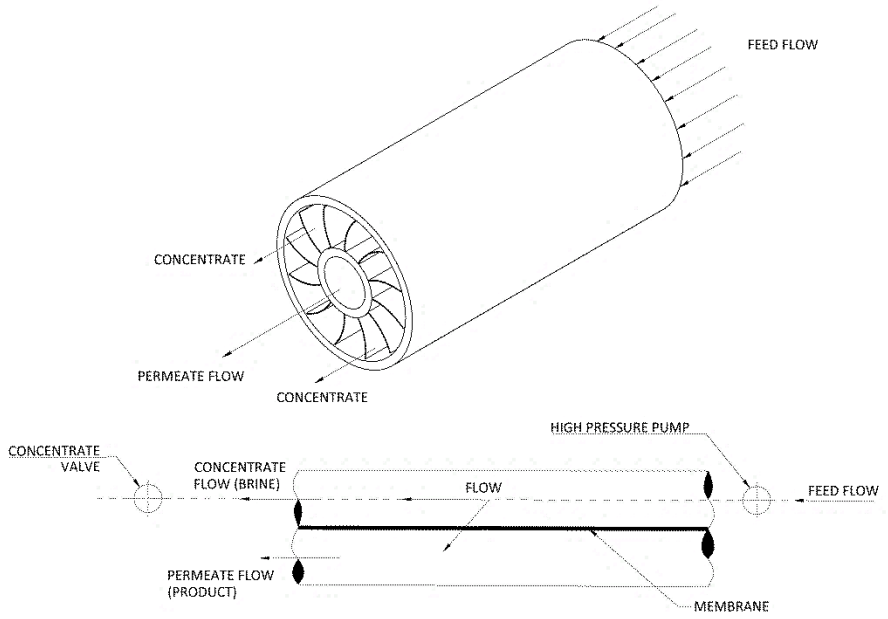

Figure 4-2 Typical Membrane Flow Characteristics [169].

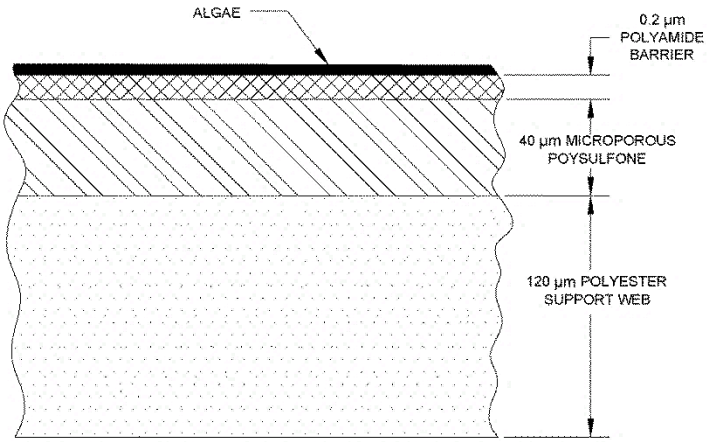

Figure 4-3 Typical Membrane Cross Section [169].

Table 4-1 Forward Analysis Parameters [169, 176, 178, 179].

Model Parameters

Algae (Film) Parameters

Film Elastic Modulus = E_f = varies

Film Thickness = t_f = varies

Aromatic Polyamide (Substrate)

Substrate Elastic Modulus = E_s = 200 $\frac{kg-\mu m}{s^2-\mu m^2}$

Substrate Thickness = t_s = 0. 2 µm

Yield Strength = σ_s = 50.0 $\frac{kg-\mu m}{s^2-\mu m^2}$

Φ = porosity = $\frac{V_v}{V_t}$ = 0.23

K= Relative Density = 1- Φ = = $\frac{V_s}{V_t}$ = 0.77

Polysulfone Base

Polysulfone Elastic Modulus = $E_{polysulfone}$ = 3.9e3 $\frac{kg-\mu m}{s^2-\mu m^2}$

Polysulfone Thickness = $t_{polysulfone}$ = 40.0 µm

Axisymmetric Model Radius = 150 µm

Indenter Radius = R = 2 µm

As shown in Figure 4-1, the specific indentation test model used requires a hardened, rigid spherical indenter that is pushed into a multilayered composite material (film/substrate/sub-base). Each different layer is considered a homogenous, isotropic elastic material, fully affixed to the adjacent layer. The polyamide substrate modeled represents a common filter material made up of a porous membrane with a defined fixed specific porosity of 0.23 [180, 181]. The polyamide substrate is rigidly attached to a microporous polysulfone sub-base that is 20 times stiffer than the polyamide barrier and 400 times thicker [178, 179, 182]. The Poisson's ratio for each material is taken to be 0.3 and considered fixed. However, it should be noted that variations in Poisson's ratio has a minor effect on indentation and therefore will not be considered in the forward analysis [85].

The rigid indenter is initially just in contact with the film, with its axis normal to the film surface. The indenter is then pushed into the film while the incremental force and corresponding displacement is recorded.

In the forward analysis (FA), the P-δ data is linked to the material properties that are to be examined. As part of the FA a general relationship that incorporates all of the important material parameters needs to first be established. From Dimensional Analysis [85, 99] we develop the following general relationship for

the spherical indenter acting on a film-substrate material through the forward analysis:

$$\frac{P}{E_f \delta R} = \prod \left(\frac{E_f}{E_s}, \frac{h_f}{R}, \frac{h_f}{h_s}, \frac{\delta}{h_f} \right) \quad \textbf{(4. 1)}$$

This is a dimensionless formulation of the criteria necessary to generally describe the P-δ data and how this P-δ data relates to the salient film/substrate material properties. The terms listed represent properties related to the indentation test/material geometry: The film Elastic Modulus (E_f), the substrate Elastic Modulus (E_s), the film thickness (h_f), the substrate thickness (h_s), the indenter radius (R), and the indentation force and depth (P-δ).

While the indenter is pushed into the test material an arbitrary distance, in order to develop a strong relational connection between film and substrate the indenter needs to be driven deep enough in order to take advantage of the so called substrate effect [126, 127, 129, 130]. Through the forward analysis two indentation loads (P_1, P_2) can be taken at two prescribed indentation depths, δ_1 = 0.1 h and δ_2 = 0.3 h, again, where h is the film thickness [165]. From these two depths the basis for two independent equations can then be deduced. The depths chosen are arbitrary, but are deep enough such that surface effects as described above are not a factor. Also, by choosing two depths we can reduce the

dimensionless variables described in Eq. (4.1), removing the $\frac{\delta}{h_f}$ term. The general Eq. (4.1) thus takes the form:

$$\frac{P_1}{E_f \delta R} = f_1\left(\frac{E_f}{E_s}, \frac{h_f}{R}, \frac{h_f}{h_s}\right) @\ \delta_1, P_1 \qquad \textbf{(4. 2)}$$

$$\frac{P_2}{E_f \delta R} = f_2\left(\frac{E_f}{E_s}, \frac{h_f}{R}, \frac{h_f}{h_s}\right) @\ \delta_2, P_2 \qquad \textbf{(4. 3)}$$

To further reduce the number of variables in this dimensionless set of equations, the analysis takes advantage of the physical relationship that is considered known and constant for the forward analysis, h_s and R. In knowing these terms, either $\frac{h_f}{R}$ or $\frac{h_f}{h_s}$ can be removed from Equations (4.2) and (4.3). Further expanded studies can examine the h_s and R terms and how these affect the dimensional relationship. For the present problem, the terms considered as unknowns are E_f as shown by the dimensionless property $\frac{E_f}{E_s}$ (EMR) or h_f through $\frac{h_f}{R}$ also a dimensionless term. And again as stated in the earlier problem parameters, the two terms, indenter radius and polyamide barrier (substrate thickness), are usually known and in this analysis, given as constants. This then provides two sets of Equations (4.4) and (4.5) available to solve for two unknowns, E_f and h_f.

$$\frac{P_1}{E_f \delta_1^2} = f_1\left(\frac{E_f}{E_s}, \frac{h_f}{R}\right) \text{ with } \frac{\delta_1}{h} = 0.1$$
$$\text{and } \frac{h_s}{R} = constant \quad \textbf{(4. 4)}$$

$$\frac{P_2}{E_f \delta_2^2} = f_2\left(\frac{E_f}{E_s}, \frac{h_f}{R}\right) \text{ with } \frac{\delta_2}{h} = 0.3$$
$$\text{and } \frac{h_s}{R} = constant \quad \textbf{(4. 5)}$$

The forward analysis was computationally performed using ABAQUS commercial software on Dell Workstations [183]. The element type used was an axisymmetric 8-node biquadratic, reduced integration element, CAX8R. Over 10,500 elements were incorporated into the model with the sub-base considered semi-infinite in depth. The contact between the indenter and film was assumed to be frictionless, and considered a minor factor [85, 135].

4.3 Forward Analysis

The parameters used in this study for the film thickness (h_f) and substrate thickness (h_s) ratio were varied as shown: $0.3 \leq h_f/h_s \leq 4.0$ such that the substrate can be either larger, smaller, or of equal thickness to the film. As noted before, the Radius and substrate thickness are constant for this problem and therefore easily interchangeable such that we can also say $0.03 \leq h_f/R \leq 0.4$. It is this term, h_f/R that is used in the forward analysis. The film/substrate elastic modulus ratio varies as: $0.00625 \leq E_f/E_s \leq 2.0$. A set of extensive simulations were performed in

order to develop a relationship between various parameters of interest. As can be seen in Figure 4.4, the load versus displacement data as plotted has a non-linear relationship. This is primarily due to the use of a spherical shaped indenter, and also the substrate effect that is developed from pushing the indenter moderately deep into the film [128]. Figure 4-5 is a typical plot from the forward analysis showing normalized indentation force versus elastic modulus ratio. As shown there is good separation between the two curves, representing distinct values for the two normalized indentation depths chosen. This in turn suggests that these relationships can be considered unique, providing through the forward analysis two independent simultaneous equations that can be used in solving for the unknown material parameters. Figures 4-6, 4-7, 4-8 are representative plots from the forward analysis. Using the data generated through extensive analysis and the equations as shown in Eqs. (4.4) and (4.5) above as a guide, a unique set of fitted functions are developed. One equation is based on a prescribed normalized depth of $\frac{\delta_1}{h} = 0.1$ and the other using $\frac{\delta_2}{h} = 0.3$.

$$\frac{P_1}{E_f \delta_1^2} = A_1 \left[\left(\frac{E_f}{E_s} - B_1 \right)^{C_1} \right] \quad \textbf{(4. 6)}$$

$$\frac{P_2}{E_f \delta_2^2} = A_2 \left[\left(\frac{E_f}{E_s} - B_2 \right)^{C_2} \right] \quad \textbf{(4. 7)}$$

$$A_i = a_{i1} + b_{i1} \left(\frac{h_f}{R} \right) + c_{i1} \left[\left(\frac{h_f}{R} \right)^2 \right] \text{ i=1,2} \quad \textbf{(4. 8)}$$

$$B_i = a_{i2} + b_{i2}\left(\frac{h_f}{R}\right) + c_{i2}\left[\left(\frac{h_f}{R}\right)^2\right] \quad \text{i=1,2} \qquad \textbf{(4. 9)}$$

$$C_1 = a_{13} + b_{13}\left(\frac{h_f}{R}\right) + c_{13}\left[\left(\frac{h_f}{R}\right)^2\right] \qquad \textbf{(4. 10)}$$

$$C_2 = y_0 + \left\{\frac{A}{W}\sqrt{\frac{\pi}{2}}\right\} e^{-2\left[\left(\frac{\frac{h_f}{R}-x_c}{W}\right)^2\right]} \qquad \textbf{(4. 11)}$$

Coefficients for a_i, b_i, c_i are shown in table 4-2

Table 4-2 Coefficients for Equations 4.6-4.9

a_{11}	0.11765	a_{21}	0.32489
b_{11}	2.52616	b_{21}	3.46195
c_{11}	-2.23205	c_{21}	12.85941
a_{12}	-0.23127	a_{22}	-0.11363
b_{12}	-5.31011	b_{22}	-3.78187
c_{12}	0.26307	c_{22}	-7.30549
a_{13}	-0.95546	y_0	-0.97282
b_{13}	2.36833	A	0.05411
c_{13}	-2.60493	W	0.23325
		x_c	0.19371

These functions are shown as discrete surfaces in Figures 4-9 and 4-10. The accompanying data points on each plot are the calculated values taken from the initial forward analysis simulations. As can be seen the fitting functions provide an excellent representation of the data points generated.

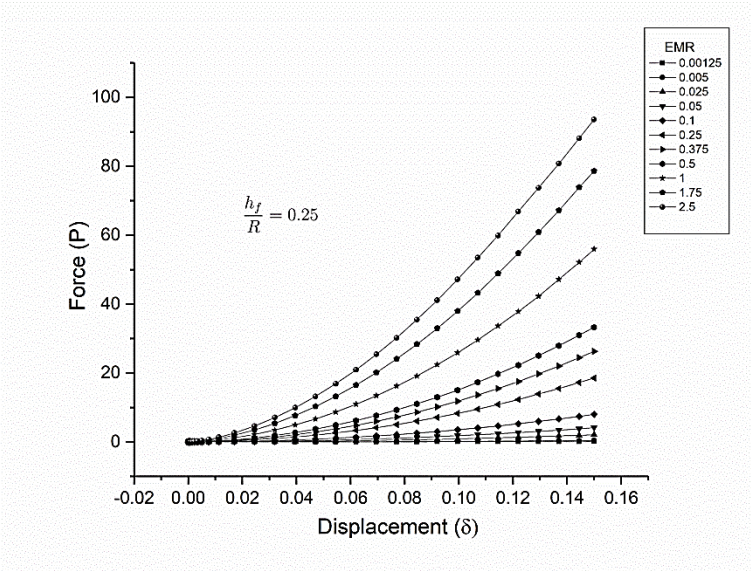

Figure 4-4 Force versus Displacement with $h_f/R=0.25$ for various EMR values.

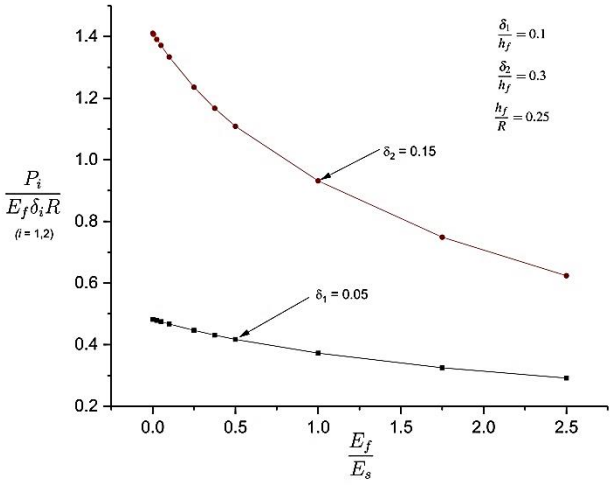

Figure 4-5 Typical Normalized Load versus Normalized Elastic Modulus Ratio at δ_1 and δ_2.

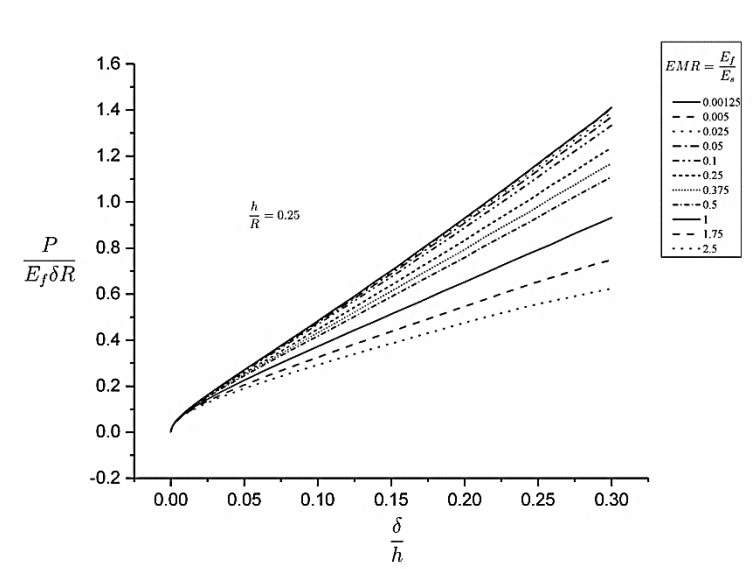

Figure 4-6 Forward Analysis - Normalized Load versus Normalized Indentation Depth with $h_f/R = 0.25$.

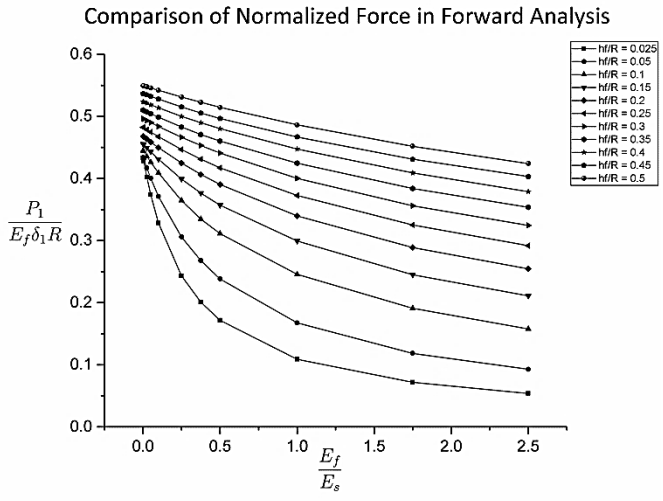

Figure 4-7 Forward Analysis - Normalized Load (P_1 at δ_1) versus Elastic Modulus Ratio (E_f/E_s) at various Normalized Film Thickness at $\delta_1/h = 0.1$.

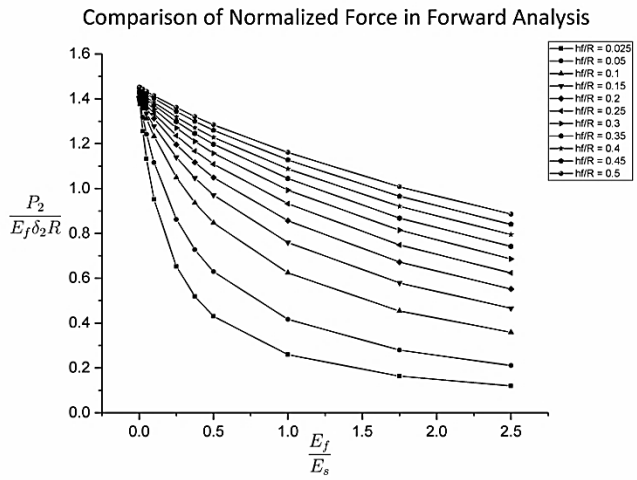

Figure 4-8 Forward Analysis - Normalized Load (P_2) versus Elastic Modulus Ratio (E_f/E_s) at $\delta_2/h = 0.3$.

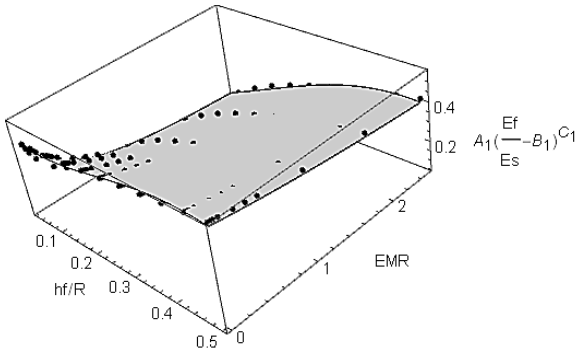

Figure 4-9 Normalized Indentation Load (points) compared to function f_1 from Forward Analysis (surface).

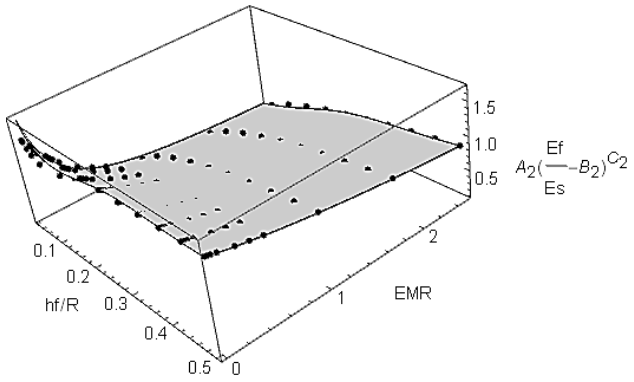

Figure 4-10 Normalized Indentation Load (points) compared to function f_2 from Forward Analysis (surface).

4.4 Reverse Analysis

As seen from the forward analysis two independent equations, Eqs. (6 and 7) with coefficients as defined in Eqs. (4.8 to 4.11) and Table 4-2, effectively describe the indentation-load relationship at $\frac{\delta_1}{h} = 0.1$ and $\frac{\delta_2}{h} = 0.3$. The reverse analysis algorithm is based on minimizing the total error of these relationships [165]. This method utilizes the complete set of P-δ data without any aforementioned bias towards the prescribed δ_1 and δ_2 values used in the forward analysis. This provides a general solution method for the unknowns. Figure 4-11 details results from a number of checks of our forward analysis equations. Each test was performed utilizing input parameters independent from the parameters used in the forward analysis. Both h_f and E_f were solved simultaneously with good results achieved. From the reverse analysis the film thickness shows maximum errors

that were less than 7.35%. The larger errors tend to occur at larger normalized film thickness.

The film elastic modulus results showed errors less than 14.55%. These errors are clustered where the film elastic modulus is high, compared to the substrate elastic modulus. Overall the results from the reverse analysis are robust across a large scale of both elastic modulus as well as relative film thickness. Errors at very large moduli suggest that the substrate effect is reduced due to the dominance of the film stiffness. A more detailed study at very high film elastic moduli is suggested.

A search of existing published experimental indentation tests of multilayered material was made in order to find P-δ data that could be used in this reverse analysis. It was the intent of the author to verify this theory with actual experimental test data. Unfortunately no applicable data that fit within the material and film parameters was found.

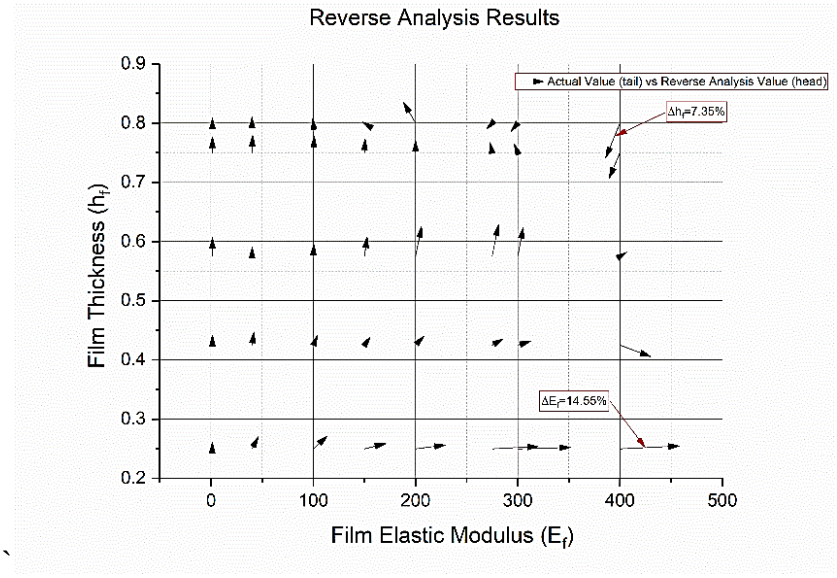

Figure 4-11 Results from Reverse Analysis.

4.5 Examination of Polysulfone Sub-Base

The sub-base, in this analysis, and as shown in Figures 4-1 to 4-3, was fixed in both thickness (h_{ps}) and stiffness (E_{ps}). However, the effect of this sub-base on the overall performance of the three-layered system needs to be explored. It is assumed that changing the sub-base parameters, h_{ps} and E_{ps}, has little to no effect on the properties of the film and substrate. To explore this effect a number of simulations were performed varying both E_{ps} and h_{ps} (while keeping all other parameters constant). From these simulations P-δ data was produced and then normalized with respect to the P-δ data from the original polysulfone thickness and elastic modulus. Two figures show the results of these simulations, the first exploring polysulfone variables within ±20% of the original values, Figure 4-12 and the second figure, Figure 4-13 shows results for values between 5% and

5000% of the original E_{ps} and h_{ps} values. From these plots it is clear that within ±20% of the original values there is very little change in the P-δ data. However, as the stiffness of the sub-base drops to ¼ of the original stiffness the P-δ data changes significantly. In this test and as shown in Fig 4-13 as the stiffness increases, the normalized P-δ data remains within an acceptable range.

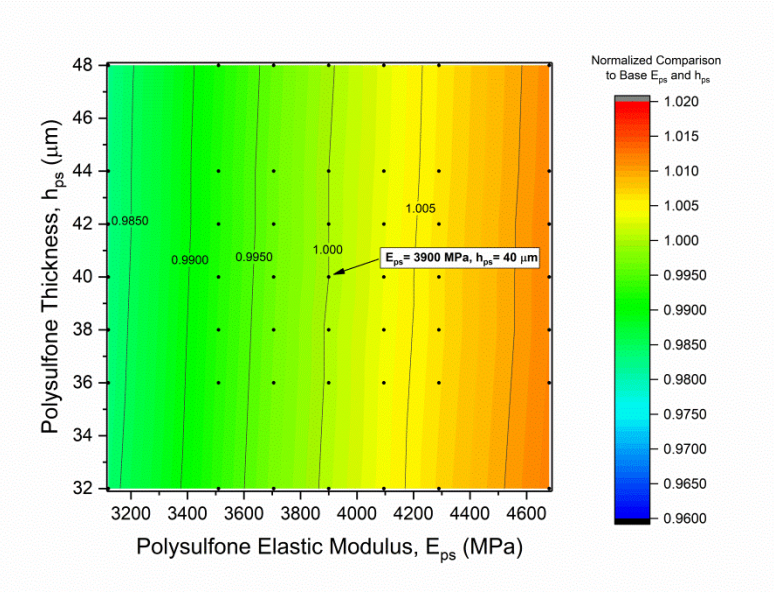

Figure 4-12 Comparison of Polysulfone E_{ps} (MPa) and h_{ps} (µm).

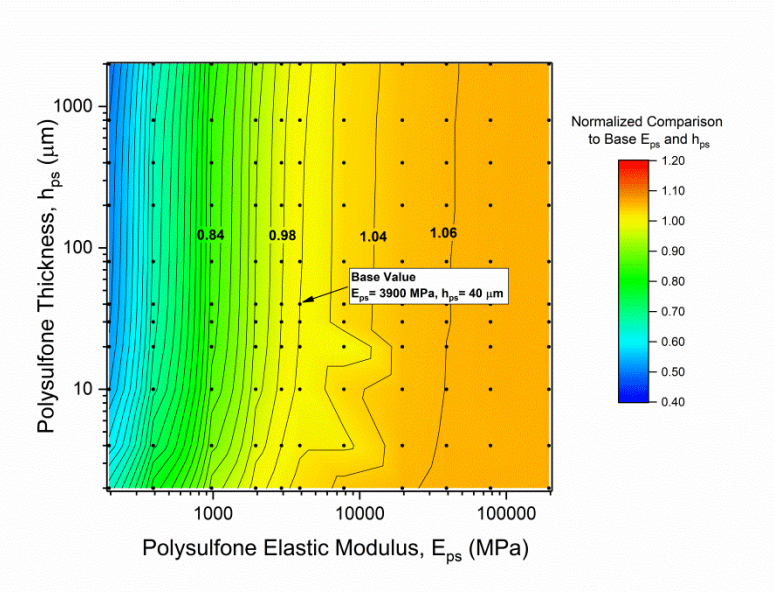

Figure 4-13 Comparison of Polysulfone E_{ps} (MPa) and h_{ps} (μm).

4.6 Error sensitivity

This section of this research focused on the unknowns, film (algae) thickness and film (algae) elastic modulus. These two parameters are the common unknowns when it comes to understanding multilayer analysis and in particular, reverse osmosis performance. The substrate (polyamide barrier) properties are usually well known and understood. If this was not the case they could also be determined based on the work described in this chapter. However, in performing an actual indentation test, the data taken has some inherent inaccuracies, both systematic and random. For example, a force measuring load cell may not be calibrated properly or the depth sensing properties of an indenter may not be accurately measuring the actual depth of indentation penetration during a force-

displacement test on a specimen. For these reasons, it is important to understand the error sensitivity of our actual measured variables, the measured depth and measured force, δ and P respectively.

Performing a general differentiation of our dimensionless equations (4.4) and (4.5) we get the following:

$$\frac{1}{E_f\delta_1 R}dP_1 - \frac{P_1}{E_f^2\delta_1 R}dE_f - \frac{P_1}{E_f\delta_1^2 R}d\delta_1 - \frac{P_1}{E_f\delta_1 R^2}dR = \frac{\partial\left[f_1\left(\frac{E_f}{E_s},\frac{h_f}{R}\right)\right]}{\partial\left(\frac{E_f}{E_s}\right)}d\left(\frac{E_f}{E_s}\right) + \frac{\partial\left[f_1\left(\frac{E_f}{E_s},\frac{h_f}{R}\right)\right]}{\partial\left(\frac{h_f}{R}\right)}d\left(\frac{h_f}{R}\right) \quad \textbf{(4. 12)}$$

$$\frac{1}{E_f\delta_2 R}dP_2 - \frac{P_2}{E_f^2\delta_2 R}dE_f - \frac{P_1}{E_f\delta_2^2 R}d\delta_1 - \frac{P_1}{E_f\delta_2 R^2}dR = \frac{\partial\left[f_2\left(\frac{E_f}{E_s},\frac{h_f}{R}\right)\right]}{\partial\left(\frac{E_f}{E_s}\right)}d\left(\frac{E_f}{E_s}\right) + \frac{\partial\left[f_2\left(\frac{E_f}{E_s},\frac{h_f}{R}\right)\right]}{\partial\left(\frac{h_f}{R}\right)}d\left(\frac{h_f}{R}\right) \quad \textbf{(4. 13)}$$

The normalized potential errors from measurements are then shown after rearranging Equations (4.12) and (4.13) as $\frac{dP_1}{P_1}$, $\frac{dP_2}{P_2}$, $\frac{d\delta_1}{\delta_1}$, and $\frac{d\delta_2}{\delta_2}$. These terms, after reorganizing, are related to the general perturbed material properties of our system, $\frac{dE_f}{E_f}$, and $\frac{dh}{h}$. This will provide us a general understanding of what the effects are from load and displacement measurement errors on the

perturbed film thickness and elastic property variables which we wish to determine. Equations (4.14) and (4.15) provide two independent equations with two unknowns, $\frac{dE_f}{E_f}$, and $\frac{dh}{h}$. Solving and rearranging terms for the perturbed film elastic modulus we get,

$$\frac{dE_f}{E_f} = \xi_1 \frac{dP_1}{P_1} + \xi_2 \frac{d\delta_1}{\delta_1} + \xi_3 \frac{dP_2}{P_2} + \xi_4 \frac{d\delta_2}{\delta_2} \quad \textbf{(4. 14)}$$

Where $\xi_1 = \frac{\Omega_1(V_2)}{Y}$, $\xi_2 = \frac{-\Omega_1(V_2)}{Y}$, and $\xi_3 = \frac{-\Omega_2(V_1)}{Y}$, $\xi_4 = \frac{\Omega_2(V_1)}{Y}$ **(4.15)**

And $Y = (V_2)\left(\Omega_1 + Q_1 \frac{E_f}{E_s}\right) - (V_1)\left(\Omega_2 + Q_2 \frac{E_f}{E_s}\right)$ **(4. 16)**

For the perturbed film thickness,

$$\frac{dh_f}{h_f} = X_1 \frac{dP_1}{P_1} + X_2 \frac{d\delta_1}{\delta_1} + X_3 \frac{dP_2}{P_2} + X_4 \frac{d\delta_2}{\delta_2} \quad \textbf{(4. 17)}$$

With values for X_1, X_2, X_3, X_4, and Y_2,

$$X_1 = \frac{\Omega_1(\Omega_2 + Q_2\frac{E_f}{E_s})}{Y_2} \qquad X_2 = \frac{-\Omega_1(\Omega_2 + Q_2\frac{E_f}{E_s})}{Y_2} \qquad \textbf{(4. 18-4.21)}$$

$$X_3 = \frac{-\Omega_2(\Omega_1 + Q_1\frac{E_f}{E_s})}{Y_2} \quad X_4 = \frac{\Omega_2(\Omega_1 + Q_1\frac{E_f}{E_s})}{Y_2}$$

Where Y_2 is: $Y_2 = \left[\left(\Omega_2 + Q_2\frac{E_f}{E_s}\right)\left(V_1\frac{h_f}{R}\right) - \left(\Omega_1 + Q_1\frac{E_f}{E_s}\right)\left(V_2\frac{h_f}{R}\right)\right]$ **(4.22)**

and $\Omega_1 = \frac{P_1}{E_f\delta_1 R} \quad \Omega_2 = \frac{P_2}{E_f\delta_2 R}$ **(4.23-24)**

Introducing terms from Eqs. (4.6 to 4.11) and Table 4-2 we get the following:

$$Q_i = \frac{\partial\left[\Pi_i\left(\frac{E_f}{E_s},\frac{h_f}{R}\right)\right]}{\partial\left(\frac{E_f}{E_s}\right)} = A_i C_i \left(\frac{E_f}{E_s} - B_i\right)^{C_i - 1} \quad \textbf{(4. 25)}$$

$$V_i = \frac{\partial\left[\Pi_i\left(\frac{E_f}{E_s},\frac{h_f}{R}\right)\right]}{\partial\left(\frac{h_f}{R}\right)} \quad \textbf{(4. 26)}$$

$$V_i = \frac{\partial A_i}{\partial\left(\frac{h_f}{R}\right)}\left(\frac{E_f}{E_s} - B_i\right)^{C_i} - A_i C_i \left(\frac{E_f}{E_s} - B_i\right)^{C_i - 1}\frac{\partial B_i}{\partial\left(\frac{h_f}{R}\right)} + A_i\left(\frac{E_f}{E_s} - B_i\right)^{C_i} ln\left(\frac{E_f}{E_s} - B_i\right)\frac{\partial C_i}{\partial\left(\frac{h_f}{R}\right)} \quad \textbf{(4. 27)}$$

$$\frac{\partial A_i}{\partial\left(\frac{h_f}{R}\right)} = b_{i1} + 2c_{i1}\left(\frac{h_f}{R}\right) \text{ i=1, 2} \quad \textbf{(4.28)}$$

$$\frac{\partial B_i}{\partial\left(\frac{h_f}{R}\right)} = b_{i2} + 2c_{i2}\left(\frac{h_f}{R}\right) \text{ i=1, 2} \quad \textbf{(4. 29)}$$

$$\frac{\partial C_1}{\partial\left(\frac{h_f}{R}\right)} = b_{13} + 2c_{13}\left(\frac{h_f}{R}\right) \quad \textbf{(4. 30)}$$

$$\frac{\partial C_2}{\partial\left(\frac{h_f}{R}\right)} = \frac{-4A}{w^3\sqrt{\frac{\pi}{2}}}\left\{e^{-2\left[\frac{1}{w}\left(\frac{h_f}{R}-x_c\right)\right]^2}\right\}\left(\frac{h_f}{R} - x_c\right) \quad \textbf{(4. 31)}$$

The terms $\xi_i \; and \; X_i$ are the general coefficients for the perturbed errors of the indentation test, with respect to load and displacement measurements. These are developed at the prescribed depths of $\frac{\delta_1}{h} = 0.1$ and $\frac{\delta_2}{h} = 0.3$. This is consistent with the forward analysis derivation and reverse analysis methodology. They provide insight into the potential error due to systematic errors in the measured values for force and displacement at δ_1 and δ_2. For example, if in a practical test there is an error in the measured value for force at δ_1 of 1% then the effect on the perturbed Film Elastic Modulus is ξ_1% (Eq. 4.14). Using the same technique the effect on the perturbed Film Elastic Modulus at δ_2 of the measured force is ξ_3%. Because the errors in measuring force at the two indentation depths δ_1 and δ_2 typically occur together and have the same order of magnitude, the total effect on the Elastic Modulus, $\frac{dE_f}{E_f}$, from these errors are summed and shown as $\xi_1 + \xi_3$.

The corresponding effect on the Elastic Modulus, $\frac{dE_f}{E_f}$, due to errors in measurement of the indenter displacements, δ_1 and δ_2 is then $\xi_2 + \xi_4$. A similar analogy holds for the perturbed film thickness. Errors due to the measured indentation force have a cumulative effect on $\frac{dh_f}{h_f}$ equivalent to $X_1 + X_3$. Errors related to measured values for δ_1 and δ_2 are $X_2 + X_4$. Plots associated with these predictive values shown over the range for this analysis are depicted in Figs. 4-14 to 4-17. In general the errors deduced from the plots are relatively low. However, there are regions where the errors can be quite high and caution is recommended.

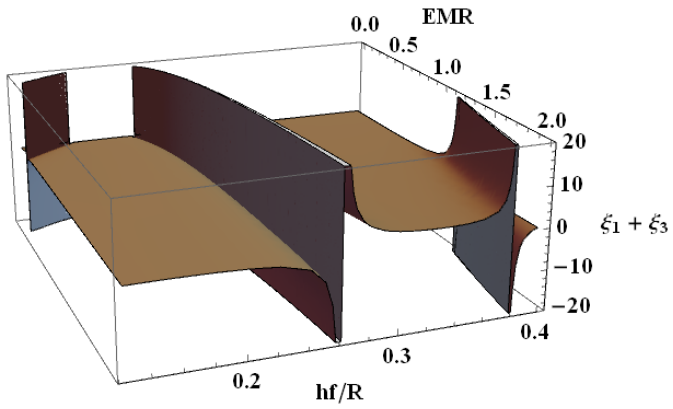

Figure 4-14 Error Sensitivity $\xi_1 + \xi_3$.

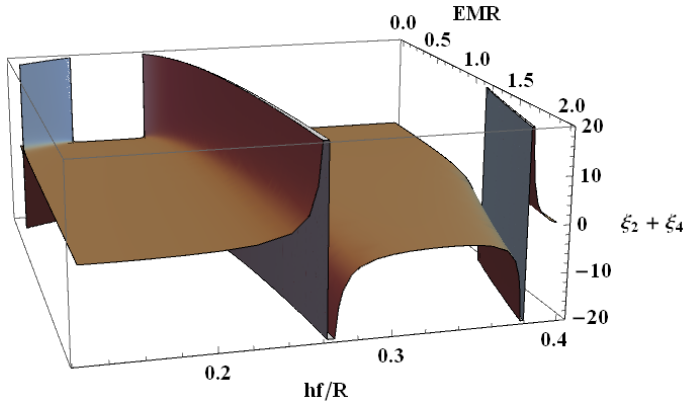

Figure 4-15 Error Sensitivity $\xi_2 + \xi_4$.

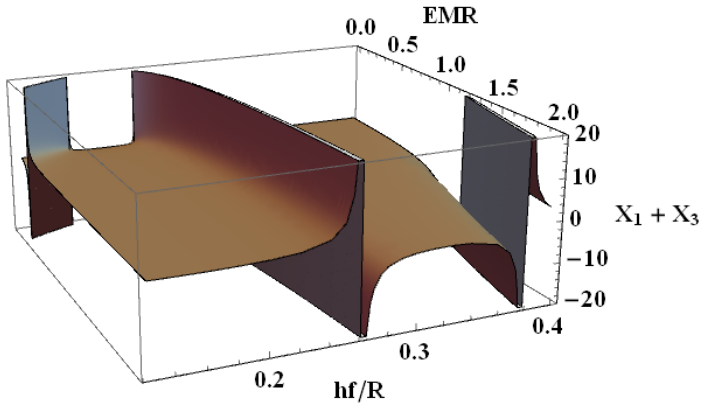

Figure 4-16 Error Sensitivity $X_1 + X_3$.

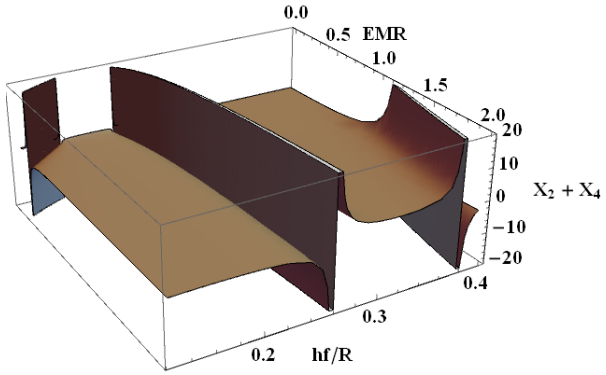

Figure 4-17 Error Sensitivity $X_2 + X_4$.

In many practical problems, all but one of the variables is known ahead of time, leaving either the film elastic modulus or the film thickness as unknowns. Under these circumstances, the errors have reasonably stable error predictions. In particular, the relationship for the potential error in the film elastic modulus due to measuring load and displacement in an indentation test is $\frac{dE_f}{E_f}$ when other film/substrate properties are known:

$$\frac{dE_f}{E_f} = \alpha_1 \frac{dP_1}{P_1} + \alpha_2 \frac{d\delta_1}{\delta_1} \qquad \textbf{(4.32)}$$

With $\alpha_1 = \frac{1}{\frac{Q_1 E_f}{\Omega_1 E_s}+1}$ and $\alpha_2 = \frac{-1}{\frac{Q_1 E_f}{\Omega_1 E_s}+1}$

If in turn E_f is known, then $dE_f = 0$ and the relationship for the error sensitivity of the film thickness is:

$$\frac{dh_f}{h_f} = \beta_1 \frac{dP_1}{P_1} + \beta_2 \frac{d\delta_1}{\delta_1} \qquad \textbf{(4.33)}$$

And with $\beta_1 = \frac{\Omega_1 R}{V_1 h_f}$ and $\beta_2 = \frac{-\Omega_1 R}{V_1 h_f}$

These terms can be shown in graphic form in Figs. 4-18 to 4. 21.

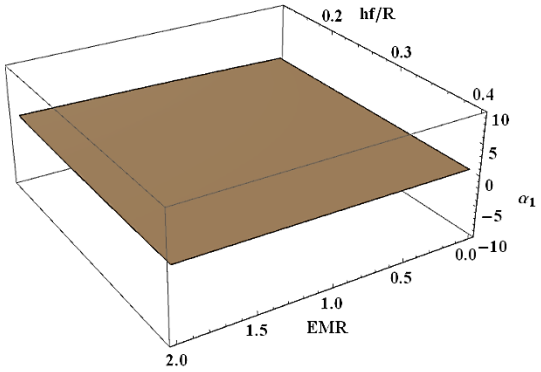

Figure 4-18 Error Sensitivity α_1.

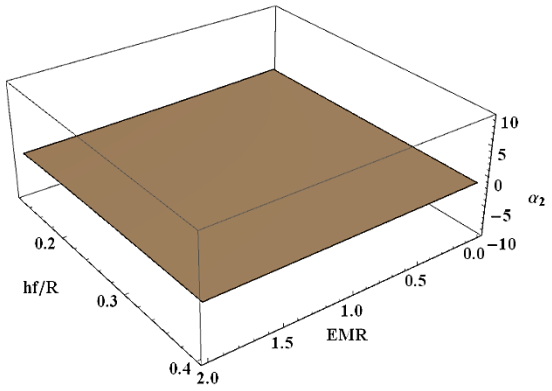

Figure 4-19 Error Sensitivity α_2.

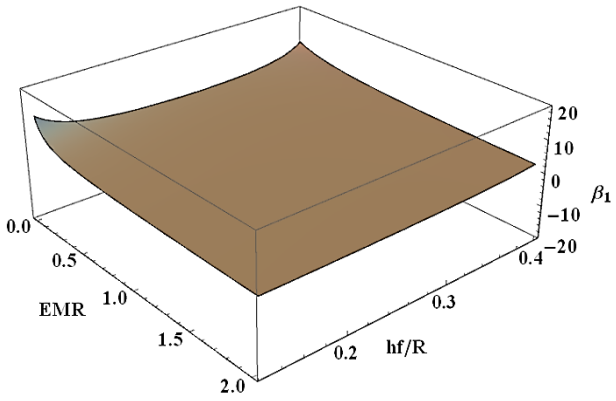

Figure 4-20 Error Sensitivity β_1.

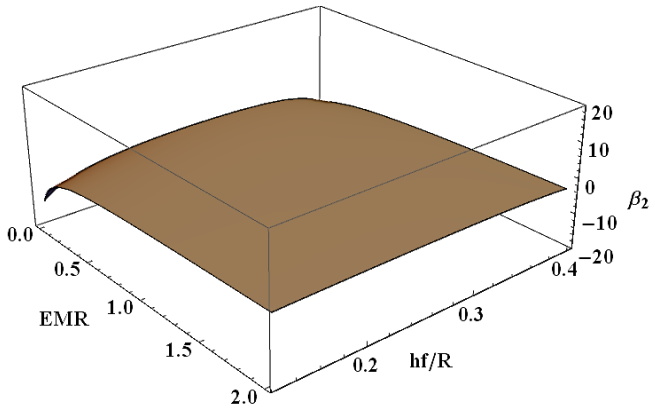

Figure 4-21 Error Sensitivity β_2.

4.7 Chapter Summary

Indentation research typically follows a standardized path of creating a model that is then analyzed, with a corresponding general principle or a set of principles learned and available to be applied across many disciplines; in essence somewhat generic in nature. This typical suite of research topics include bulk materials, film on substrate, viscoelastic film on substrate, stressed film on substrate, etc. It is often assumed that the film thickness or substrate properties are known a priori. However, for many problems this is not the case. And in many instances the substrate plays a significant role in the elastic response of the film and its contribution needs to be understood.

In this study we have instead performed a proof-of-principle examination of a very specific type of multi-layer composite material that can be eventually extended to a more general relationship. A practical example of this type of

problem is the reverse osmosis membrane problem where there is an algae buildup on a filter. It is suggested that with the analysis as described in this paper as well as further work, certain material characteristics can be learned from a single spherical indentation test. As noted, using a spherical indenter and pushing into the test material to a moderate depth lets us explore not just the film material properties but also the substrate and in particular how the substrate affects the film/substrate continuum. By using the spherical indenter, the film is less likely to become damaged as the indenter is pushed in. The model in this study incorporated the use of two indentation depths, the first to a depth of 10% of the film thickness and then, while continuing to move the indenter, to a depth of 30% into the film. Because the two depths are significantly different along with the substrate effect we are able to develop two distinct independent equations. These two equations then provided the framework to solve for two unknowns simultaneously, film elastic modulus (the algae elastic modulus), E_f, and film thickness (algae thickness), h_f. Or just as easily one could solve for the polyamide elastic modulus (E_s) if for some reason this is not known (in this situation, E_f or h_f must be known). A reverse analysis algorithm was then established, the results of which, using independent parameters than those used in the forward analysis agree well with the actual values used in the computational simulations.

A systematic error analysis was also performed, examining the effects from perturbations of the recorded indentation force and depth. The potential for error

can be due to inaccuracy in recording data, out-of-calibration testing equipment, etc. There are certain regions, at specific h_f/R values where errors are significant. Under circumstances where large errors could occur, it is suggested that multiple tests be made using different indenter radii until results converge.

This analysis, using spherical indentation at moderate depths is a first step towards the goal of understanding the full range of multi-layered material types. This work will ultimately be extended to a larger variety of multi-layered systems. It is also the author's intent to verify these results by laboratory experiment.

While this study was started as a general examination of a three-layered system, the added benefit of being able to accurately examine various algae types with different elastic modulus and thickness in a reverse osmosis water filtration problem has shown practical significance. If the elastic properties and thickness can be determined from a simple indentation test, it may lead to a more effective way to monitor algae build-up or provide a tailored method for cleaning more common built-up algae materials.

5 Dissertation Summary, Conclusions, and Future Work

5.1 Summary of work

Indentation analysis over the last 100 years has transformed our research and industrial understanding of materials from steel of the early 20th century to electronics and high-tech materials in the later part of the century and early 21st century. The means to easily understand the quality and fundamental mechanical properties of steel plate being fabricated issued in the need for developing an easy, straightforward way to deduce this important information. Hardness testing proved to be the bridge forming a general if not somewhat empirical correlation between material quality and hardness value while also providing a rough estimate of the material strength of the manufactured product. From the 1970's through the 1990's new and novel materials were developed for use in electronics and other high-tech industries paving the way for the introduction of special systems such as thin films on substrates. The first chapter of this thesis examined the development and important research breakthroughs in this area. Chapters 2, 3, and 4 (as shown in Figure 5-1) introduced the reader to thin film indentation using a relatively new and novel technique in determining the engineering and geometric material properties of the film-substrate system. In particular the use of a relatively deep single indentation could be used to not only examine properties

of the film but because the indenter extends to a moderate depth it allows us to examine substrate properties. Essentially by performing this moderately deep indentation there is a substrate effect which then also contributes to the force-depth relationship developed from the test.

Thesis Chapter 2	Material Systems	Material Elasticity	Stress State	Indenter Type	Load/Displacement Property	Load/Unload Condition	Study Type
	Bulk Material	Elastic	Unstressed Film	Flat Punch	Shallow Indentation	Loading Data	Numerical Analysis
	Film-Substrate	Elastic-Perfectly Plastic	Prestressed Film	Conical Punch	Moderately Deep Indentation	Unloading Data	Experimental Testing
	2-Film-Substrate	Elastic-Plastic		Vickers (4-sided pyramidal)			
		Elastic-Viscoelastic		Berkovitch Indenter (3-sided pyramidal)			
				Spherical Indenter			

Thesis Chapter 3	Material Systems	Material Elasticity	Stress State	Indenter Type	Load/Displacement Property	Load/Unload Condition	Study Type
	Bulk Material	Elastic	Unstressed Film	Flat Punch	Shallow Indentation	Loading Data	Numerical Analysis
	Film-Substrate	Elastic-Perfectly Plastic	Prestressed Film	Conical Punch	Moderately Deep Indentation	Unloading Data	Experimental Testing
	2-Film-Substrate	Elastic-Plastic		Vickers (4-sided pyramidal)			
		Elastic-Viscoelastic		Berkovitch Indenter (3-sided pyramidal)			
				Spherical Indenter			

Thesis Chapter 4	Material Systems	Material Elasticity	Stress State	Indenter Type	Load/Displacement Property	Load/Unload Condition	Study Type
	Bulk Material	Elastic	Unstressed Film	Flat Punch	Shallow Indentation	Loading Data	Numerical Analysis
	Film-Substrate	Elastic-Perfectly Plastic	Prestressed Film	Conical Punch	Moderately Deep Indentation	Unloading Data	Experimental Testing
	2-Film-Substrate	Elastic-Plastic		Vickers (4-sided pyramidal)			
		Elastic-Viscoelastic		Berkovitch Indenter (3-sided pyramidal)			
				Spherical Indenter			

Figure 5-1 Summary of decision matrix for indentation analysis related to thesis chapters.

For a thin film fully affixed to a substrate the basic understanding of the material properties of the film are typically of most interest, while the substrate properties and the film thickness are considered less important. In most instances it is assumed that the substrate properties and film thickness are known explicitly. However, there oftentimes are instances where this is not true and where there is a need to understand the mechanical properties of the substrate or the thickness of the film as well. For example in many applications, the substrate provides the structural backbone to the film/substrate system. Irregularities in the substrate properties could prove catastrophic to the system. An example of this is the engine turbine blade, where the outer coating (film) is simply a thermal and wear barrier to the blade (substrate), the blade providing the structural load carrying capability of the system. Another example of this is in the civil engineering field where the cladding (film) over building siding (substrate) panels plays a role in the preservation of the siding, but it is the siding that provides the structural integrity of the system. Conventional building roofing is also a common application of film on substrate systems where the substrate, the roof panel, is as important a gauge of the health of a roofing system as is the protective coating over the top of it. Failure or reduction in the load carrying capability of the panel as a unit could cause a premature failure of the panel. The same is true for a helicopter rotor blade, where the blade itself is as important if not more important than the coating on it. In these examples as well as many others it is important to

note that it is extremely difficult and costly to try to directly examine substrate properties of such systems. In order to do so the film would need to be removed which at best is difficult and costly. Therefore to have the ability to examine both film and substrate together, without having to remove one or the other is very appealing.

In discussing the examples above it is important however, not to diminish the role of the film. Through manufacturing processes or in use the film may thin due to erosion, wear, or perhaps catastrophically may actually delaminate from the cladding. Understanding the state of the film, including its thickness is very important. If the film acts as an electrical or thermal insulator for example, knowing the status of the thickness is crucial in evaluating the overall performance of the system.

There are many examples of these types of systems and for this reason it would be extremely useful to be able to examine both the substrate properties and film thickness as part of a test that is unfortunately typically only used to examine the film mechanical properties such as elastic modulus and hardness. However, through a model system of elastic film on substrate, a framework in this thesis has been established to close such a gap. Through a comprehensive computational study, and applying Dimensional Analysis to minimize the number of unknown terms, a set of explicit relationships were developed that provide a close

correlation between the indentation load-displacement data and the mechanical properties of both the film and substrate of a fully elastic system. And in most studies of film on substrate properties where the film properties are of primary interest, the total indentation depth should be limited to approximately 10% of the overall film thickness. However by incorporating the substrate effect into the testing, deeper indentation depths can be achieved without sacrificing accuracy. By indenting to these moderately deep depths we avoid random errors introduced in shallow depth indentation which can be caused by surface roughness of the film, indenter tip adhesion, as well as strain gradient effects.

In chapter 2 numerical simulations were performed over a range of elastic modulus ratios (EMR, E_f / E_s) from 0.04 to 25.00 and an indenter radius (R/h) varied from 0.5 to 3.0. This analysis was a first step toward the goal of measuring substrate properties in a film/substrate system, using the substrate effect at moderate indentation depths. This chapter in particular provided a method of determining the film elastic modulus, substrate elastic modulus, and film thickness.

The third chapter and second component of this research extends the development of film-substrate testing at moderate depths to also include the study of the effects on a film-substrate system due to an applied pre-stress to the film. This is an important consideration and a relatively common problem as most film/substrate

systems experience this phenomenon. Powered electronics certainly have a heat component in operations that can create thermal stresses in the film due to differences in the thermal expansion properties of the film and substrate. During material fabrication and the cooling done at the end of such a process there can be an unintended build-up of thermal stresses in the film. The system of a thin barrier (paint or vinyl) that is affixed to a building wall panel can potentially experience, during operations, the unintended application of a tensile or a compressive stress component due to changes in outdoor ambient air temperature. In fact cycling from tensile to compressive stresses is quite possible under the heating and cooling from changes in weather; conditions which can potentially affect the film substrate system. This third chapter developed as a proof-of-principle analysis, shows how a system of equations can be established that relates the elastic material properties of both the film and substrate, along with also relating the prestress of the film, to the load-depth data generated from an indentation test. In particular this work has established two fundamental equations that can simultaneously be solved in order to determine two unknowns; film elastic modulus, substrate elastic modulus, or film prestress, with one of the three being known a priori.

The fourth chapter of this thesis introduces the concept of multi-layer systems under the influence of a moderately deep spherical indentation test. Through a specific study of a multi-layered reverse osmosis water filtration system a set of

numerical simulations were performed and by adopting the terms from a Dimensional Analysis of the problem a set of formulas were developed that strongly relate a standard indentation test to the mechanical properties of the underlying layers. This too was a proof of principal study that allowed us to introduce a third layer specific to this problem and yet still be able to develop a useful correlation between indenter load-displacement data and the engineering features of the film and underlying substrate.

A detailed systematic error analysis was also performed for each section of this research. This work provided a useful exploration of the relationships developed and located specific areas of potentially large instability in the calculation of results. However, in interpreting this analysis a roadmap on how to possibly mitigate or minimize potential errors was obtained which provides a validation to the usefulness of each concept.

The work done in this paper fundamentally changes how certain indentation tests can be performed and what kinds of valuable test data can be determined from such a test. By using a spherical indenter relatively deep penetrations can be made without damaging the material, with the added benefit of not having to test the material to failure as would be required if a simple tensile or compressive test were to be performed. The indentation test can be performed relatively quickly with very little preparation required. This is important because the indentation

test does not require the need to remove the film before trying to perform a tensile test on the substrate. The tensile test would be a common method used to determine the mechanical properties of the substrate. Because of the non-self-similarity features of a spherical indenter we can make a single indentation test but still obtain two separate and unique indenter force-displacement relationships allowing us to solve for any two unknowns out of the three unknowns established through Dimensional Analysis.

5.2 Future Research and Emerging Indentation Technologies

From the research described in this thesis a set of simple relationships between indentation force-displacement data and material properties has been established. This was done by performing a series of numerical simulations of a spherical indentation test, to moderate depth, which invokes the substrate effect, into materials with various properties. We then incorporated this simulation data into a comprehensive set of relationships spanning various material properties. Applying these formulas in a reverse analysis to the data generated from a single indentation test we can directly solve for material unknowns of an elastic film/substrate system. Unknowns such as film elastic modulus, film thickness, film prestress, and substrate elastic modulus can be determined.

The work conducted and described in this thesis is broad in scope and allows for many interesting future steps in research. Referring to the matrix shown in Fig.

5-2 an interesting, important, and natural extension to the research already performed is to establish an experimental program (providing additional data) that tests the theory developed from chapter 2 in this thesis (chapters 3 and 4 have similar proposed future research paths). This is of importance in order to validate the theory with real data generated from actual indentation tests, that spans over the range of variables used, and to examine any errors whether systematic or randomly generated.

Future Work	Material Systems	Material Elasticity	Stress State	Indenter Type	Load/Displacement Property	Load/Unload Condition	Study Type
	Bulk Material	Elastic	Unstressed Film	Flat Punch	Shallow Indentation	Loading Data	Numerical Analysis
	Film-Substrate	Elastic-Perfectly Plastic	Prestressed Film	Conical Punch	Moderately Deep Indentation	Unloading Data	Experimental Testing
	2-Film-Substrate	Elastic-Plastic		Vickers (4-sided pyramidal)			
		Elastic-Viscoelastic		Berkovitch Indenter (3-sided pyramidal)			
				Spherical Indenter			

Figure 5-2 Future research related to validating results from chapter 1 by experimental testing.

Another natural extension beyond the scope of this research is to examine film-substrate systems that are not perfectly elastic but instead follow power law work hardening principles. Materials indented to moderate depth may very well undergo some degree of plastic deformation directly under the indenter. An examination of materials that exhibit the properties of a power law work hardening material would be an important extension to the current research. This type of material as discussed earlier in Chapter 1 of this thesis can undergo both elastic and plastic deformation and can be described by the stress-strain

relationship as shown in Equations (1.44 to 1.46). Typical to this type of problem an understanding of the unloading portion of an indentation test may prove to be a valuable tool in further understanding the variables associated with work hardening such as elastic modulus, work hardening exponent, and yield stress, Fig. 5-3.

Future Work	Material Systems	Material Elasticity	Stress State	Indenter Type	Load/Displacement Property	Load/Unload Condition	Study Type
	Bulk Material	Elastic	Unstressed Film	Flat Punch	Shallow Indentation	Loading Data	Numerical Analysis
	Film-Substrate	Elastic-Perfectly Plastic	Prestressed Film	Conical Punch	Moderately Deep Indentation	Unloading Data	Experimental Testing
	2-Film-Substrate	Elastic-Plastic		Vickers (4-sided pyramidal)			
		Elastic-Viscoelastic		Berkovitch Indenter (3-sided pyramidal)			
				Spherical Indenter			

Figure 5-3 Future research extending into the elastic-plastic region of films and substrates.

One of the areas of emerging discovery is in the research and study of the biomechanics of the brain. Indentation may help in the understanding of many aspects of research such as young brain development, trauma of the brain, brain disease, and aging of the brain. The brain is a very complex organ with different locations having different properties. The brain is made up of and can be modelled as a homogenous or non-homogenous, isotropic or anisotropic, elastic or elastic-viscoelastic material.

By extending the research outlined in this thesis, specifically in the determination of elastic modulus of both film and substrate, some of the unanswered questions surrounding brain function may be answered. Of particular present-day interest is in the study of traumatic brain injury, see Goldsmith, [184], which has led to a quest to further understand the mechanical properties, acceleration, and forces on the brain during severe trauma. Widely referenced literature developed in the late twentieth century focused on the work done by Versace [185], called Head Injury Criterion. This was correlated with additional work done at Wayne State University by Gurdjian, et al [186]. This work was based on the assumption that the acceleration of the head was linear. Further work was done by Bandak and Eppinger [187], Brands, et al. [188], Claessens et al. [189], and other researchers which used finite element analysis in modelling the effects from large accelerations to the brain. Research specifically related to the development of finite element modeling of the brain was conducted by Taylor and Sackman [131]. However, the mechanical properties assumed in these analyses had large variations from one study to another, especially when it came to determining the differences in gray (isotropic) and white (anisotropic) brain matter. As another example, in 1960 Lee and Radok [190] developed a model that represents the mechanical shear modulus (G_s) and how this is related to force-depth data for a spherical indenter as it is pushed into a homogenous, isotropic linear viscoelastic half space:

$$G_s = \frac{3P}{16\delta\sqrt{R\delta}} \quad for \sqrt{\frac{\delta}{R}} \ll 1 \qquad \textbf{(5.1)}$$

P is the indenter force, R is the indenter radius, and δ is the indentation depth. Recall that our general term for shear modulus is the following which provides a correlation to material elastic modulus and Poisson's ratio:

$$G = \frac{E}{2(1+\nu)} \quad \textbf{(5.2)}$$

Geffen and Margulies [191] verified that this was applicable and representative for brain tissue when performed with an indenter radius between 2mm ≤ R ≤ 4mm. However, verification of the modulus of various sections of the brain still need to be further understood and verified. A better and more accurate method of determining these mechanical properties is needed in order to make representative FEA modelling more accurate. One possible theory for this discrepancy is that much of the data that is related to the mechanical properties was done from rheological experiments using large samples. The size of the sample examined can have engineering properties that changes from one location to another [192]. It is possible that indentation, at the micro or nano level targeting much smaller material locations can fill this gap and help in determining some of these different mechanical parameters.

Another ongoing area of research with regard to the brain, and brain development is in the area of gyrification. Gyrification is the term used to describe the folding of the cortical section of the human brain. This convoluted surface is what gives

the brain its characteristic ridges (gyri) and valleys (sulci). This distinctive feature creates more surface area of the brain and is believed to provide a better means for processing information in the brain [193, 194]. This condition is believed to be caused by the rapid growth of the brain with the number of folds varying between different species. For mice the brain surface is relatively smooth whereas for a mammalian there may be multiple folds. This act of brain folding naturally allows for substantial growth in brain size despite the restrictions due to the confining skull. As stated by Sun and Hevner [195] the growth of the cortex is dependent on the expansion of neural stem cells and neural progenitors. Consequently, deviations from this brain growth, microcephaly (a small brain) or macrocephaly (an enlarged brain) tends to lead to problems related to cognitive development, such as memory, judgement, reasoning, or comprehension.

An interesting and important question associated with gyrification is how does it occur? What is the driving mechanism that creates these folds in the cerebral cortex? There are three popular theories about how these ridges and valleys form. The first is that the gyri simply grows much more rapidly and to a greater extreme than the sulci. As such the folding is formed simply by this growth differential. The second theory considers the differences between the gray matter of the brain and the white matter. The grey matter is the outer part of the brain and is made up primarily of neurons while the inner white matter has long thin axons which are connected to the neurons. It has been proposed that these axons tend to pull on

the neurons of the grey matter creating this folding action. However there is growing speculation that neither of these two theories fully explains this folding action. The third hypothesis is based on the mechanics of the developing grey and white matter. If the gray matter grows faster than the white matter it may introduce buckling in the cortex, and this buckling would naturally create the gyri/sulci surface. Tallinen, Chung, Biggins and Mahadevan [196] proposed that this latter theory is the most probable and performed a set of experiments to try and simulate this effect. Along with this they qualitatively extended the analytical work done by Chen and Hutchinson [197] in Herringbone Buckling Patterns of Compressed Thin Films on Compliant Substrates in order to map this work directly to the buckling questions associated with brain development. While Tallinen, et al [196] stated that the folding of the brain cortex is different than wrinkles, they did propose that the work done by Chen and Hutchinson [197] can qualitatively help to describe this phenomenon. However they did conclude that a rigorous analytical study of this phenomenon is still not complete. The work done by Tallinen, et al. [196] was based on Gray and White matter having the same elastic properties. While this has been proposed by others [198, 199] further testing is warranted as there are varying thoughts that the elastic modulus of the two may in fact be quite different. In the paper by Chen and Hutchinson a critical buckling stress relationship was developed that is a function of the film and substrate elastic modulus. Understanding these elastic moduli is thus a very important and critical set of values to know accurately. Indentation could be the

tool used to fully understand the elastic values of each of the components of the brain and could be a viable tool in predicting when and how these folds occur. In particular it should be noted that indentation from the work described in this paper, specifically that related to the prestress of the film in chapter 3 could also be applied to the study of buckling and gyrification. It could specifically help link the correlation between tissue elastic modulus and the modes of buckling under gray matter compression or white matter tension.

In another study of the brain as it relates to gray and white matter stems from work done by Budday, et al [200]. They performed flat punch indentation tests on various gray and white matter producing an average elastic modulus for bovine brain tissue. They found that white matter was about 39% stiffer than gray matter. However what is not fully understood is the interface between the white and gray matter regions. In effect, what happens at this interface region? Can we learn anything from examining the system, both gray and white matter simultaneously? The research done and outlined in this thesis could be extended and may help to understand this relationship.

While the study of the brain offers many opportunities in extending the research done in this thesis another very important and growing area of interest is in spinal tissue research. Kawchuk and Fauvel [201] stated that indentation is a useful tool in helping to determine the force-displacement properties of spinal tissue and is

thought to have clinical significance. However, this is an emerging research area with many variables still left to be studied. Indentation may help in identifying some of these important mechanical properties. Like the brain this tissue has viscoelastic properties making it a complex non-linear elastic physical structure [202]. Bilston and Thibault [202] describe the interior of the spinal region to be made up of a combination of white matter of parallel axial fibers and inside this a central gray matter region made up of neurons that has no discernable isotropic pattern. One area of interest may be in trying to understand the mechanical performance of the spine under different loading scenarios, and in particular during severe trauma conditions where the spinal cord is under high loading rates, both axial as well as torsional. Understanding the mechanical properties of both the white matter and gray matter may help in understanding the mechanics of the spine. However, because the gray matter has no discernable isotropic pattern, the difficulty will be in how to statistically perform enough sampling to garner a relatively accurate statistical average. Because of the ease and minimal cost in performing indentation testing, it could be a useful tool in performing multiple tests, and if supported and enhanced by computational analysis could help further understand these materials.

Another area in biomedical research that may be influenced by indentation is in the field of biometric forensic identification. Here there are techniques using optical instrumentation to measure the microscopic features of tooth growth in an

effort to determine the characteristics of the human tooth [203]. Could indentation play a role in this research? Are there areas where we could correlate the age of tooth development to hardness? Can the measure of the tooth elastic modulus give us an indication of tooth health? All are interesting questions in which indentation may play a role in helping to answer.

While the future work proposed in the previous paragraphs suggests the use of indentation at the micro and nano scale, could indentation also help with macro problems as well? Can large data, using statistical methods be useful tools of the future for indentation testing? For example, could an in-situ multi step or continuous measurement of an indenter along the length of a support cable of a suspension bridge, testing the casing over the cable allow for a running chronology of the status of the material properties of the casing? Could it give us useful information about the stranded cable underneath it? Is there a way to determine the level of stress below the casing on a strand? Could the monitoring of a ship's hull by indentation provide useful long term information of the existing thickness and structural properties of the plating, differentiating between the paint on the plate surface and the underlying steel plate itself? Presently plate thickness is measured using ultrasonic testing, but no method is available other than removing test coupons from the hull itself in order to determine the elastic properties of the steel. Corrosion and thinning of a ship's hull may cause premature failure of the system or require costly repairs and time spent in a

shipyard. Can an indenter test system be developed that can be small enough to be able to move along a ship's hull easily such that a system such as this is viable, quick, and efficient? The simplicity of indentation begs these questions of the potential field application of in-situ testing of film/substrate systems. Indentation could indeed be a cost effective practical solution to solving many problems in industry.

Another emerging area where indentation could potentially play a role in the field testing of materials is in the long-term operation of large underground and above ground piping systems. Some piping systems can span hundreds if not thousands of kilometers. One such system is the Trans-Alaska Pipeline which delivers oil from the North Slope of Alaska to the port of Valdez, over 1200 kilometers away. The pipe is made of steel, continuously welded, 122 cm in diameter, with a nominal wall thickness of 1.25 cm. Natural gas, growing in popularity as a newly reliable energy alternative to coal and oil specifically in the commercial power generating and residential heating industry also has long piping systems installed throughout the world. Natural gas mains, running at pressures up to 10 MPa also use steel pipe to transport its medium to customers all around the world. As these piping systems operate, changes in pipe properties can potentially affect the safe operation of the system. This can come from environmental or mechanical effects to the pipe such as corrosion from moisture or wall deterioration from unanticipated corrosives, vibrational loading from pulsating flow, high strain rates

due to ground motion from a seismic event or frost heave in cold climates. Each can cause unacceptable mechanical changes to the pipe. If there is a coating or liner (film) applied to the pipe this too can be directly affected by environmental or mechanical effects. Again, indentation could play a role in determining not only the thickness and mechanical properties of an environmental coating over the pipe, but also the thickness and structural integrity of the pipe itself. Indentation may be a viable alternative for long-term monitoring of large piping systems such as this. Can an indenter be developed such that it is small enough to be able to run along the inside or outside of a pipe, taking indentation force-depth data? Could such a system provide real-time mass data to operators and maintenance personnel? All of these questions are interesting topics that extends the work done in this thesis to further research that can have a profound influence on critical areas of energy, infrastructure, and transportation.

A summary flow chart of possible future work is shown in Figure 5-4.

The research presented in this thesis provides a novel set of relationships that when applied through indentation at moderate depths to various geometric and prestress conditions provides information on film elastic modulus, thickness and prestress. It also and sometimes more importantly provides an easy, accurate, and straightforward method of determining the substrate elastic modulus, without

having to remove the film. This makes this technique unique, extremely attractive, and certainly worthy of further research.

Future Work - Brain Tissue Research	Material Systems	Material Elasticity	Stress State	Indenter Type	Load/Displacement Property	Load/Unload Condition	Study Type
	Bulk Material	Elastic	Unstressed Film	Flat Punch	Shallow Indentation	Loading Data	Numerical Analysis
	Film-Substrate	Elastic-Perfectly Plastic	Prestressed Film	Conical Punch	Moderately Deep Indentation	Unloading Data	Experimental Testing
	2-Film-Substrate	Elastic-Plastic		Vickers (4-sided pyramidal)			
		Elastic-Viscoelastic		Berkovitch Indenter (3-sided pyramidal)			
				Spherical Indenter			

Future Work - Brain Tissue Research	Material Systems	Material Elasticity	Stress State	Indenter Type	Load/Displacement Property	Load/Unload Condition	Study Type
	Bulk Material	Elastic	Unstressed Film	Flat Punch	Shallow Indentation	Loading Data	Numerical Analysis
	Film-Substrate	Elastic-Perfectly Plastic	Prestressed Film	Conical Punch	Moderately Deep Indentation	Unloading Data	Experimental Testing
	2-Film-Substrate	Elastic-Plastic		Vickers (4-sided pyramidal)			
		Elastic-Viscoelastic		Berkovitch Indenter (3-sided pyramidal)			
				Spherical Indenter			

Future Work field testing of hull plating and piping systems (initial investigation)	Material Systems	Material Elasticity	Stress State	Indenter Type	Load/Displacement Property	Load/Unload Condition	Study Type
	Bulk Material	Elastic	Unstressed Film	Flat Punch	Shallow Indentation	Loading Data	Numerical Analysis
	Film-Substrate	Elastic-Perfectly Plastic	Prestressed Film	Conical Punch	Moderately Deep Indentation	Unloading Data	Experimental Testing
	2-Film-Substrate	Elastic-Plastic		Vickers (4-sided pyramidal)			
		Elastic-Viscoelastic		Berkovitch Indenter (3-sided pyramidal)			
				Spherical Indenter			

Figure 5-4 Summary decision tree for possible future research.

Citations

1. Hertz, H., *Über die Berührung fester elastischer Körper (On the contact of elastic solids).* J. reine und angerwandte Mathematik, 1882a. **92**: p. 156-171.

2. Hertz, H., *Über die Berührung fester elastischer Körper and über die Harte (On the contact of rigid elastic solids and on hardness).* Verhandlungen des Vereins zur Beförderung des Gewerbefleisses, Leipzig, 1882b. **92**.

3. Johnson, K.L., *Contact Mechanics*. 1985, Cambridge: Cambridge University Press.

4. Boussinesq, J., *Application des potentiels à l'étude de l'équilibre et du mouvement des solides élastiques : principalement au calcul des déformations et des pressions que produisent, dans ces solides, des efforts quelconques exercés sur une petite partie de leur surface ou de leur intérieur : mémoire suivi de notes étendues sur divers points de physique, mathematique et d'analyse*. 1885, Paris: Gauthier-Villars.

5. Huber, M.T., *Zur Theorie der Berührung fester elastischer Körper.* Annalen der Physik, 1904. **319**(6): p. 153-163.

6. Fuchs, S., *Hauptspannungstrajektorien bei der Berührung einer Kugel mit einer Platte.* Phys. Z., 1913. **14**: p. 1282-1285.

7. Fuchs, M.T.H.a.S., Phys. Z. , 1914. **15**: p. 298.

8. Timoshenko, S., S. Timoshenko, and J.N. Goodier, *Theory of elasticity, by S. Timoshenko and J.N. Goodier, ... 2nd edition*. 1951, New York-Toronto-London: McGraw-Hill Book Co.

9. Flamant, A., *Sur la répartition des pressions dans un solide rectangulaire chargé transversalement.* C. R. Acad. Sci., 1892. **114**: p. 1465-1468.

10. Mindlin, R.D., *Compliance of elastic bodies in contact.* Journal of Applied Mechanics, 1949. **16**: p. 259-268.

11. Love, A.E.H., *BOUSSINESQ'S PROBLEM FOR A RIGID CONE.* The Quarterly Journal of Mathematics, 1939. **os-10**(1): p. 161-175.

12. Sneddon, I.N., *FOURIER TRANSFORMS*. 1951.

13. Gladwell, G.M.L., *Contact Problems in the Classical Theory of Elasticity*. 1980: Springer Netherlands.

14. Harding, J.W. and I.N. Sneddon, *The elastic stresses produced by the indentation of the plane surface of a semi-infinite elastic solid by a rigid punch.* Mathematical Proceedings of the Cambridge Philosophical Society, 1945. **41**(1): p. 16-26.

15. Titchmarsh, E.C., *Introduction to the theory of Fourier integrals*. 1937, Oxford: Clarendon Press. x, 390 p., 1 L.

16. Sneddon, I.N., *Boussinesq's problem for a flat-ended cylinder.* Mathematical Proceedings of the Cambridge Philosophical Society, 1946. **42**(1): p. 29-39.

17. Sneddon, I.N., *Boussinesq's problem for a rigid cone.* Mathematical Proceedings of the Cambridge Philosophical Society, 1948. **44**(4): p. 492-507.

18. Sneddon, I.N., *The relation between load and penetration in the axisymmetric boussinesq problem for a punch of arbitrary profile.* International Journal of Engineering Science, 1965. **3**(1): p. 47-57.

19. Chong, F., *Indentation of a semi-infinite medium by an axially symmetric rigid punch.* Iowa State College J. of Science, 1952. **026**: p. 1-15.

20. Segedin, C.M., *The relation between load and penetration for a spherical punch.* Mathematika, 1957. **4**(2): p. 156-161.

21. Tabor, D., *The hardness of metals*. 1951, Oxford: Clarendon Press.

22. Mohs, F., *Grundriss der Mineralogie*. 1822: Dresden.

23. Bierbaum, C., *Iron Age.* Trans. Amer. Inst. Mining Met. Engrs., 1920. **69**: p. 972.

24. Hankins, G.A., *Proc. Instn. Mech. Engr. .* 1, 1923: p. 423.

25. O'Neill, H., *The Hardness of Metals and Its Measurement*, C.a. Hall, Editor. 1934: London.

26. Brinell, J.A., in *II. Cong. Int. Méthodes d'Essai*. 1900: Paris.

27. Wahlberg, A., *On Brinell's method of determining hardness and other properties of iron and steel.* Journal of Iron and Steel Institute, 1901. **59**: p. 234-271.

28. Meyer, E., Zeits. d. Vereines Deutsch. Ingenieure, 1908. **52**: p. 645.

29. Smith, R.L. and G.E. Sandland, *An Accurate Method of Determining the Hardness of Metals, with Particular Reference to Those of a High Degree of Hardness.* Proceedings of the Institution of Mechanical Engineers, 1922. **102**(1): p. 623-641.

30. Shore, A.F., *Report on hardness testing: relation between ball hardness and scleroscope hardness.* Journal of the Iron and Steel Institute, 1918. **2**: p. 59-78.

31. Rockwell, S.P., *The testing of metals for hardness.* Transactions of American Society for Steel Treating, 1922. **2**: p. 1013-1033.

32. Knoop, F., Peters, C.G., Emerson, W.B. , *A sensitive pyramidal-diamond tool for indentation measurements.* Journal of Research of the National Institute of Standards and Technology, 1939. **23**(1): p. 39-61.

33. Stone, D., et al., *An investigation of hardness and adhesion of sputter-deposited aluminum on silicon by utilizing a continuous indentation test.* Journal of Materials Research, 2011. **3**(1): p. 141-147.

34. Pethicai, J.B., R. Hutchings, and W.C. Oliver, *Hardness measurement at penetration depths as small as 20 nm.* Philosophical Magazine A, 1983. **48**(4): p. 593-606.

35. Bhushan, B.K., A.; Bonin, W.; Wyrobek, J., *Nanoindentation and picoindentation measurements using a capacitive transducer system in atomic force microscopy.* Philosophical Magazine A, 1996. **74**(5): p. 1117-1128.

36. Berkovich, E.S., *Three-faceted diamond pyramid for micro-hardness testing.* Industrial Diamond Review, 1951. **11**(127): p. 129-133.

37. Doerner, M.F. and W.D. Nix, *A method for interpreting the data from depth-sensing indentation instruments.* Journal of Materials Research, 1986. **1**(4): p. 601-609.

38. Oliver, W.C. and G.M. Pharr, *An improved technique for determining hardness and elastic modulus using load and displacement sensing indentation experiments.* Journal of Materials Research, 1992. **7**(6): p. 1564-1583.

39. Bulychev, S.I., et al., *Determining Young's modulus from the indentor penetration diagram.* Ind Lab (USSR), 1975. **41**: p. 1409-1412.

40. Bulychev, S.I., et al., *Mechanical properties of materials studied from kinetic diagrams of load versus depth of impression during microimpression.* Strength of Materials, 1976. **8**(9): p. 1084-1089.

41. Pharr, G.M., W.C. Oliver, and F.R. Brotzen, *On the generality of the relationship among contact stiffness, contact area, and elastic modulus during indentation.* Journal of Materials Research, 2011. **7**(3): p. 613-617.

42. Loubet, J.L., et al., *Vickers Indentation Curves of Magnesium Oxide (MgO).* Journal of Tribology, 1984. **106**(1): p. 43-48.

43. Newey, D., M.A. Wilkins, and H.M. Pollock, *An ultra-low-load penetration hardness tester.* Journal of Physics E: Scientific Instruments, 1982. **15**(1): p. 119-122.

44. Pethica, J.B., *Microhardness Tests With Penetration Depths Less Than Ion Implanted Layer Thickness* in *Ion Implantation Into Metals*, V. Ashworth, W.A. Grant, and R.P.M. Procter, Editors. 1982, Pergamon. p. 147-156.

45. Field, J.S., *Understanding the penetration resistance of modified surface layers.* Surface and Coatings Technology, 1988. **36**(3): p. 817-827.

46. Lawn, B.R.H., V.R., *Elastic recovery at hardness indentations.* Journal of Materials Science, 1981. **16**(10): p. 2745-2752.

47. Stilwell, N.A. and D. Tabor, *Elastic Recovery of Conical Indentations.* Proceedings of the Physical Society, 1961. **78**(2): p. 169-179.

48. Oliver, W.C., R. Hutchings, and J.B. Pethica, *Measurement of Hardness at Indentation Depths as Low as 20 Nanometres*, P.J. Blau and B.R. Lawn, Editors. 1985, ASTM International: West Conshohocken, PA. p. 90-108.

49. Love Augustus Edward, H., *IX. The stress produced in a semi-infinite solid by pressure on part of the boundary.* Philosophical Transactions of the Royal Society of London. Series A, Containing Papers of a Mathematical or Physical Character, 1929. **228**(659-669): p. 377-420.

50. Tabor, D. and I. Taylor Geoffrey, *A simple theory of static and dynamic hardness.* Proceedings of the Royal Society of London. Series A. Mathematical and Physical Sciences, 1948. **192**(1029): p. 247-274.

51. Oliver, W.C. and G.M. Pharr, *Measurement of hardness and elastic modulus by instrumented indentation: Advances in understanding and refinements to methodology.* Journal of Materials Research, 2011. **19**(01): p. 3-20.

52. Pharr, G.M. and W.C. Oliver, *Measurement of Thin Film Mechanical Properties Using Nanoindentation.* MRS Bulletin, 2013. **17**(7): p. 28-33.

53. Pharr, G.M., *Measurement of mechanical properties by ultra-low load indentation.* Materials Science and Engineering A, 1998. **253**: p. 151-159.

54. Menčík, J., et al., *Determination of elastic modulus of thin layers using nanoindentation.* Journal of Materials Research, 2011. **12**(9): p. 2475-2484.

55. Knapp, J.A., et al., *Finite-element modeling of nanoindentation.* Journal of Applied Physics, 1999. **85**(3): p. 1460-1474.

56. Randall, N.X., *Direct measurement of residual contact area and volume during the nanoindentation of coated materials as an alternative method of calculating hardness.* Philosophical Magazine A, 2002. **82**(10): p. 1883-1892.

57. Xu, Z.-H. and D. Rowcliffe, *Method to determine the plastic properties of bulk materials by nanoindentation.* Philosophical Magazine A, 2002. **82**(10): p. 1893-1901.

58. Tsui, T.Y. and G.M. Pharr, *Substrate effects on nanoindentation mechanical property measurement of soft films on hard substrates.* Journal of Materials Research, 2012. **14**(1): p. 292-301.

59. Tsui, T.Y., J. Vlassak, and W.D. Nix, *Indentation plastic displacement field: Part I. The case of soft films on hard substrates.* Journal of Materials Research, 1999. **14**(6): p. 2196-2203.

60. Miyahara, K., N. Nagashima, and S. Matsuoka, *Development and application of a combined atomic force microscopy-nanoindentation system with a silicon tip and a diamond indenter.* Philosophical Magazine A, 2002. **82**(10): p. 2149-2160.

61. Lim, Y.Y., M.M. Chaudhri, and Y. Enomoto, *Accurate determination of the mechanical properties of thin aluminum films deposited on sapphire flats using nanoindentations.* Journal of Materials Research, 2011. **14**(6): p. 2314-2327.

62. Hainsworth, S.V., H.W. Chandler, and T.F. Page, *Analysis of nanoindentation load-displacement loading curves.* Journal of Materials Research, 2011. **11**(8): p. 1987-1995.

63. Hendrix, B.C., et al., *The Indentation Elastic Response - Indentation Shape and the Stress Distribution.* MRS Proceedings, 2011. **356**: p. 699.

64. Min, L., et al., *A numerical study of indentation using indenters of different geometry.* Journal of Materials Research, 2011. **19**(1): p. 73-78.

65. Qin, J., et al., *The equivalence of axisymmetric indentation model for three-dimensional indentation hardness.* Journal of Materials Research, 2011. **24**(3): p. 776-783.

66. Joslin, D.L. and W.C. Oliver, *A new method for analyzing data from continuous depth-sensing microindentation tests.* Journal of Materials Research, 2011. **5**(1): p. 123-126.

67. Fischer-Cripps, A.C., *Study of analysis methods of depth-sensing indentation test data for spherical indenters.* Journal of Materials Research, 2011. **16**(6): p. 1579-1584.

68. Field, J.S. and M.V. Swain, *Determining the mechanical properties of small volumes of material from submicrometer spherical indentations.* Journal of Materials Research, 2011. **10**(1): p. 101-112.

69. Francis, H.A., *Phenomenological Analysis of Plastic Spherical Indentation.* Journal of Engineering Materials and Technology, 1976. **98**(3): p. 272-281.

70. Swadener, J.G., E.P. George, and G.M. Pharr, *The Correlation of Indentation Size Effect Experiments with Pyramidal and Spherical Indenters.* MRS Proceedings, 2011. **695**: p. L11.5.1.

71. Williams, J.S., et al., *Ultra-micro-indentation of silicon and compound semiconductors with spherical indenters.* Journal of Materials Research, 2011. **14**(6): p. 2338-2343.

72. Field, J.S. and M.V. Swain, *A simple predictive model for spherical indentation.* Journal of Materials Research, 2011. **8**(2): p. 297-306.

73. Choi, I.-C., et al., *Indentation creep revisited.* Journal of Materials Research, 2011. **27**(1): p. 3-11.

74. Stone, D. and A.A. Elmustafa, *Analysis of Indentation Creep.* MRS Proceedings, 2011. **1049**: p. 1049-AA10-02.

75. Stone, D.S., et al., *Analysis of indentation creep.* Journal of Materials Research, 2011. **25**(4): p. 611-621.

76. Ngan, A.H.W. and B. Tang, *Viscoelastic effects during unloading in depth-sensing indentation.* Journal of Materials Research, 2011. **17**(10): p. 2604-2610.

77. Fu, G., *A Theoretical Study on the Indentation of Viscoelastic Materials.* MRS Proceedings, 2011. **795**: p. U11.16.

78. Cheng, Y.-T. and C.-M. Cheng, *Modeling indentation in linear viscoelastic solids.* MRS Proceedings, 2011. **841**: p. R11.2.

79. Oyen, M.L., *Indentation of Nonlinearly Viscoelastic Solids.* MRS Proceedings, 2011. **1049**: p. 1049-AA06-06.

80. Lawn, B.R., *Indentation fracture*, in *Fracture of Brittle Solids*, B. Lawn, Editor. 1993, Cambridge University Press: Cambridge. p. 249-306.

81. Mooney, R.G., et al., *Indentation micromechanics of three-dimensional fibrin/collagen biomaterial scaffolds.* Journal of Materials Research, 2006. **21**(8): p. 2023-2034.

82. Guidoni, G.M., et al., *Influence of the indenter tip geometry and environment on the indentation modulus of enamel.* Journal of Materials Research, 2011. **24**(3): p. 616-625.

83. Zhao, Y., et al., *Indentation experiments and simulation of ovine bone using a viscoelastic-plastic damage model.* Journal of Materials Research, 2011. **27**(1): p. 368-377.

84. Peterson, M.A., *Galileo's discovery of scaling laws.* American Journal of Physics, 2002. **70**: p. 575-580.

85. Cheng, Y.T. and C.M. Cheng, *Scaling, dimensional analysis, and indentation measurements.* Materials Science and Engineering, 2004. **R**(44): p. 91-149.

86. Barenblatt, G.I., *Introduction*, in *Scaling, Self-similarity, and Intermediate Asymptotics: Dimensional Analysis and Intermediate Asymptotics*, G.I. Barenblatt, Editor. 1996, Cambridge University Press: Cambridge. p. 1-27.

87. Rayleigh, *The Principle of Similitude.* Nature, 1915. **95**(2368): p. 66-68.

88. Rayleigh, *The Principle of Similitude.* Nature, 1915. **95**(2389): p. 644-644.

89. Riabouchinsky, D., *The Principle of Similitude.* Nature, 1915. **95**(2387): p. 591-591.

90. Bridgman, P.W., *Dimensional Analysis*, Y.U. Press, Editor. 1922: New Haven.

91. Sedov, L.I., *Similarity and Dimensional Methods in Mechanics*, Academic, Editor. 1959: New York.

92. Simon, V., B. Weigand, and H. Gomaa, *Some Fundamentals of Dimensional Analysis*, in *Dimensional Analysis for Engineers*. 2017, Springer International Publishing: Cham. p. 1-25.

93. Szirtes, T., *Applied Dimensional Analysis and Modeling*, McGraw-Hill, Editor. 1997: New York.

94. Taylor, E.S., *Dimensional Analysis for Engineers*, C. Press, Editor. 1974: Oxford.

95. L, J., *The Principle of Similitude.* Nature, 1915. **95**(2389): p. 644-644.

96. Astarita, G., *Dimensional analysis, scaling, and orders of magnitude.* Chemical Engineering Science, 1997. **52**(24): p. 4681-4698.

97. Butterfield, R., *Dimensional analysis for geotechnical engineers.* Géotechnique, 1999. **49**(3): p. 357-366.

98. Macagno, E.O., *Historico-critical review of dimensional analysis.* Journal of the Franklin Institute, 1971. **292**(6): p. 391-402.

99. Tan, Q.-M., *Dimensional Analysis*. 2011, Springer: Berlin, Heidelberg.

100. Maxwell, J.C.A., *Treatise on Electricity and Magnetism*, C. Press, Editor. 1871: Cambridge.

101. Buckingham, E., *On Physically Similar Systems; Illustrations of the Use of Dimensional Equations.* Physical Review, 1914. **4**(4): p. 345-376.

102. Buckingham, E., *The principle of similitude.* Nature, 1915. **96 (2406)** p. 396–397.

103. Buckingham, E., *Model experiments and the forms of empirical equations.* Transactions of the American Society of Mechanical Engineers, 1915. **37**: p. 263–296.

104. Cheng, Y.-T., Z. Li, and C.-M. Cheng, *Scaling Relationships for Indentation Measurements*. Philosophical Magazine A. Vol. 82. 2002. 1821-1829.

105. Cheng, Y.-T. and C.-M. Cheng, *Scaling approach to conical indentation in elastic-plastic solids with work hardening* Journal of Applied Physics, 1998. **84**(3): p. 1284-1291.

106. Cheng, Y.T. and C.M. Cheng, *Analysis of indentation loading curves obtained using conical indenters.* Philosophical Magazine Letters, 1998. **77**(1): p. 39-47.

107. Lubliner, *PlasticityTheory*, Macmillan, Editor. 1990: New York.

108. Dieter, G., *Mechanical Metallurgy*, McGraw-Hill, Editor. 1976: New York.

109. Fischer-Cripps, A.C., *Nanoindentation*. 2013: Springer New York.

110. Cheng, C.-M. and Y.-T. Cheng, *On the initial unloading slope in indentation of elastic-plastic solids by an indenter with an axisymmetric smooth profile.* Applied Physics Letters, 1997. **71**(18): p. 2623-2625.

111. Cheng, Y.-T. and C.-M. Cheng, *Further analysis of indentation loading curves: Effects of tip rounding on mechanical property measurements.* Journal of Materials Research, 2011. **13**(4): p. 1059-1064.

112. Cheng, Y.-T. and C.-M. Cheng, *Relationships between hardness, elastic modulus, and the work of indentation.* Applied Physics Letters, 1998. **73**(5): p. 614-616.

113. Cheng, Y.-T. and C.-M. Cheng, *Scaling relationships in conical indentation of elastic-perfectly plastic solids.* International Journal of Solids and Structures, 1999. **36**(8): p. 1231-1243.

114. Huang, H. and F. Spaepen, *Tensile testing of free-standing Cu, Ag and Al thin films and Ag/Cu multilayers.* Acta Materialia, 2000. **48**(12): p. 3261-3269.

115. Vlassak, J.J. and W.D. Nix, *A new bulge test technique for the determination of Young's modulus and Poisson's ratio of thin films.* Journal of Materials Research, 2011. **7**(12): p. 3242-3249.

116. Xiang, Y., X. Chen, and J.J. Vlassak, *Plane-strain Bulge Test for Thin Films.* Journal of Materials Research, 2011. **20**(9): p. 2360-2370.

117. Weihs, T.P., et al., *Mechanical deflection of cantilever microbeams: A new technique for testing the mechanical properties of thin films.* Journal of Materials Research, 2011. **3**(5): p. 931-942.

118. Kurapati, S.N.V.R.K., Y.C. Lu, and F. Yang, *Indentation Load-Displacement Relations for the Spherical Indentation of Elastic Film/Substrate Structures.* CMC: Computers, Materials & Continua, 2010. **20**(1): p. 1-18.

119. Chen, X. and J.J. Vlassak, *Numerical study on the measurement of thin film mechanical properties by means of nanoindentation.* Journal of Materials Research, 2001. **16**(10): p. 2974-2982.

120. Gao, H., C. Cheng-Hsin, and L. Jin, *Elastic contact versus indentation modeling of multi-layered materials.* International Journal of Solids and Structures, 1992. **29**: p. 2471-2492.

121. Hu, X.Z. and B.R. Lawn, *A simple indentation stress-strain relation for contacts with spheres on bilayer structures.* Thin Solid Films, 1998. **322**(1-2): p. 225-232.

122. Gouldstone, A., et al., *Indentation across size scales and disciplines: Recent developments in experimentation and modeling.* Acta Mater., 2007. **55**: p. 4015-4039.

123. Saha, R. and W.D. Nix, *Effects of the substrate on the determination of thin film mechanical properties by nanoindentation.* Acta Materialia, 2002. **50**: p. 23-38.

124. Saha, R., et al., *Indentation of a soft metal on a hard substrate: strain gradient hardening effects.* J. Mech. Phys. Solids, 2001. **49**: p. 1997-2014.

125. Swadener, J.G., E.P. George, and G.M. Pharr, *The correlation of the indentation size effect measured with indenters of various shapes.* Journal of the Mechanics and Physics of Solids, 2002. **50**: p. 681-694.

126. Zhao, M., et al., *A new approach to measure the elastic-plastic properties of bulk materials using spherical indentation.* Acta Materialia, 2006b. **54**: p. 23-32.

127. Zhao, M., et al., *Measuring elastoplastic properties of thin films on an elastic substrate using sharp indentation.* Acta Materialia, 2007. **55**: p. 6260-6274.

128. Chen, X., et al., *On the Uniqueness of Measuring Elastoplastic Properties from Indentation: the Indistinguishable Mystical Materals.* Journal of Mechanics and Physics of Solids, 2007. **55**: p. 1618-1660.

129. Chen, X., Y. Xiang, and J.J. Vlassak, *A novel technique to measure mechanical properties of porous materials by nanoindentation.* Journal of Materials Research, 2006. **21**(3): p. 715-724.

130. Zhao, M., et al., *A new sharp indentation method of measuring the elastic-plastic properties of soft and compliant materials by using the substrate effect.* Journal of Materials Research, 2006a. **21**: p. 3134-3151.

131. Taylor, R.L., et al., *Contact-impact problems*. 1980, Washington, D.C.; Springfield, Va.: The Administration ; National Technical Information Service [distributor].

132. Hughes, T., et al., *Finite Element Formulation and Solution of Contact-Impact Problems in Continuum Mechanics - IV.* 1976: p. 99.

133. Hughes, T.J.R., et al., *A finite element method for a class of contact-impact problems.* Computer Methods in Applied Mechanics and Engineering, 1976. **8**(3): p. 249-276.

134. ABAQUS, *ABAQUS 6.7 User's Manual*. 2007, Pawtucket, Rhode Island: ABAQUS Inc.

135. Bucaille, J.-L., et al., *Determination of plastic properties of metals by instrumented indentation using different sharp indenters.* Acta Materialia, 2003. **51**(6): p. Pages 1663-1678.

136. Dintwa, E., E. Tijskens, and H. Ramon, *On the accuracy of the Hertz model to describe the normal contact of soft elastic spheres.* Granular Mater, 2007. **10**(3): p. 209-221.

137. *OriginPro*. OriginLab Corporation: Northampton, MA, USA.

138. Shiwa, M., et al., *Acoustic emission and precision force-displacement observations of spherical indentations into TiN films on silicon.* Surface and Coatings Technology, 1994. **68-69**: p. 598-602.

139. Gan, L., B. Ben-Nissan, and A. Ben-David, *Modelling and finite element analysis of ultra-microhardness indentation of thin films.* Thin Solid Films, 1996. **290-291**: p. 362-366.

140. Kim, M.T., *Influence of substrates on the elastic reaction of films for the microindentation tests.* Thin Solid Films, 1996. **283**(1): p. 12-16.

141. Dolbow, J. and M. Gosz, *Effect of out-of-plane properties of a polyimide film on the stress fields in microelectronic structures.* Mechanics of Materials, 1996. **23**(4): p. 311-321.

142. Hess, P., *Laser diagnostics of mechanical and elastic properties of silicon and carbon films.* Applied Surface Science, 1996. **106**: p. 429-437.

143. Bhushan, B. and X. Li, *Micromechanical and tribological characterization of doped single-crystal silicon and polysilicon films for microelectromechanical systems devices.* Journal of Materials Research, 2011. **12**(1): p. 54-63.

144. Swain, M.V. and J. Menčík, *Mechanical property characterization of thin films using spherical tipped indenters.* Thin Solid Films, 1994. **253**(1): p. 204-211.

145. Fischer-Cripps, A.C., *Nanoindentation*. Mechanical Engineering Series, ed. F.F. Ling. 2002: Springer.

146. Eda, G. and M. Chhowalla, *Graphene-based Composite Thin Films for Electronics.* Nano Letters, 2009. **9**(2): p. 814-818.

147. Jang, K.-I., et al., *Rugged and breathable forms of stretchable electronics with adherent composite substrates for transcutaneous monitoring.* Nature Communications, 2014. **5**: p. 4779.

148. Zhang, Q.C., et al., *Bio-Inspired Engineering of Honeycomb Structure - Using Nature to Inspire Human Innovation.* Progress in Materials Science, 2015. **74**: p. 332-400.

149. Diez-Pascual, A., et al., *Nanoindentation in polymer nanocomposites.* Progress in Materials Science, 2014. **67**.

150. Duan, P., S. Bull, and J. Chen, *Modeling the nanomechanical responses of biopolymer composites during the nanoindentation.* Thin Solid Films, 2015.

151. Mallikarjunachari, G. and P. Ghosh, *Analysis of strength and response of polymer nano thin film interfaces applying nanoindentation and nanoscratch techniques.* Polymer, 2016. **90**: p. 53-66.

152. Mallikarjunachari, G. and P. Ghosh, *Application of Nanomechanical Response of Wrinkled Thin Films in Surface Feature Generation.* European Polymer Journal, 2017. **89**.

153. Huajian, G., C. Cheng-Hsin, and L. Jin, *Elastic Contact Versus Indentation Modelling of Multi-Layered Materials.* International Journal of Solids and Structures, 1992. **29**: p. 2471-2492.

154. Evans, A.G. and J.W. Hutchinson, *On the mechanics of delamination and spalling in compressed films.* International Journal of Solids and Structures, 1984. **20**(5): p. 455-466.

155. Hu, M.S., M.D. Thouless, and A.G. Evans, *The Decohesion of Thin Films From Brittle Substrates.* Acta Metallurgica, 1988. **36**(5): p. 1301-1307.

156. Suresh, S. and A.E. Giannakopoulos, *A New Method For Estimating Residual Stresses By Instrumented Sharp Indentation.* Acta Metallurgica, 1998. **46**(16): p. 5755-5767.

157. Tsui, T.Y., J. Vlassak, and W.D. Nix, *Indentation plastic displacement field: Part II. The case of hard films on soft substrates.* Journal of Materials Research, 1999. **14**(6): p. 2204-2209.

158. Drory, M., D.,Hutchinson, J. W. , *Measurement of the adhesion of a brittle film on a ductile substrate by indentation.* Proceedings of the Royal Society of London. Series A: Mathematical, Physical and Engineering Sciences, 1996. **452**(1953): p. 2319-2341.

159. Hu, M.S. and A.G. Evans, *The cracking and decohesion of thin films on ductile substrates.* Acta Metallurgica, 1989. **37**(3): p. 917-925.

160. Chen, Z., et al., *A review on the mechanical methods for evaluating coating adhesion.* Acta Mechanica, 2014. **225**(2): p. 431-452.

161. Lin, C.K. and C.C. Berndt, *Measurement and analysis of adhesion strength for thermally sprayed coatings.* Journal of Thermal Spray Technology, 1994. **3**(1): p. 75-104.

162. Hull, T.R., J.S. Colligon, and A.E. Hill, *Measurement of thin film adhesion.* Vacuum, 1987. **37**(3): p. 327-330.

163. Yeo, A., M. Liu, and K. Zhou, *Indentation damage evaluation on metal-coated thin-films stacked structure*. Vol. 30. 2015. 13.

164. Yeo, A., et al., *A combined experimental and modelling study of indentation damage test on thin-film stacked structures.* Thin Solid Films, 2016. **615**: p. 74-83.

165. Mills, J.A. and X. Chen, *Spherical Indentation on an Elastic Coating/Substrate System: Determining Substrate Modulus.* Journal of Engineering Mechanics, 2009. **135**(10): p. 1189-1197.

166. ABAQUS, *ABAQUS 6.11 Documentation Suite*. 2010, Dassault Systèmes Simulia Corporation: Providence, Rhode Island.

167. Quinn, G., P. J. Patel, and I. Lloyd, *Effect of Loading Rate Upon Conventional Ceramic Microindentation Hardness*. Vol. 107. 2002. 9.

168. *ASTM E384-17, Standard Test Method for Microindentation Hardness of Materials*. 2017, ASTM International: West Conshohocken, PA.

169. DOW, *FILMTEC™ Reverse Osmosis Membranes* in *Technical Manual*. Dow Chemical Company.

170. Connor, R., *Water for a sustainable World*, in *The United Nations World Water Development Report*. 2015, United Nations Educational, Scientific and Cultural Organization: Spello, Umbria, Italy.

171. Cadotte, J.E., et al., *A NEW THIN-FILM COMPOSITE SEAWATER REVERSE OSMOSIS MEMBRANE* Desalination, 1980. **32**: p. 25-31.

172. Petersen, R.J., *Composite reverse osmosis and nanofiltration membranes* Journal of Membrane Science, 1993. **83**: p. 81-150.

173. Ghosh, A.K., R.C. Bindal, and S. Prabhakar, *Composite Polyamide Reverse Osmosis (RO) Membranes – Recent Developments and Future Directions*, B.N.-T.D. ARTICLE, Editor. JULY - AUG. 2011 BARC p. 43-51.

174. Kurihara, M. and Y. Himeshima, *The Major Developments of the Evolving Reverse Osmosis Membranes and Ultrafiltration Membranes.* Polymer Journal, 1990. **23**(5): p. 513-520.

175. Lee, K.P., T.C. Arnot, and D. Mattia, *A review of reverse osmosis membrane materials for desalination - Development to date and future potential.* Journal of Membrane Science, 2011. **370**: p. 1-22.

176. Shawky, H.A., *Performance of aromatic polyamide RO membranes synthesized by interfacial polycondensation process in a water–tetrahydrofuran system.* Journal of Membrane Science, 2009. **339**(1-2): p. 209-214.

177. Shawky, H.A., et al., *Synthesis and characterization of a carbon nanotube/polymer nanocomposite membrane for water treatment.* Desalination, 2011. **272**: p. 46-50.

178. Callow, J.A., et al., *The application of atomic force microscopy to topographical studies and force measurements on the secreted adhesive of the green alga Enteromorpha.* Planta, 2000. **211**(5): p. 641-647.

179. Chaudhury, M.K., et al., *The influence of elastic modulus and thickness on the release of the soft-fouling green alga Ulva linza (syn. Enteromorpha linza) from poly(dimethylsiloxane) (PDMS) model networks.* Biofouling, 2005. **21**(1): p. 41-48.

180. Mi, B., et al., *Physico-chemical characterization of NF/RO membrane active layers by Rutherford backscattering spectrometry.* Journal of Membrane Science, 2006. **282**(1): p. 71-81.

181. Kotelyanskii, M.J., N.J. Wagner, and M.E. Paulaitis, *Atomistic simulation of water and salt transport in the reverse osmosis membrane FT-30.* Journal of Membrane Science, 1998. **139**: p. 1-16.

182. Hughes, Z. and J.D. Gale, *A Computational Investigation of the Properties of a Reverse Osmosis Membrane.* Journal of Materials Chemistry, 2010. **20**: p. 7788-7799.

183. ABAQUS, *ABAQUS 6.12 Documentation Suite*. 2012, Dassault Systèmes Simulia Corporation: Providence, Rhode Island.

184. Goldsmith, W., *Impact - The Theory and Physical Behaviour of Colliding solids*. 1960, London: EDWARD ARNOLD (PUBLISHERS) LTD.

185. Versace, J., *A Review of the Severity Index*. 1971, SAE International.

186. Gurdjian, E.S., H.R. Lissner, and L.M. Patrick, *Protection of the Head and Neck in Sports.* JAMA, 1962. **182**(5): p. 509-512.

187. Bandak, F.A. and R.H. Eppinger, *A Three-Dimensional Finite Element Analysis of the Human Brain Under Combined Rotational and Translational Accelerations.* SAE Transactions, 1994. **103**: p. 1708-1726.

188. Brands, D.W.A., P.H.M. Bovendeerd, and J.S.H.M. Wismans, *On the Potential Importance of Non-Linear Viscoelastic Material Modelling for Numerical Prediction of Brain Tissue Response: Test and Application*. 2002, The Stapp Association.

189. Claessens, M., F. Sauren, and J. Wismans, *Modeling of the Human Head Under Impact Conditions: A Parametric Study.* SAE Transactions, 1997. **106**: p. 3829-3848.

190. Lee, E.H. and J.R.M. Radok, *The Contact Problem for Viscoelastic Bodies.* Journal of Applied Mechanics, 1960. **27**(3): p. 438-444.

191. Gefen, A. and S.S. Margulies, *Are in vivo and in situ brain tissues mechanically similar?* Journal of Biomechanics, 2004. **37**(9): p. 1339-1352.

192. van Dommelen, J.A.W., et al., *Mechanical properties of brain tissue by indentation: Interregional variation.* Journal of the Mechanical Behavior of Biomedical Materials, 2010. **3**(2): p. 158-166.

193. Striedter, G.F., *Principles of brain evolution*. Principles of brain evolution. 2005, Sunderland, MA, US: Sinauer Associates. xii, 436-xii, 436.

194. Lui, Jan H., David V. Hansen, and Arnold R. Kriegstein, *Development and Evolution of the Human Neocortex.* Cell, 2011. **146**(1): p. 18-36.

195. Sun, T. and R.F. Hevner, *Growth and folding of the mammalian cerebral cortex: from molecules to malformations.* Nature Reviews Neuroscience, 2014. **15**: p. 217.

196. Tallinen, T., et al., *Gyrification from constrained cortical expansion.* Proceedings of the National Academy of Sciences, 2014. **111**(35): p. 12667-12672.

197. Chen, X. and J.W. Hutchinson, *Herringbone Buckling Patterns of Compressed Thin Films on Compliant Substrates.* Journal of Applied Mechanics, 2004. **71**(5): p. 597-603.

198. Prange, M.T. and S.S. Margulies, *Regional, Directional, and Age-Dependent Properties of the Brain Undergoing Large Deformation.* Journal of Biomechanical Engineering, 2002. **124**(2): p. 244-252.

199. Kaster, T., I. Sack, and A. Samani, *Measurement of the hyperelastic properties of ex vivo brain tissue slices.* Journal of Biomechanics, 2011. **44**(6): p. 1158-1163.

200. Budday, S., et al., *Mechanical properties of gray and white matter brain tissue by indentation.* Journal of the Mechanical Behavior of Biomedical Materials, 2015. **46**: p. 318-330.

201. Kawchuk, G.N. and O.R. Fauvel, *Sources of variation in spinal indentation testing: Indentation site relocation, intraabdominal pressure, subject movement, muscular response, and stiffness estimation.* Journal of Manipulative and Physiological Therapeutics, 2001. **24**(2): p. 84-91.

202. Bilston, L.E. and L.E. Thibault, *The mechanical properties of the human cervical spinal cordIn Vitro.* Annals of Biomedical Engineering, 1995. **24**(1): p. 67-74.

203. Elhechmi, I., et al., *Accelerated measurement of perikymata by an optical instrument.* Biomedical Optics Express, 2013. **4**(10): p. 2124-2137.